Department of Precision and Microsystems Engineering

A NEW APPROACH TO PRINT HEAD MOVEMENT: PROOF OF CONCEPT FOR LINEAR MOTOR POSITIONING IN AN ULTIMAKER 3D PRINTER

AARON ALKEMADE

Report no : 2019:008
Coach : Dr. ir. O.S. van de Ven
Professor : Ir. J.W. Spronck
Specialisation : Mechatronic System Design
Type of report : MSc Thesis
Date : 11-02-2019

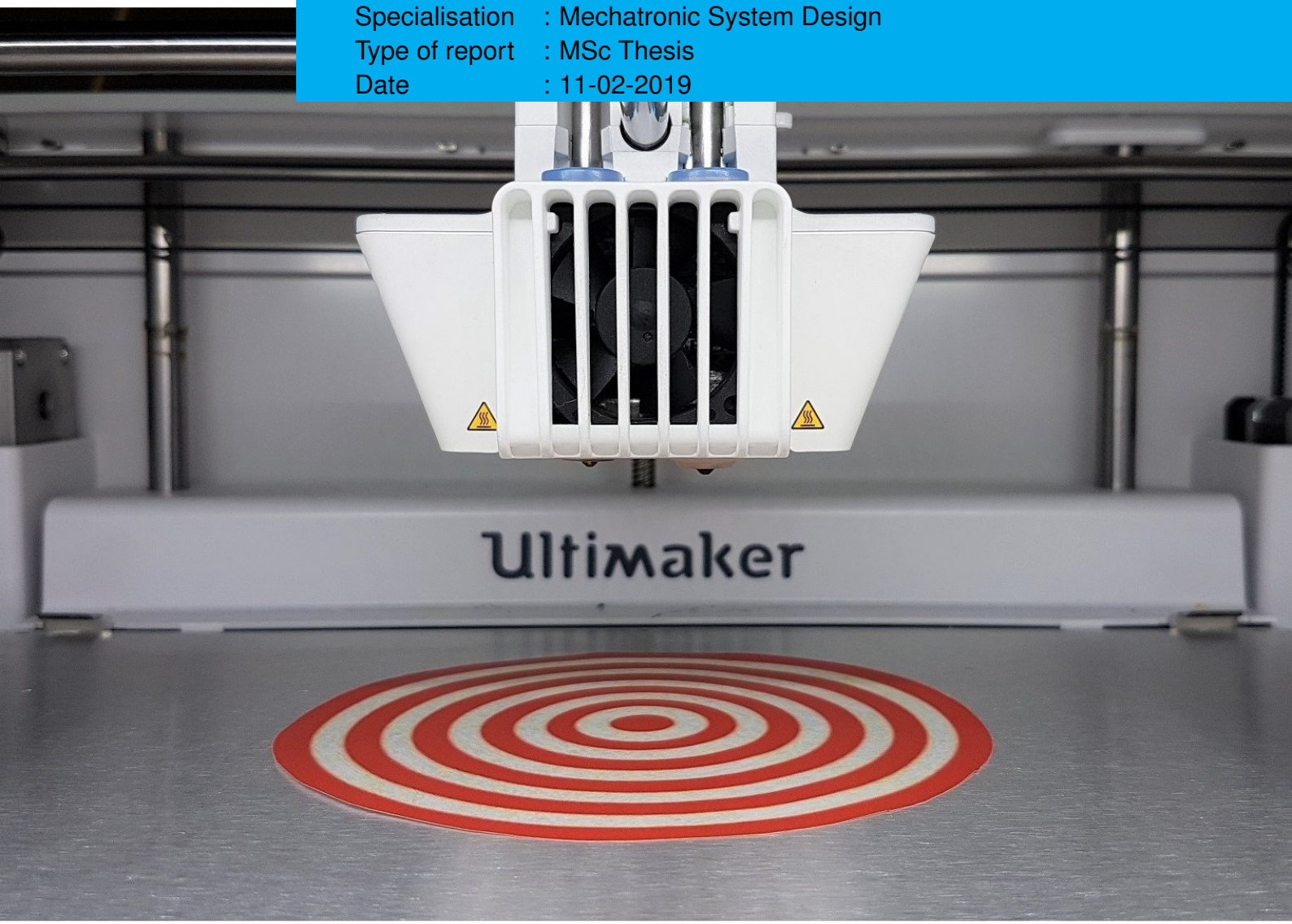

TU Delft Delft University of Technology

Challenge the future

A new approach to print head movement

Proof of concept for linear motor positioning in an Ultimaker 3D printer

by

Aaron Alkemade

to obtain the degree of Master of Science
at the Delft University of Technology,
to be defended publicly on Tuesday February 26, 2019 at 12:45 PM.

Student number:	4155572	
Project duration:	May 1, 2018 – February 28, 2019	
Thesis committee:	Dr. ir. O.S. van de Ven,	Ultimaker, daily supervisor
	Ir. J.W. Spronck,	TU Delft, supervisor
	Dr. N. Saikumar,	TU Delft
	Dr. J.J. van den Dobbelsteen,	TU Delft

This thesis is confidential and cannot be made public until February 1, 2024.

TU Delft

Summary

Ultimaker is a company that produces fused filament fabrication (FFF) 3D printers. To push the performance of the next generation 3D printers further, a new positioning system is required to improve the printing speed, print accuracy and print repeatability. The expectation is that a linear motor positioning system will perform significantly better than a conventional belt driven system. Linear motors are widely used in other positioning systems. The challenge however, is to make the positioning system affordable for implementation in an Ultimaker 3D printer. For this reason, the aim of this MSc Thesis is to demonstrate the feasibility of a low-cost linear motor positioning system for use in a 3D printer.

A review of the state of the art concerning the use of linear motors in FFF 3D printers reveals that these are not commonly implemented. The only record of a commercial 3D printer using linear motors was just released in Q4 2018 and falls outside the price category Ultimakers are marketed at. Linear motors are common in other type of positioning systems found in both commercial products as in research papers, however, no system is found which meets the performance requirements of Ultimaker at the given cost price. A further review of the field of precision engineering has provided terminology, common errors and design principles which should be considered when designing a linear positioning system.

For further analysis, the linear motor positioning system is divided in different subsystems; linear drive, position sensor, guide and controller. To be able to narrow down the design choices during the concept phase, a classification of these subsystems is made from literature. The choice of drive system is narrowed down to flat, ironless, synchronous linear motors. Whether a double sided, semi-double sided or single sided configuration is preferable needs to be determined. Position sensors are selected which are expected to provide the right accuracy, repeatability and linearity and are also affordable for implementation in an Ultimaker 3D printer. The eligible technologies are narrowed down to optical encoders, hall effect sensors, magnetoresistive sensors and inductive sensors. Linear ball bearings are the only eligible guides for use in the 3D printer, mainly out of cost perspective, however it can be decided if one or two guide blocks are preferable for the application. A closed-loop control system must be employed, equipped with necessary control schemes. Apart from the basic PID control functions, other advanced control strategies can be implemented to enhance the performance of the linear motor positioning system.

A single axis experimental set-up is realized in order to demonstrate the feasibility of a linear motor positioning system in a 3D printer. The use of a single axis is sufficient to evaluate the effect of different linear drives, sensors, guides and controllers on the performance of the system. A bottom-up design approach can be used to examine the effect of various components on the performance of the total system by replacing each component with a cheaper one. The frame is currently out of scope and can be designed when a multi-axis system is realized. As a basis, a linear synchronous motor from Tecnotion is chosen for the drive system. A Heidenhain linear optical encoder is selected as reference encoder because of the high accuracy grade and the small measuring step. A Hiwin linear guideway is used which can support the load on the mover and the force generated by the motor. Lastly, an Elmo servo drive is used which will be able to control the linear motor combined with different types of feedback sensors.

In order to make a statement about the performance of the positioning system, five measurement procedures are used to create a benchmark for the system and will be carried out when a new component of a subsystem is evaluated. The first measurement determines the maximum acceleration and velocity by measuring the motor force which can be generated per unit of current. The second measurement determines the accuracy and repeatability. ISO standard 230-2 is used, which specifies test procedures to determine the accuracy and repeatability of positioning of numerically controlled axes. The third measurement detects the motor stiffness and bandwidth. A motor stiffness follows from the proportional gain of the controller and the bandwidth can be found by performing a system identification. The fourth measurement determines the root mean square error, maximum absolute error, overshoot and settling time. This measurement uses a series of movements and monitors actual position relative to a position setpoint during movement. During the fifth

and last measurement the system is heated up and the encoder error is measured, determining the error by thermal expansion.

It is investigated whether a single sided, double sided or semi-double sided motor magnet track is optimal for the specific application of Ultimaker. Apart from the generated force in the motor, the weight of the moving axis also plays a large role in the consideration of the motor configuration. Measurements show that the semi-double sided configuration produces 54% force and the single sided configuration produces 43% force compared to the double sided configuration. This corresponds with results from a simulation of the magnet track in COMSOL. All three motor configurations feature virtually the same dynamic position error. Difference can be found in the continuous and maximum force the motor can generate. Both the semi-double sided and single sided configuration cannot reach continuous acceleration of 1 g in the y axis. All the motor configurations can, however, reach a 1 g peak acceleration. From a cost perspective, it would be beneficial to use a single sided configuration for both the x and y axes of the linear motor positioning system.

Various sensor types are mounted on the experimental set-up in order to evaluate the impact of the different sensor types on the performance of the positioning system. One optical encoder (Heidenhain), one magnetic hall encoder (RLS) and one inductive encoder (POSIC) is selected to compare the difference in performance and cost. It can be concluded that the choice of sensor type only has minor effect on the motor stiffness, bandwidth and dynamic position error. The choice of sensor type does affect the accuracy of the system. The RLS encoder can reach an accuracy of 14 μm and a repeatability of 2.8 μm. Even though the POSIC encoder has even better accuracy and repeatability, this sensor is very sensitive to temperature changes and deviations in scale distance. For this reason, the RLS encoder is preferred for this application. In an attempt to cut costs even further, effort has been made to develop a custom position sensor using Honeywell hall effect sensors, which can determine the position using the motors magnetic field. Even after calibration, an accuracy of 110 μm is maximum achievable. The principle of a custom build position sensor can be considered unsuitable for position feedback in the Ultimaker 3D printer.

Because of the large contribution of the guides to the accuracy and stiffness of the linear motor positioning system, the effect on performance by using one or two guide blocks is also examined. Linear recirculating ball bearings of HIWINs MGN series are used for this evaluation. The accuracy and repeatability stay virtually the same when one or two guide blocks are used. The frequency of the first eigenmode shifts from 120 Hz to 140 Hz and a decrease in dynamic position error is also noticeable when two guide blocks are used. Because of the increase in performance, and because the guide blocks are relatively inexpensive compared to the rails, the double guide block is preferable in this specific application.

Controllers are distinguished by communication interfaces, feedback interfaces, user interfaces, control strategies and hardware components. What effect these functions have on the performance of the motion system, is investigated through the use of an industrial controller (Elmo) and an open-source controller (ODrive). From the measurements it can be concluded that the error mapping function is an important tool to improve the accuracy of the positioning system. The ODrive is a promising controller for the linear motor positioning system. Before the ODrive is eligible as controller for a final product, there are few essential functions which are needed to be built in; error mapping, acceleration feed-forward during step and direction input, peak current limitation and a notch filter. Because the ODrive offers open source software, it is believed that the implementation of these functions can be done relatively quickly, making the gain by reduction in cost of the control system outweigh the effort of adjusting the firmware.

A linear motor positioning system that satisfies the requirements set by Ultimaker is feasible, as far as can be concluded from single axis experiments. The bottom up design approach led to a single axis positioning system that can reach an acceleration of 15 m/s^2, a velocity of 3.7 m/s, an accuracy of 14 μm and a repeatability of 4.1μm. In the final concept, a single sided Tecnotion linear motor is used combined with a RLS Hall effect encoder, HIWIN guiderail with two guide blocks and an ODrive controller. It is shown that a 2DOF, 3 axis positioning system using the components of the final set-up can be realized for €854.

Contents

1 Introduction **1**
- 1.1 Background . . . 1
- 1.2 Requirements of new system . . . 1
- 1.3 Research plan . . . 2

2 Literature Review **3**
- 2.1 Introduction . . . 3
- 2.2 Introduction to linear motors . . . 3
  - 2.2.1 Working principle of linear motors . . . 3
  - 2.2.2 Benefits of linear motors . . . 4
- 2.3 State of the art linear motors and 3D printers . . . 5
  - 2.3.1 Closed-loop rotary servo 3D printers . . . 5
  - 2.3.2 Linear motor motion systems . . . 5
  - 2.3.3 Linear motor 3D printers . . . 6
- 2.4 Introduction to precision engineering . . . 7
  - 2.4.1 Terminology . . . 7
  - 2.4.2 Classification of errors . . . 7
  - 2.4.3 Design principles . . . 8
- 2.5 Classifications of subsystems . . . 9
  - 2.5.1 Classification of linear drives . . . 9
  - 2.5.2 Classification of sensors . . . 10
  - 2.5.3 Classification of guiding . . . 12
  - 2.5.4 Classification of controllers . . . 13
- 2.6 Conclusion . . . 14

3 Experimental Set-up **15**
- 3.1 Introduction . . . 15
- 3.2 Proposed concept . . . 15
- 3.3 Conceptual design . . . 16
  - 3.3.1 Abbe errors . . . 16
  - 3.3.2 Balance of force . . . 17
  - 3.3.3 Prediction of distortions . . . 17
  - 3.3.4 Structural stiffness . . . 17
  - 3.3.5 Guide stiffness . . . 17
  - 3.3.6 Natural frequencies . . . 17
- 3.4 Measurement procedures . . . 18
  - 3.4.1 Maximum acceleration and velocity . . . 18
  - 3.4.2 Accuracy and Repeatability . . . 19
  - 3.4.3 Motor stiffness and bandwidth . . . 21
  - 3.4.4 Dynamic position error . . . 21
  - 3.4.5 Error due to thermal expansion . . . 22
- 3.5 Conclusion . . . 23

4 Motor configuration **25**
- 4.1 Introduction . . . 25
- 4.2 Expectation . . . 27
- 4.3 Measurement set-up . . . 27
- 4.4 Measurement results . . . 28

5 Position sensor **29**
5.1 Introduction . . . 29
5.2 Expectation . . . 30
5.3 Measurement set-up . . . 30
5.4 Measurement results . . . 31

6 Linear guide **33**
6.1 Introduction . . . 33
6.2 Expectation . . . 33
6.3 Measurement set-up . . . 34
6.4 Measurement results . . . 34

7 Controller **37**
7.1 Introduction . . . 37
7.2 Expectation . . . 38
7.3 Measurement setup . . . 38
7.4 Measurement results . . . 39

8 Conclusion and Recommendations **41**
8.1 Conclusion . . . 41
8.2 Recommendations . . . 42

A Conceptual design **45**
A.1 Solidworks simulations of the bracket . . . 45
A.2 Position plant bode plot . . . 46

B COMSOL model of motor configurations **47**

C Position sensor **49**
C.1 Sensor calibration . . . 49
C.1.1 RLS . . . 49
C.1.2 POSIC . . . 50
C.1.3 Honeywell . . . 52
C.1.4 AMS . . . 54
C.1.5 Comparison of the sensors . . . 55
C.2 Measurement results thermal error . . . 56
C.3 Contour lines of 50 mT magnetic field strength . . . 57

D Yaw stiffness guide **59**

E Controller **61**
E.1 Elmo control loop . . . 61
E.2 ODrive control loop . . . 61
E.3 Error mapping . . . 62
E.4 Step responses of Elmo and ODrive . . . 62

F Supplementary figures **65**

Bibliography **69**

1 Introduction

1.1. Background

Ultimaker is a company that produces fused filament fabrication (FFF) 3D printers. FFF techniques create 3D solid objects directly from a computer model using a 3D printer, depositing successive layers of material in different shapes only where required. Dispensing material over complex geometries requires a motion system with multiple degrees of freedom to move the printing head or the substrate. Overall system accuracy and throughput are vitally important to creating complex structures with a commercially viable process.[14]

The current motion system of the Ultimaker 3D printers consist of two stepper motors, connected via belts to axes on which the print head slides. This system is shown in figure 1.1. To push the performance of the next generation 3D printers even further, a new motion system is required to improve the printing speed, print accuracy and print repeatability. There are two possibilities to realize this goal, improve the current system or come up with a new design. The expectation is that a linear motor motion system will perform significantly better than a conventional belt driven system.

Linear motors are widely used in other positioning systems. The challenge however, is to make the positioning system affordable for implementation in an Ultimaker 3D printer while meeting performance requirements. The question is, if the linear motor system will still outperform a belt driven system after the cost-down. For this reason, the aim of this MSc thesis is to demonstrate the feasibility of a low-cost linear motor positioning system for use in a 3D printer.

1.2. Requirements of new system

The functional requirements of the new motion system are given by Ultimaker and can be found in table 1.1.

Table 1.1: Typical performance of the Ultimaker S5 along with requirements for the new positioning system

	Unit	Ultimaker S5	Target
Travel speed	mm/s	150	2000
Print speed	mm/s	50	250
Acceleration	m/s^2	5	10
Positioning accuracy	μm	230	10
Positioning repeatability	μm	90	10
Print accuracy	μm	200+0.4%	100
Print repeatability	μm	-	50
Total cost (BOM)	€	-	<1000
Build volume	mm (LxWxH)	240x330x300	300x420x300

1.3. Research plan

To be able to demonstrate the feasibility of a linear motor positioning system in a 3D printer, an experimental set-up is needed. The literature study from chapter 2 is used to gather information about linear motors and their benefits. This study also reveals the state of the art in linear motors and 3D printers, to show the originality of this thesis. The field of precision engineering is investigated to get familiar with terminology, common errors and design principles in this field. The positioning system is divided in five different subsystems; linear drive, sensor, guide, controller and frame. A classification of first four subsystems is made, which helps designing the first concept and narrows down the search for the best component for each subsystem.

A single axis experimental set-up is realized, and can be found in chapter 3. The use of a single axis is sufficient to evaluate the effect of different linear drives, sensors, guides and controllers on the performance of the system. The frame is currently out of scope and can be designed when a multi-axis system is realized. The details about the conceptual design can also be found in this chapter. A series of measurements is created which can be used to benchmark the system and enables the comparison of different components on the performance of the entire system.

From the literature study a selection of components follows which are eligible for use in the linear motor positioning system. In the following four chapters the performance of these components will be investigated. In chapter 4 the drive will be investigated, in chapter 5 different sensors will be investigated, chapter 6 zooms in on the guide and finally chapter 7 investigates the performance of different controllers. For references to a multi-axis system, a gantry stage configuration is used, because of the small footprint of this type of motion system and the higher stiffness than a compound configuration of the same number of axes[14].

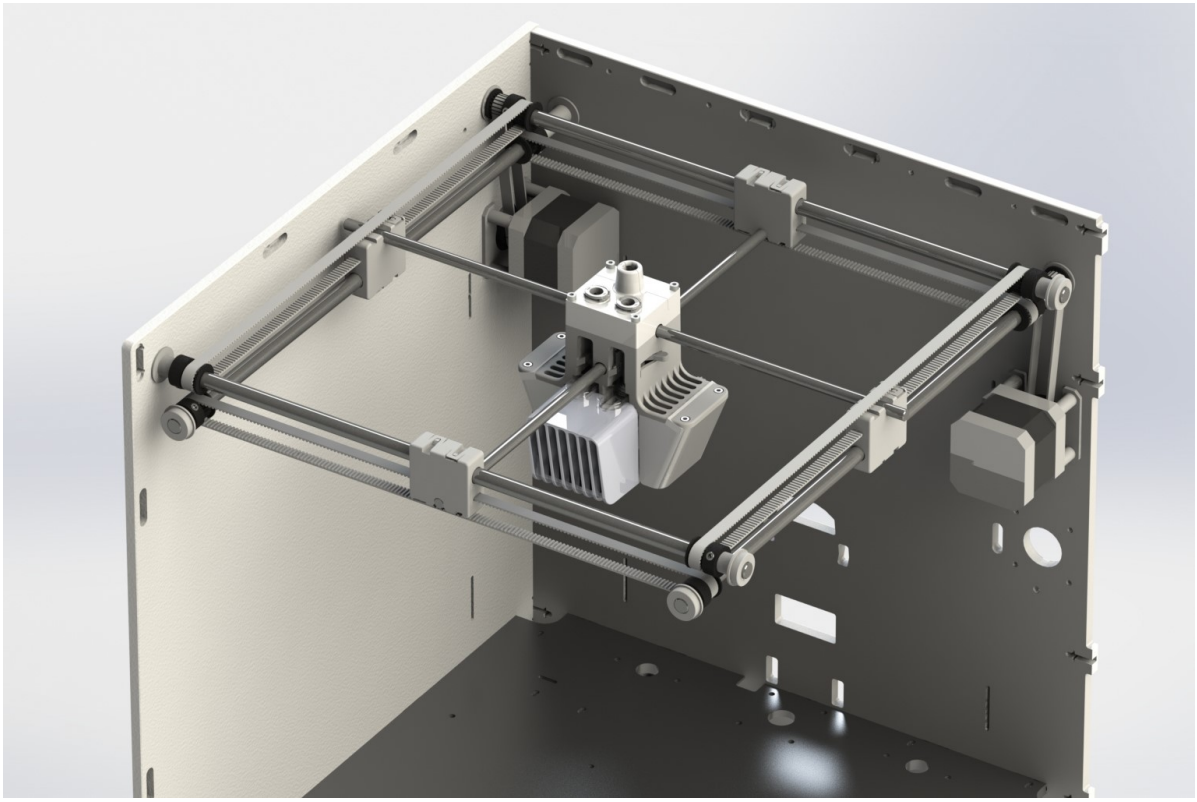

Figure 1.1: The motion system of the Ultimaker 3. Components unrelated to motion are hidden for clarity.

2

Literature Review

2.1. Introduction

The scope of this literature review is to reveal the state of knowledge in the field of linear motor systems, give an overview of dominant methodologies used when selecting a linear motor and to initiate the design process by generating an classification of the subsystems of a linear motor. First of all, the working principle and benefits of linear motors are explained. An overview of the state of the art in the field of linear motor 3D printers is given. The field of precision engineering is investigated to become familiar with the terminology in this field, tackle some errors that are common in this field and come up with a design strategy when designing a precision mechanism. Finally, a classification is made of four subsystems to consider when designing a linear motor; the linear drive, sensor, guide and controller. Using this classification a selection is made of components that are eligible for use in the linear motor positioning system.

2.2. Introduction to linear motors

2.2.1. Working principle of linear motors

A linear motor is an electrical machine that converts electrical energy into mechanical energy. Linear motors operate through the interaction between a magnetic field and winding currents to generate force. Magnetism is created from an electric current or by a permanent magnet.[39]. Unrolling a rotary electromagnetic machine will lead to its linear counterpart. Because of this relation, it is expected to encounter numerous conventional or easy to visualize linear motor configurations. Figure 2.1 illustrates the now classic birth of the linear counterpart of a rotary induction machine by simply unrolling it. A flat single-sided topology is thus obtained. Alternatively, if the stator and rotor of a rotary machine are halved and "squashed" subsequently, a flat double-sided configuration results, as shown in figure 2.2.[23]

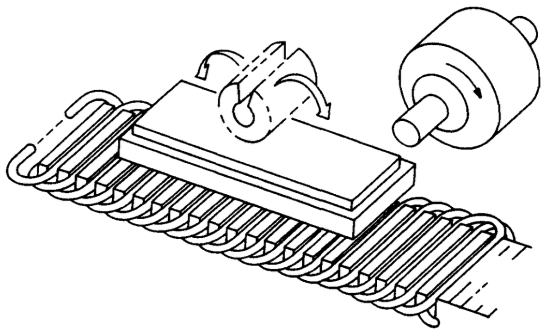

Figure 2.1: Unrolling a rotary electric machine. [23]

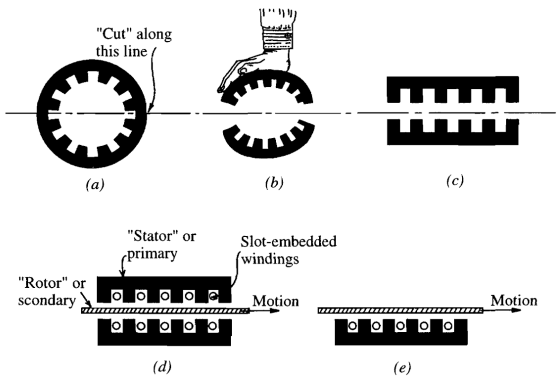

Figure 2.2: Halving and squashing a rotary electric machine. [23]

The linear flat configuration may be used as is, or it may be re-rolled along the direction of motion to form a tubular linear topology. The air gap between the stator and the mover may be kept below 1 mm for most cases. Consequently, the energy conversation performance is rather high. This is especially true for devices utilizing high-energy permanent magnets to produce the magnetic fields. Forces in magnetic fields may be either electromagnetic (by virtue of attraction) or electrodynamic (Lorentz type). Single sided flat linear motors experience, besides the thrust force, a non-zero normal force worthy of consideration for design purposes since the normal force may be greater than the thrust.[23]

2.2.2. Benefits of linear motors

Mostly high speed electric motors with associated gearing elements for torque and angular velocity conversion are used in numerically controlled machines for motion generation.[39] Belts and pulleys are the workhorses of the automation world. They provide high speeds and reasonable positioning repeatability for an economical component cost, but there are inherent limitations to using belt drives. All the torsional windup, backlash, and belt stretching of the components contribute to inaccuracies in the system. Typical repeatability of a belt drive system is around 0.2 mm whereas repeatability for a common linear motor system can be 1 μm. Additionally, all of the mechanical components are spring like by nature and cause ringing and longer settling time. So while belt drive systems can operate at high speeds, they can be difficult to tune for dampening and quick settling. This problem only gets worse at longer lengths, as belts tend to sag the longer they have to span.[18]

For high-end applications where good speed stability and high precision is required, the eligible drive technologies are based on screw drives, linear motors and piezo motors.[4] Because the direct linear drive does not require transmission elements to convert rotational movement to translational movement, it lacks the gears and ball screw mechanisms and their associated elasticities of the conventional drive system.[39]. Piezo motors only provide short stroke motion. For this reason a linear motor seems the perfect solution for the new positioning system in the Ultimaker 3D printer. Linear positioning stages offer the best available accuracy, repeatability and long-term reliability. [14]

The linear motor drive has several advantages[48].

- **Unlimited travel** - Linear motors do not have limitations on travel displacements. Since the stationary magnet assemblies can be easily joined to form any length of motor, the travel length can be made as long as necessary. Since the same moving coil assembly could be used for any travel length, there is no trade-off in the performance as a function of travel.
- **Velocity** - Linear servo motors can be used in both very low and very high velocity applications. They can precisely operate at velocities ranging from less than 1 $\mu m/sec$ to more than 10 m/sec.
- **Acceleration** - Linear motors have a high ratio of peak force to motor inertia. Therefore, almost all of the motor force can be used to accelerate the moving load and perform useful work.
- **Smoothness of motion** - Brushless linear servo motors can provide an extremely smooth motion, since they have no contacting surfaces to cause a jitter.
- **Accuracy and repeatability** - With linear motors, the only limit to total system accuracy and repeatability is the sensing device and the bearings of the positioning system. In rotary driven systems, there are additional factors, which affect these performance variables, including backlash, hysteresis, lost motion and jitter.
- **Stiffness** - Linear servo motors have a very high stiffness, typically higher than a stage's bearings and structural members. With ball screws and rack-and-pinion drives, the couplings, ball nut, and pinions are the highest contributors to the low stiffness of a stage. Low stiffness reduces frequency response and increases settling times.
- **Maintenance and life expectancy** - In brushless linear servo motors, there is no contact between the two working members. Therefore, they have an extremely long, virtually maintenance-free life. The non-contact design eliminates lubrication and periodic adjustment to compensate for wear.

2.3. State of the art linear motors and 3D printers

2.3.1. Closed-loop rotary servo 3D printers

The reader might ask why a closed-loop rotary servo system is not suitable for positioning. To be able to answer this question, a recent study of Go et al. [26] points out the performance that can be achieved with closed-loop rotary servos. A prototype is build using a servo-driven parallel gantry system to achieve fast gantry motion. The static and dynamic accuracy and repeatability of the H-frame gantry was measured along each axis (x, y) using a laser displacement sensor (Keyence LKG-152). Static accuracy was measured by moving the gantry with a velocity of 280 mm/s by a specified distance, and comparing its final position to the command position after coming to rest. The static positional accuracy was determined to fall within a band of ±0.1 mm. Dynamic accuracy was measured by the endpoint positions of the printhead when commanded to execute a continuous back-and-forth motion. The repeatability is defined as the standard deviation of the respected errors, sampled over a series of identical measurements. To examine dynamic positioning, the gantry was commanded to move repetitively between two positions along the axis at gantry speeds ranging from 35 to 280 mm/s at a prescribed acceleration of 10 m/s^2. The dynamic positional accuracy was determined to fall within a band of ±0.3 mm. This research provides an excellent target for the linear motor stage.

2.3.2. Linear motor motion systems

Gantry table for use in a semiconductor packaging machine Gaunekar et al.[16] describe the design optimization of a high speed, high accuracy, linear motor driven gantry table, for use in a semiconductor packaging machine. An air cored, moving coil, 3-phase linear motor drives the upper axis upon which the load is placed, while two similar, independently controlled linear motors drive the bottom axis. Each linear motor will have an associated high-resolution linear optical encoder. The system design of the gantry table is presented, as well as the design optimization and choice of the linear motor topology. Mechanical design aspects, such as the selection of the bearings, gantry system construction and placement of the encoders are also explored.

To meet the specifications, the motion system must have a high control bandwidth and impart a negligible temperature rise to the structure. The authors note that, to achieve the first of these requirements, higher order mechanical transmission systems that introduce low resonant frequencies, such as ball screws, gears and cams, should be eliminated. Instead, direct drive, non-contact linear motors and linear motion recirculating ball guides are preferable. Moving coil type linear motors were chosen for this application because the large attraction forces associated with the slotted moving magnet motors require larger bearings. The elimination of cogging force also reduces the variation of settling time with position. The authors provide the following design specifications:

- **Average acceleration** 20 m/s^2
- **Max. velocity** 2.0 m/s
- **Repeatability** 3.0 μm
- **Accuracy** 10.0 μm
- **Envelope dimensions** 950*800*200 mm
- **Load** 7.0 kg

In this work the authors predict the airgap flux density by a lumped parameter model and a finite element analysis. Using this flux density, also the force distribution is determined with respect to the position of the motor. These predictions are verified by measurements on a test setup of the y axis. The authors do not make a statement whether the design specifications are met nor they provide any measurement data regarding the evaluation of the design specifications. For this reason, this study is not usable for the design of a linear motor positioning system in a 3D printer.

Design and Metrology of a Precision XY Planar Stage J.M. Gorniak[15] presents a novel ultra-precision machine tool with the intent to bridge the gap between traditional machine tools with larger work volumes and lower accuracy, and ultra-precision machine tools with high accuracy and small work volumes. The machine was designed using a T-type gantry and worktable configuration with a precision ground granite base, to achieve a work area of 300x300 mm^2, with a maximum velocity of 1 m/s and a maximum acceleration of 10 m/s^2. Actuation is provided by direct drive linear motors with high resolution feedback supplied by 4 μm grating linear encoders with 4096x interpolation. Aerostatic porous bearings are employed to reduce the effect of friction while maintain high stiffness of the guideways and structure.

The following error was measured 2.7 μm and 2.4 μm in the x and y axes respectively, during a high speed (200 mm/s) test . Metrology tests using laser interferometry were performed in accordance with international and American metrology standards for linear positioning, vertical and horizontal straightness, and yaw and pitch errors. The results will be used for geometric error compensation in future work. Finally, an overall error budget is presented with focus on the geometric, dynamic, servo, and thermal errors, where the maximum static resultant error of the machine was estimated to be 1.44 μm, and the maximum dynamic resultant error of 3.69 μm.

This research provides a gantry stage that will meet specifications and could be used in the Ultimaker 3D printer. It is however expected that, because of the three double-sided linear synchronous motors and the use of air bearings, this system will be too expensive for use in the 3D printer. This research also describes a very useful design approach of a linear motor gantry system from the mechanical design up to measurements of a working prototype.

2.3.3. Linear motor 3D printers

Essentium HSE There is one record of a 3D FFF printer using linear motors for x-y positioning. The newly announced Essentium HSE 3D printer is scheduled for release in Q4 2018, the HSE 3D printer will cost $75,000. The company claims a print at speeds up to 1 m/s and a resolution of 13 μm for the x and y axis.[37]

Although the Essentium HSE uses a linear motor gantry system, it is far off from the desired solution for the new Ultimaker series. The Essentium HSE has a heavy print head, which makes the complete gantry system large and as well heavy. It is believed that a lighter and cheaper gantry system can be realized for use in the new Ultimaker series.

3D bioprinter Kim and Cho[27][28][29] introduce the development of precision deposition system, which is one of rapid prototyping technologies. A 3D bioprinter is built, containing two different cell types for osteochondral tissue regeneration. The system consists of two linear synchronous ironless motors, one for each axis. A reflective photoelectric linear encoder is used for positional feedback and roller bearings are used for guidance. This system is shown in figure 2.3 and 2.4. The authors claim that a repeatability of ± 1 μm was achieved by conducting the error mapping process based on static accuracy measurement data with a laser interferometer. The authors developed a linear motor gantry system with the following requirements:

- **Acceleration** 10 m/s^2
- **Max. velocity** 0.5 m/s
- **Repeatability** 1.0 μm
- **Accuracy** 2.4 μm
- **Resolution** 1.9 nm
- **Working area** 180*180*50 mm
- **Load** 9.0 kg

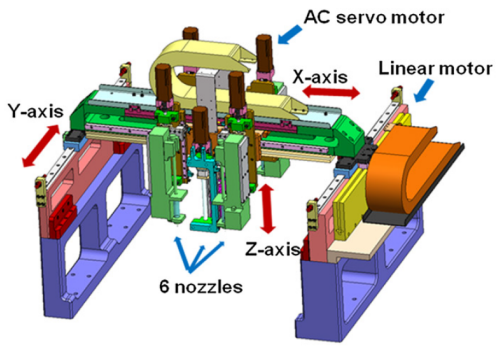

Figure 2.3: CAD modeling of the bioprinter.

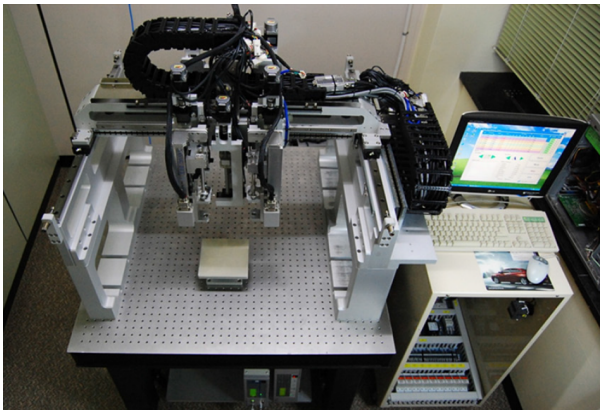

Figure 2.4: A front view of the bioprinter.

Unfortunately, no additional measurement data was made available in this research. The authors add that a single line test was performed to determine the precision of the structure; this confirmed that it was possible to fabricate a minimum line width of 100 μm with a precision of $\pm$20 μm.

Although this research proves that a linear motor FFF printer can achieve the desired specifications on accuracy and repeatability, the speed of the positioning system is still not as fast as it should be. Because the bioprinter uses six print heads, the overall weight of the printhead is a magnitude more than the printhead used in the Ultimaker printer. For this reason, it is believed that even better performance can be achieved when a similar system is implemented in the Ultimaker 3D printers.

2.4. Introduction to precision engineering

2.4.1. Terminology

Error An error is defined as the amount by which a assumed value deviates from its true value. Errors belong to two distinct classes: random and systematic errors. Random errors are related to precision of results and may be treated statistically. The magnitude of such errors may be judged from the results of a set of repeated measurements and could be reduced with the high number of observations. Systematic errors are those that occur in the same way at every measurement and therefore cannot be discovered only by examining the results.

Accuracy and precision The term accuracy refers to the degree of agreement of the measured dimension with its true magnitude or, in other words, it is the ability to hit what is aimed at. The term precision refers to the degree to which an instrument can give the same value when repeated measurements of the same standard are made. In short, precision pertains to the repeatability of a process. The distinct difference between accuracy and precision is shown in Figure 2.5. The figure shows the possible outcomes of attempts to hit a target, illustrating the difference between the terms accuracy and precision.[48]

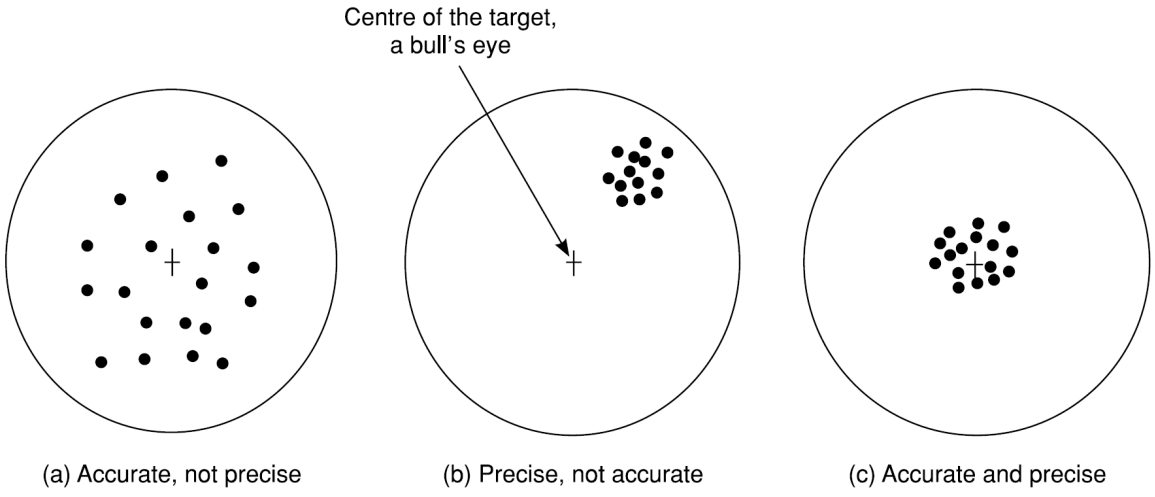

Figure 2.5: The difference between accuracy and precision. The cross represents the centre of the target.[48]

2.4.2. Classification of errors

Errors can fall into general categories such as geometric errors, thermal errors or controller errors. Some are beyond the control of the machine builder. It is important to make an accurate list of errors and to measure or estimate their magnitude. By building upon previous experience, extensive testing, and different operating conditions, it is possible to analyze the uncertainty of any machine.[31]

A classification is made for systematic and random errors and can be found in table 2.1. The reason for this categorization of errors in systematic and random is that it would help the error identification and compensation strategy. As long as we have specified the systematic errors, we can easily and permanently compensate for them by performing correction actions, concerning calibration. Most of the systematic errors are not

costly to compensate for. Unfortunately, random errors cannot be permanently compensated for, because of their random nature. They can exhibit random characteristics and thus, it is difficult to model and predict them. The only way to compensate for these errors is to monitor them during the process. Eliminating random errors can be elaborate and costly.[31]

Table 2.1: Systematic and Random Error Classification. Freely adopted from [31]

Systematic Errors	**Random Errors**
Geometric and kinematic errors	*Geometric and kinematic errors*
Positioning errors	Backlash errors
Straightness error of each axis in its perpendicular axis	Contouring error of each axis
Pitch angular error	Hysteresis errors
Roll angular error	Friction and stick-slip errors
Yaw angular error	Inertia forces while braking/accelerating
Nonperpendicularity of axes	Machine assembly errors
Reversal errors	*Thermal errors*
Acceleration of axes (Stiffness)	Perpendicular expansion of the linear motor
Abbé error	*Force-induced errors*
Thermal errors	Vibrations
Expansion of the linear motor in direction of motion	Instrumentation errors
Expansion of bed and frame	*Fixturing errors*
Force-induced errors	Wear
Workpiece, bed and frame elastic deformation	*Controller errors*
Wear	Servo errors
Fixturing errors	Interpolation errors
Production tolerances	Instrumentation random errors
Controller errors	Noise
Mismatch of position loop gain (different following errors)	
Instrumentation systematic errors	

2.4.3. Design principles

Standard machine design methods are no longer appropriate to design precision machines and satisfy tight requirements. Many principles have been defined for the design of precision systems. The design methodology will encompass a few critical steps such as the choice of design concepts with higher stiffness. The following are most of the principles required in the design of a precision system.[31] These design principles will be used for the design of the experimental set-up.

Conceptual design analysis

- Kinematic design
- Minimization of known errors induced by the system such as Abbe errors

Structural analysis

- Structure Stiffness
- Balance of force, damping, and dynamic stability over machine axes
- Thermal drift stabilization and compensation

Sensing and metrology

- Sensing system independent from machine distortions
- Direct measurement to avoid Abbe errors
- Sensors with appropriate resolution, repeatability, and time response

Control

- Control-securing high axis stiffness and high bandwidth
- Servo-drive stiffness, position loop synchronization
- Error compensation techniques

2.5. Classifications of subsystems

The linear motor positioning system consist of five different subsystems. A classification is made for four of these subsystems, namely the linear drive, position sensor, guide and controller. This classification will be followed by a selection to narrow down the design choices during the concept phase.

2.5.1. Classification of linear drives

The drive system is an important element to consider. It has a major influence on the load capacity, motion sensitivity, and dynamics of a motion system.[4] This section will provide an overview and selection of the linear drive. A classification of linear drives can be found in figure 2.6.

Non-eligible drives In the classification, depicted in yellow, are the drive technologies that are not eligible for use in the specific application discussed in this thesis. A few short-stroke motion technologies are mentioned which are not suited for the Ultimaker 3D printer because it will have a 420 mm stroke. As stated in the introduction, the performance of rotary drives with mechanical transmission elements is expected to be too poor for the application. What remains are linear synchronous, asynchronous (induction) and DC motors. Unlike a rotary DC motor, the DC linear motor with a commutator is not a very practical device.[25] The linear DC brush motor is plagued by the brush wear, noise and EMI.[24] Because of the small thrust per mass and volume, low efficiency, low power factor and because they emit large amounts of heat linear induction motors are, in general, not satisfactory as servo-motors for industrial robots. Much smaller dimensions and higher thrust can be obtained using permanent magnet linear motors. Permanent magnet linear synchronous motors are also a better alternative, because they are smaller and can provide efficiency over 75%, high power factor and fast response.[12][14][39]

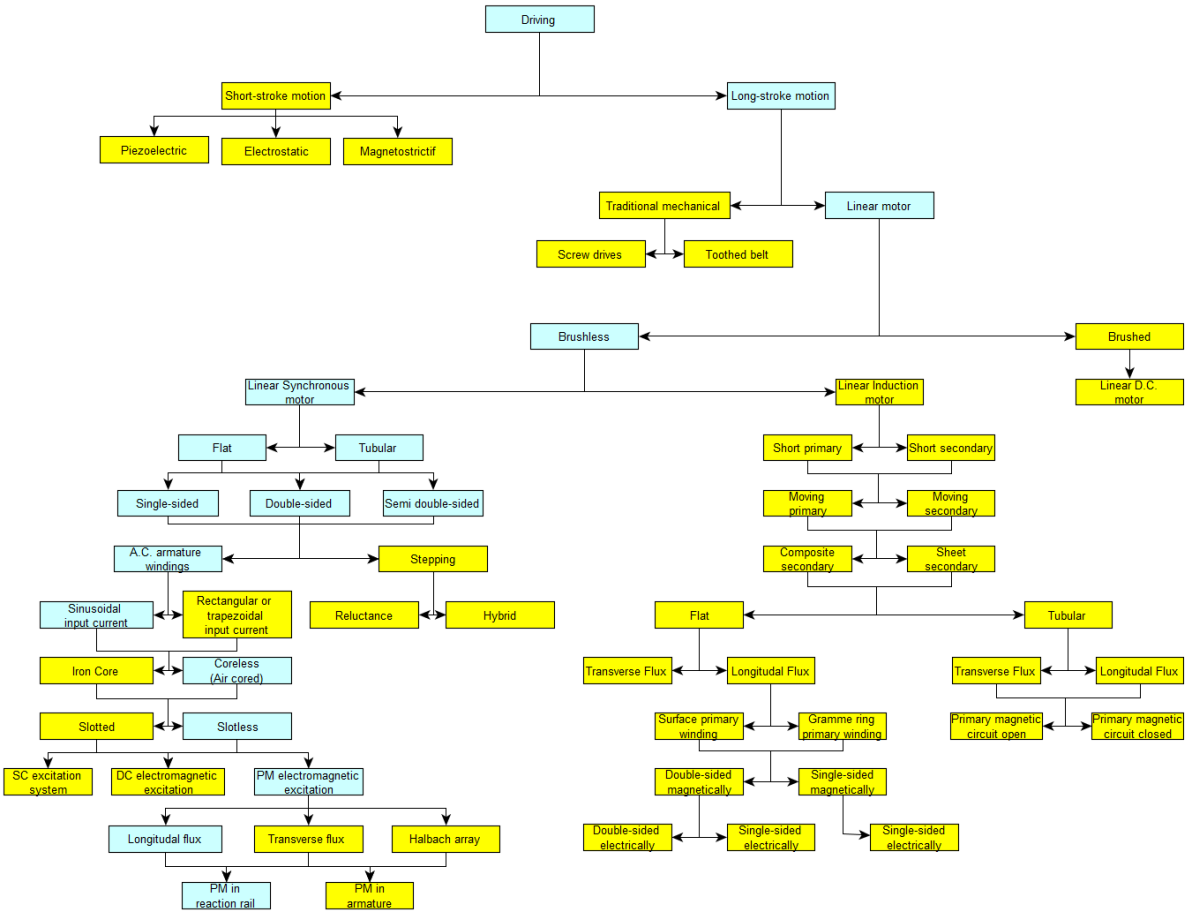

Figure 2.6: An overview and classification of linear drives. Freely adapted from [13], [25] and [6]. In yellow highlighted are the technologies not eligible for the application studied in this thesis.

A linear synchronous motor (LSM) is a linear motor in which the mechanical motion is in synchronism with the magnetic field, i.e., the mechanical speed is the same as the speed of the travelling magnetic field.[13] Zooming in on the field of linear synchronous motors, a choice needs to be made between AC armature and reluctance motors. The thrust (propulsion force) can be generated as an action of either travelling magnetic field produced by a polyphase winding and an array of magnetic poles (LSMs with a.c. armature windings) or magnetic field produced by electronically switched DC windings and variable reluctance ferromagnetic rail (switched reluctance motors).[13] A reluctance motor experiences high attractive force[6] and has an ferromagnetic mover, increasing the weight of the motor and the guiding system and is therefore not suited for use in the 3D printer. The polyphase (usually three-phase) armature winding can be distributed in slots, made in the form of concentrated-parameter coils or made as a coreless (air cored) winding layer.[13] Stampfli[45] presents an engineering based comparison of the two predominant linear motor types, iron core and ironless, with the objective of providing the reader with the knowledge needed to properly specify the correct type of motor for a given application. The author presents a comparative table between the two types of motors. In [14] J.F. Gieras indicates that an ironless armature assembly has no electromagnetic attractive force to the stationary permanent magnet assembly, which reduces the load on, and increases the life of, the bearing system. Because of the small thrust forces needed in the application and the low weight of the print head compared to the weight of iron core movers, it is expected that the benefits of an ironless motor will outweigh the benefits of an iron core motor. Finally, replacement of DC electromagnets with permanent magnets (PMs) is common. PMs are the most popular field excitation systems for short travelling distances (less than 10 m), because a long PM rail would be expensive.

Flat and tubular synchronous motors LSMs can be designed as flat motors or tubular motors. Cruise et al.[3] present a comparative study of force to weight ratios between single-sided and tubular linear synchronous machine topologies. The single-sided linear synchronous machine has already been built and tested, and physical test results compare favourably with finite element analysis. On this basis, the tubular linear synchronous machine has been designed purely through finite element analysis, and then compared to the single-sided topologies. It appears that the tubular LSM has an advantage of an improved force to weight ratio over both the buried and surface mounted magnet systems in the single-sided LSM. This is mainly due to the fact that the air gap area has been increased by a factor of two compared to that of the single-sided system. These results can be used to compare flat and tubular synchronous motors, however, only the iron core synchronous motors are compared. Because it is decided to use an ironless linear motor for the positioning system of the 3D printer and only iron core variants of tubular synchronous motors are found in practice, flat synchronous motors will be used in this thesis.

Single sided, double sided and semi-double sided synchronous motors In a recent study between different toothless motors Chevailler et al. [43] compare the maximum force per surface unit of four different motor configurations. The four motor configurations consist of a singe sided magnet yoke, a double sided magnet yoke, a semi-double sided magnet yoke and a Hallbach array single sided magnet yoke. The double magnet track uses more magnet material and therefore has higher thrust force than the single sided version. In the semi-double sided version an extra ferromagnetic yoke is needed, which also adds to the costs of the motor. Hallbach array linear motors are not found in practice. The consideration between single sided, double sided and semi-double sided synchronous motors is investigated further in chapter 4 of this thesis.

2.5.2. Classification of sensors

A variety of methods exist to provide linear positional feedback to the motion controller. There are analog transducers, rack-and-pinion style potentiometers, and laser interferometers, to name a few. Each has its own level of accuracy and cost.[18] A distinguishing feature of position measuring systems is the design of the sensors used. The measuring principle in such systems is usually optical, magnetic or inductive[2], but various other types can be found in literature. Different types of sensors are derived from [36]. A classification of linear position sensors can be found in figure 2.7.

Non-eligible sensors In the classification, depicted in yellow, are the sensor technologies that are not eligible for use in the specific application discussed in this thesis. The optical interference and magnetorestrictive position sensor are not suited for the application due to the high cost of these type of sensors. The resistive sensor is not eligible due to the fact that a contact pair is needed for the sensor to work. Especially for the application in a 3D printer, where small repetitive movements are common, a contact will be

exposed to wear resulting in faulty measurements or even failure. The LVDT is not eligible due to the fact that the sensor that takes up as much space as the motion range and therefore the measurement range is limited. Finally, the ultrasonic and capacitive position sensors are not suited for the application because they depend on environmental conditions. For the capacitive sensor, this can be solved by using a solid dielectric material against which the sensor is mounted. This however, introduces wear and is thus not favourable for this certain application. Eligible technologies are based upon optical encoders, hall effect sensors, magneto-resistive sensors and inductive sensors.

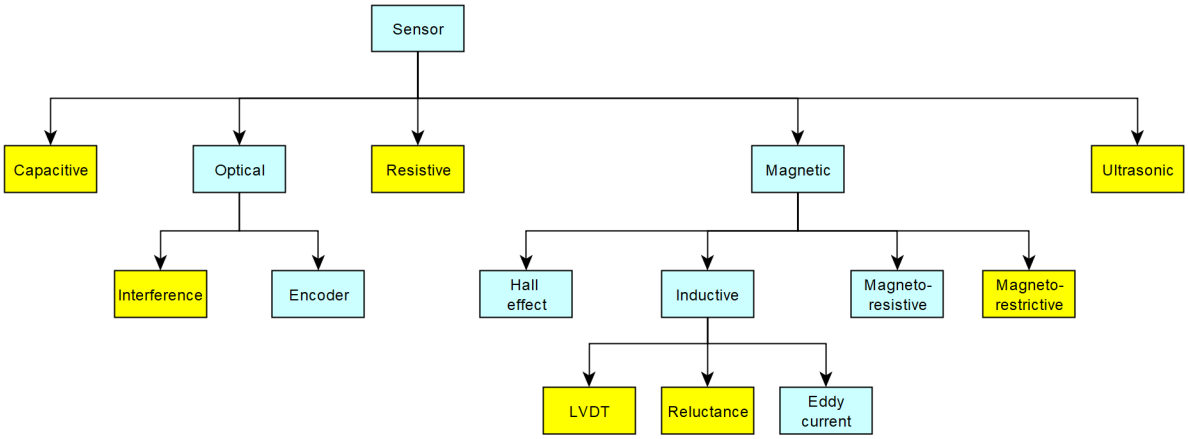

Figure 2.7: An overview and classification of linear position sensors. Freely adapted from [36]. In yellow highlighted are the technologies not eligible for the application studied in this thesis.

Optical encoder Most linear motor stages use optical scale and reading-head type encoders, although it is also possible to use magnetic encoder systems that are extremely robust and useful for hostile environment applications. Optical encoders use reflected light scanning techniques to provide feedback with extremely high resolution and accuracy. For precision applications, linear optical encoders are capable of higher levels of accuracy than their magnetic counterparts due to their finer scale pitch.[1] Optical encoders are also capable of providing feedback in the nanometer resolutions.[18] A disadvantage of optical encoders is the high sensitivity to dirt and contamination.[2]

Hall effect sensor Position sensors based on the Hall effect are often used in automotive and industrial products because they can provide long life at a relatively low cost. Hall effect sensors measure the strength and polarity of a magnetic field. A Hall effect linear position sensor includes at least a Hall device, a position magnet and associated electronic circuits. The position magnet is attached to the element to be measured. As the magnet approaches the Hall device, the strength of the magnetic field increases, and the output of the Hall device increases. Since the change in magnetic field strength is due to a change in the magnet position, the Hall device produces an electrical output that varies with changes in the location of the position magnet. Longer stroke length sensors can be made by incorporating an array of sensing elements.[36] Magnetic encoders can typically offer resolutions down between the 1 to 5 micron range.[18]. A disadvantage of hall effect sensors is the sensitivity to extreme static magnetic fields[2], which may be the case when a linear motor is used.

Magneto-resistive A magneto-resistive position sensor includes a transduction element known as a magneto-resistor. Magneto-resistive linear position sensors are non-contact. The measuring range of an individual element or bridge is limited to a maximum of about 25 mm, but practical linear sensors have been designed by using multiple sensing elements in a linear array to obtain sensors with a full-scale range (FSR) of over 2 m. These linear array sensors can have an overall nonlinearity of less than 0.25%. Popular applications include positioning of industrial machinery and measuring of small displacements in commercial products and industrial control systems.[36] Unfortunately, the availability of this type of sensor is very limited and therefore no magneto-resistive sensor is included as position feedback in the experimental set-up.

Inductive This method involves travel-dependent influencing of electromagnetic inductance by reciprocal displacement of AC-powered coil systems and iron cores. These sensors are insensitive to dirt and shavings and also insensitive to magnetic fields. The repeatability however, is less than that of the optical and magnetic encoder types.[2] Inductive position sensors use various working principles. The inductive sensor that is most common in combination with linear motors uses AC coils can generate a magnetic field that induces eddy currents on a metal padded scale. The closer the target is, the greater the induced eddy currents are and the more effect their resulting opposing magnetic fields have on the magnitude and frequency of the oscillation. Copper or aluminium is used to create the scale, because highly magnetically permeable material like iron increase the coil inductance, lowering the frequency of oscillation.

2.5.3. Classification of guiding

A guide constraints the motion to the desired direction. It is the main component that determines the trajectory accuracy, stiffness, and load capacity. This chapter will provide an overview of linear motor guides. A classification of linear guides can be found in figure 2.8.

Non-eligible guides In the classification, depicted in yellow, are the guide technologies that are not eligible for use in the specific application discussed in this thesis. The magnetic suspended bearing, hydrostatic bearing and aerostatic bearing are not suited for the application due to the high cost of these type of systems.[2] Flexure and kinematic motion (delta) types fall off because the design space is limited compared to the stroke that the motion needs to realize, making it unable to fit a rigid suspension into the design space. Metal/Metal and Metal/Plastic type of bearings provide limited accuracy and speed and are exposed to large friction forces, limiting the linear motor performance and wear over time.[2]. Finally, rollers offer a large contact are with far higher load capacity in terms of resistance to indenting the guiding due to a high load. Due to the high stiffness of the rollers they are, however, far more demanding than balls in terms of contact geometry. [4]. Because of the larger contact area, roller bearings tend to have higher resistive load than ball bearings. Eligible technologies are based upon recirculating ball bearings and cam rollers.

Linear ball bearings Balls are defined with accuracy grades that allow quality ranking down to micrometers. The accuracy and reproducibility of the diameters make the balls arrange in rows and fit in between the moving elements with contacts placed on a straight line. When moving, all balls move at the same speed, involving less resistance and frictions with the elements. The balls are in general maintained at a given position with a linear ball cage that prevents any migration or spacing deviations. The contact profile in between balls and moving elements is an important point: the larger the contact, the better is the load capacity and guide stiffness. On the other hand, the larger the contact area, the higher is the resistive load on the bearing. The required specifications for dynamics and service life define the ball bearing type: linear with translation of the ball cage or recirculating ball bearing that enables faster moving cycles. The recirculating ball bearings will also offer an easy way to manage cantilever loads by changing the bearing spacing.[4]

In general, linear ball bearings also offer very good lifetime, especially those with recirculating ball cages that improve the balls' lubrication during motion. These solutions are unfortunately not perfect – compared with a non recirculating ball solution, they are in general less straight and with induced angular deviations and noise due to the balls entering and exiting the bearing guide.[4] However, because of the limited travel range of the ball cage type bearing, the only eligible ball bearing for the specific application of this thesis, is the recirculating ball bearing.

Cam roller bearings In cam roller bearings there are cam rollers supported on ball bearings between the moving and fixed machine parts. Although cam roller bearings are quite affordable, they are still a factor 4 more expensive than linear ball bearings. A linear recirculating ball bearing in the line-up of MiSUMi[32] (SSE2B13-545) will cost €75. A cam roller bearing, with the same rail width as the recirculating ball bearing, can be provided by HepcoMotion.[20] A GV3 linear guide system (AU2018L100NS + NV20 P1) will cost €348. Cost-wise, it will thus be preferable to use linear recirculating ball bearings in the linear motor motion system.

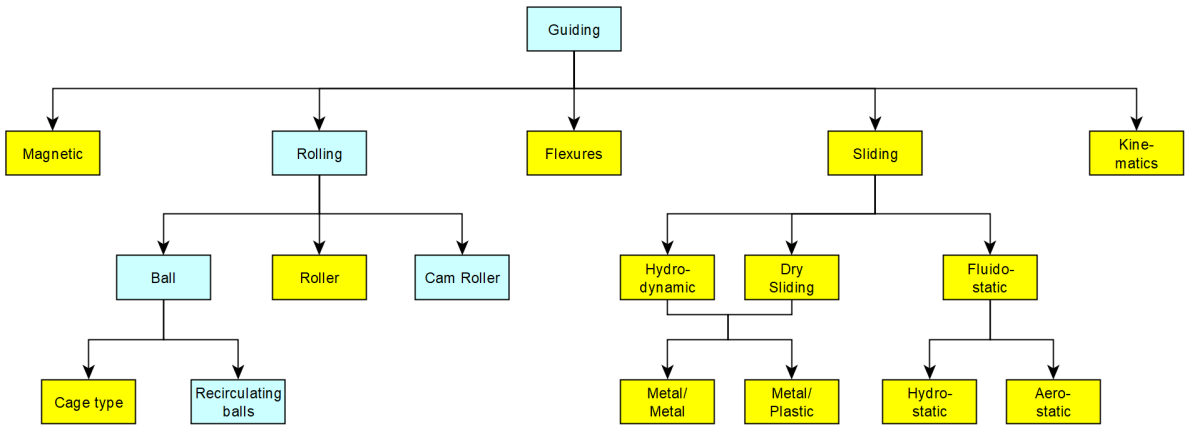

Figure 2.8: An overview and classification of linear guides. Freely adapted from [4] and [2]. In yellow highlighted are the technologies not eligible for the application studied in this thesis.

2.5.4. Classification of controllers

Generally, the objective of a servo control system is to make a controlled signal follow or track a reference input signal, sometimes also called the set-point, at certain speed and accuracy, and to remain robust to keep the controlled signal on track, despite possible undesirable disturbances affecting the system. Disturbances to the achievement of this objective may arise in the form of load changes and the existence of motion impeding forces such as friction, backlash, and cogging forces. The motion control variables of an electric drive mainly evolve around torque, speed, and position. To enable the drive system to perform according to the prescribed specifications, a closed-loop control system is employed, equipped with necessary control schemes and sensors to provide feedback of the controlled variables. Apart from the basic PID control functions, other advanced control strategies can be implemented to enhance the motion performance of the linear motor motion system. These functions will now be discussed and are derived from Kiong et al.[30]

Sensor calibration Sensors are mostly nonlinear in the relationship between the output and the input of the device. The reason for this is that the sensors are often not measuring directly the quantity of interest, but rather an indirect quantity which is related to it. A control system may include functions to calibrate the feedback sensor using a reference trajectory or a reference sensor.

Friction compensation In electric motors, friction will feature at the interface of all moving mechanisms where the power generated is transformed into mechanical motion. Friction can be broken down into two categories: static and dynamic. Many empirical friction models have been developed which attempt to capture specific components of observed friction behavior, but generally it is acknowledged that a precise and accurate friction model is difficult to be obtained in an explicit form, especially for the dynamical component. A common friction model used in this case is the Tustin friction model, which uses velocity dependent friction compensation. If a friction model is available, then based on the velocity reference signal from the trajectory generator, a counter-force can be generated to eliminate or minimize the frictional effects, so that to the feedback controller, the system appears to be friction-free.

Cogging compensation In almost all variations of electric motors where a ferromagnetic core is used for the windings, force ripples exist. The primary component of the force ripple is the cogging force. The cogging force arises as a result of the mutual attraction between the magnets and iron cores of the translator. The force ripple has significant effects on the position accuracy achievable and it may also cause oscillations. A controller may include functions to map and compensate for cogging forces.

Filters High-frequency components present in the controlled variables are usually generated in the sensor or the lead from the sensor. They can also arise due to switching power moderators such as pulse-width moderators. These high-frequency disturbances or noise should not be addressed at the controller. In most modern controllers, the facility is therefore provided for passing the controlled signal through a low-pass filter. Also, mechanical vibration in servo drives and equipment can occur. To prevent equipment damage

from the severe shaking that occurs when machines vibrate at resonant frequencies, a real-time monitoring or control device will be very useful. The task of eliminating/suppressing undesirable narrow-band frequencies can be efficiently accomplished using a notch filter. Ideally, the filter highly attenuates a particular frequency component and leaves the others relatively unaffected.

2.6. Conclusion

Linear motors have several advantages when compared to conventional drive systems. They can operate very precise at both low and high velocities, can reach high accelerations because of the high ratio of peak force to inertia and they can reach high levels of accuracy and repeatability. Nevertheless, linear motors are not commonly implemented in commercial 3D printers. The only occurrence of a commercial 3D printer which uses linear motors to position the printhead can be found at Essentium. Linear motors are common in other type of positioning systems found in both commercial products as in research papers. However, all of these systems are either too expensive or they lack data about the performance of the positioning system. A low-cost linear motor positioning system for use in an Ultimaker 3D cannot be obtained by means of a literature study.

During the classification of subsystems of the linear motor positioning system, a selection has been made of components eligible for the use in an Ultimaker 3D printer. Concluded can be that from all the linear motor drives available, a flat, ironless, synchronous linear motor is preferable for the specific application of the Ultimaker 3D printer. From all the available position sensors either an optical encoder, hall effect encoder or an inductive encoder needs to be used for position feedback on the motion system. Regarding the guide system, the only eligible technology is the recirculating linear ball bearing. Finally, various control functions are highlighted which can be used in linear motor positioning systems. This selection acts a basis for the design of a positioning system for the Ultimaker 3D printer and limits the design choices during the concept phase to a reasonable amount of components.

3

Experimental Set-up

3.1. Introduction

To reach the goal of this thesis, that is to demonstrate the feasibility of a linear motor positioning system in a 3D printer, an experimental set-up is needed to evaluate the performance of the system. The use of a single axis is sufficient to evaluate the performance of different linear motors, sensors, guides and controllers. Each subsystem will be evaluated and optimized such that the positioning system will meet the functional requirements as stated in section 1.2. The frame is currently out of scope and can be designed in a later stage when a multi-axis system is realized.

A series of measurements is created in order to evaluate the performance of the experimental set-up. These measurements can be carried out when a certain component of the set-up is replaced by another. The comparison between different components can be carried out fairly, through the use of these standardized measurements.

3.2. Proposed concept

Based on conclusions from the literature review and some basic design principles presented in 2.4.3 a concept for the experimental set-up is generated. An exploded view of the experimental set-up is shown in figure 3.1 along with a collapsed view in figure 3.2. As a starting point various components are used which are over-dimensioned for the specified requirements and will thus be too expensive for integration in a final product. However, with this test set-up, a bottom-up design approach can be used to evaluate the effect of different components on the performance of the total system by replacing each component with a cheaper one. The alternatives for the motor, sensor, guide and controller will be presented in chapter 4, 5, 6 and 7 respectively.

The initial set-up consists of the following components:

- **Cable trunking chain:** Igus E08.20.048.0
- **Linear guideway block:** HIWIN MGN12CZ0HM
- **Linear guideway rail:** HIWIN MGNR12R550HM
- **Linear optical encoder scanning head:** Heidenhain LIC 211
- **Linear optical encoder scale:** Heidenhain LIC 2107
- **Linear ironless motor:** Tecnotion UF3
- **Servo drive and motion controller** Elmo G-DCBEL10/100EE

Based on the literature review, a linear synchronous motor is chosen as drive system for the experimental set-up. Specifically, the UF3 linear ironless motor from Tecnotion[47] is chosen because it delivers high acceleration and dynamics, no cogging and low force ripple.[46] The Heidenhain linear optical encoder[19] is chosen because of the high accuracy grade (± 15 μm) and the small measuring step (50 nm). There is some free space left on the base frame to mount another encoder. In this way, the effect on performance of the system by using a different encoder can be measured. In this setting the Heidenhain encoder will function as reference encoder for the motor position. A Hiwin linear guideway[21] is used which can support the load on the mover and the force generated by the motor. The motor, encoder and guideway are connected by a

custom built bracket. The Elmo servo drive[34] will be able to control the linear motor combined with different types of feedback sensors. Finally, a mass of 0.5 kg is fixed to the mover to represent the mass of the print head.

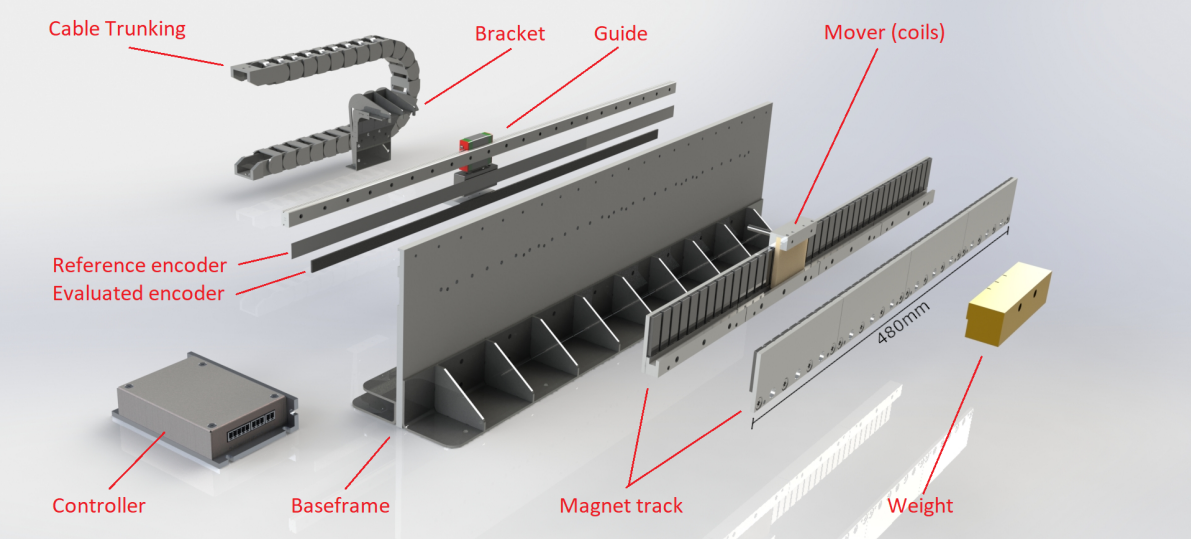

Figure 3.1: Exploded view of single axis experimental set-up.

3.3. Conceptual design

In this section, the mechanical design of the proposed concept is explained. Design principles from section 2.4.3 are used for the design of the experimental set-up.

3.3.1. Abbe errors

One important source of errors is based on angular movements combined with long arms. If errors in parallax are to be avoided, the measuring system must be placed coaxially with the axis along which the displacement is to be measured on the workpiece.[44] Because there is no print head installed on this experimental set-up, the measuring system is placed as close as possible to the bearing centerline, where it will measure the linear position free from rotational effects (Abbe errors). The placement of the encoder and the guide is shown in figure 3.3. As soon as a print head is mounted on the positioning system, the tip of the nozzle should be placed coaxially with the reading head of the linear encoder.

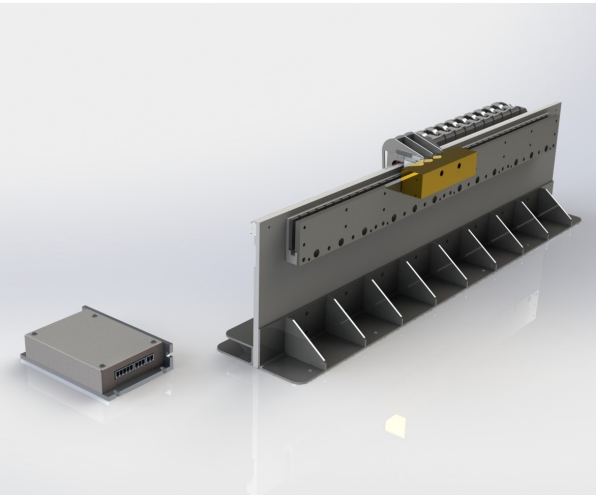

Figure 3.2: Single axis experimental set-up (collapsed).

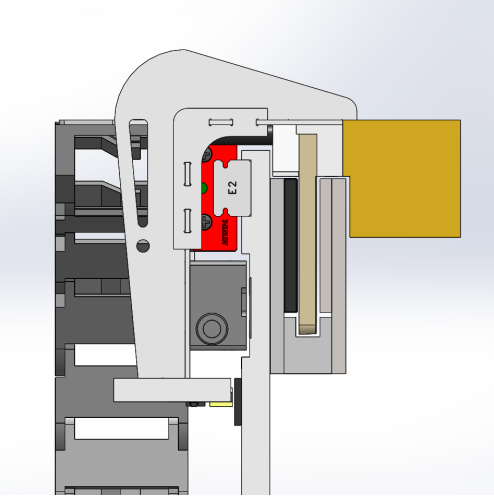

Figure 3.3: Side view (left) of the experimental set-up.

3.3.2. Balance of force

The balancing of driving forces from the motor and acceleration forces on the load reduces the forces acting on the bearing system. As shown in figure 3.3, the point where the motor force is generated is placed as close as possible to the center of the guide and coaxially with the center of gravity of the load.

3.3.3. Prediction of distortions

Frames are never infinitely rigid and therefore disturbance forces acting on the system cause deformations. The dynamic analysis of the effects of reaction forces is equally important in the design of a precision mechatronic system as the controlled actuation forces to the precisely positioned body itself.[44] Measurements on the Ultimaker 3 show that 1 N disturbance forces are introduced by the fact that the nozzle needs to cross printed lines in the same layer. Other predictions are hard to make because the new Ultimaker printers will differ much from the current generation.

3.3.4. Structural stiffness

To achieve a certain level of accuracy, the stiffness of a system is a very important property. A system with a high stiffness will deform less in response to an applied force and in most cases that is a benefit for a precision system.[44] The coupling between end effector and sensor has to be stiff enough to avoid position errors that cannot be measured and controlled. A SOLIDWORKS static deformation analysis is performed on the bracket, which couples the motor to the sensor. The simulation can be found in appendix A.1 and shows an error between the encoder and end effector of 1 μm when a 10 N force is applied by the motor. In reality, because of the balance of driving forces and acceleration forces on the load the deformation will be even less than the simulated 1 μm. It can be concluded that the stiffness of the bracket is sufficient for use in this experimental set-up.

3.3.5. Guide stiffness

An exploded view of the guide system is shown in figure 3.4. This design has 1 degree of freedom in the direction of motion and constraints the other directions. In the figure it is shown that a second guide block can be added to increase the stiffness of the bearing, making the mover rotate less with respect to the base in response to an applied force. In an ideal case the two guide blocks are perfectly aligned in the direction of motion, preventing the guide system from clamping on the rails.

3.3.6. Natural frequencies

The experimental set-up permits to determine the eigenfrequencies of the parts involved in the generation of motion. The first eigenfrequencies have to be above the servo-control bandwidth to avoid any excitation

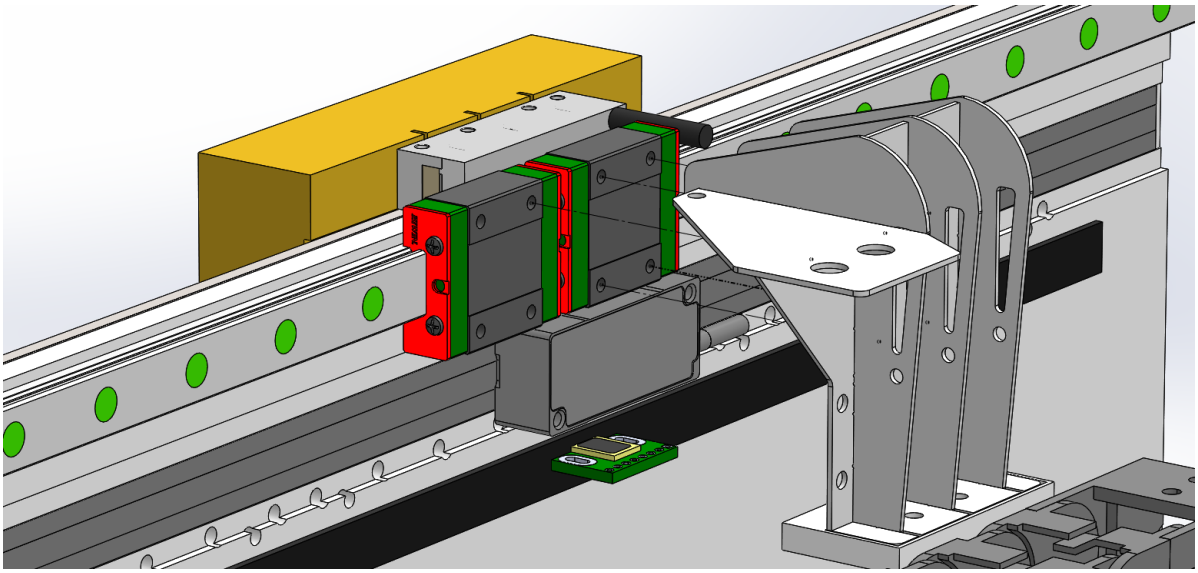

Figure 3.4: Exploded view of the guide design. The left guide block can be added to increase the stiffness of the bearing

of the vibration mode that may degrade the accuracy of the axis.[31] When positioning at high speeds, the resonance at the first mode-shape causes oscillations, which adversely affect the tracking accuracy. Often a notch filter is applied, with an inverse characteristic of the resonating eigenmode to suppress this specific resonance by pole-zero cancellation. Another method can simply be arranged by inserting a simple low-pass filter in the loop at a frequency around the eigenfrequency of the decoupling mass.[44] The system identification, displayed in appendix A.2, shows a resonance frequency around 140 Hz when two guide blocks are used. For this reason, a notch filter is applied at 140 Hz to suppress this resonance.

3.4. Measurement procedures

To be able to make a statement about the performance of the linear motor positioning system, five measurements are needed to be carried out in a systematic way to benchmark the performance of the system. These measurements can be carried out when a certain component of the set-up is replaced by another. The comparison between different components can be carried out fairly, through the use of these standardized measurements. Not all measurements are applicable to each subsystem. Whether measurements are carried out when evaluating a certain subsystem, will be discussed in the following chapters.

The following properties are determined using these measurements:

- Maximum acceleration
- Maximum velocity
- Accuracy
- Repeatability
- Motor stiffness
- Bandwidth
- Root mean square error
- Maximum absolute error
- Overshoot
- Settling time
- Error due to thermal expansion

3.4.1. Maximum acceleration and velocity

Motivation 3D printed models consist of varying geometries. Many of the models are built up by both short stroke and long stroke motion. A higher acceleration will mainly shorten the printing time when short stroke motions are dominant, because the print head is accelerating and decelerating most of the time. Small models are build up by mainly short stroke motion. Therefore, a high acceleration is needed to shorten the printing time.

In contrast to the acceleration, a higher velocity will mainly increase the printing time when long stroke motions are dominant, because maximum speed is not reached during short stroke motion. Large models can be built up by long stroke motions. Therefore, a high velocity is needed to shorten the printing time.

What to measure According to Newton's second law acceleration is directly related to the force acting on an object and its mass. For this reason, the maximum acceleration that can be achieved by the linear motor positioning system is limited by the maximum force the motor can generate. The maximum force is limited by the motor force constant $K_{rms}[\frac{\mathrm{N}}{\mathrm{A_{rms}}}]$ and the maximum current allowed in the motor coils. The maximum current allowed in the motor coils is a function of the ability of the coils to loose heat. Thus the motor force constant $K_{rms}[\frac{\mathrm{N}}{\mathrm{A_{rms}}}]$ and the maximum current allowed in the motor coils at a maximum temperature are to be measured.

The maximum velocity is limited by the maximum count frequency of the sensor and controller and the back EMF of the motor. The maximum count frequency limits the number of counts that the sensor can supply to the controller. The induced EMF over the motor coils is a function of the velocity. When the EMF voltage equals the supply voltage, current can no longer flow through the motor coils and further acceleration is not possible. The maximum velocity of the sensor is given in the data sheet of the sensor, thus does not need to be measured. The back EMF can be measured and is directly related to the motor constant (K_{peak}).

Method The motor force constant can be measured by applying a known current to the motor, and observe the force generated by this current. A schematic overview of the set-up is shown in figure 3.5. A force gauge is fixed to the base and measures the force generated by the motor. The current is measured using the ELMO application studio. The force gauge is moved 6 mm along the length of the motor, to get rid of any periodic effects which may be introduced by the magnetic pole pitch. A set of 3 measurements is repeated in both motor directions. The motor force constant can also be measured by applying a known load on the motor, and observe the current needed to counteract this load. A schematic overview of this set-up is shown in figure 3.6. The load is fixed to the motor, the motor moves slowly (10 mm/s) from 0 to 430 mm and back to 0 mm. The current supply to the motor is measured during this move using the ELMO application studio. The maximum current allowed in the motor coils is determined by the ability of the coils to loose heat. This specification is given by the manufacturer of the coil unit and thus does not need to be measured.

Because the motor constant is already measured, the back EMF does not need to be measured and follows from the relation given in equation 3.1

$$BackEMF_{peak}\left[\frac{\mathrm{V}}{\mathrm{m/s}}\right] = \sqrt{3}\cdot BackEMF_{spool} = \sqrt{3}\cdot K_{spool} = \sqrt{3}\cdot\frac{K_{peak}}{3} = \sqrt{3}\cdot\frac{\sqrt{2}K_{rms}}{3} \tag{3.1}$$

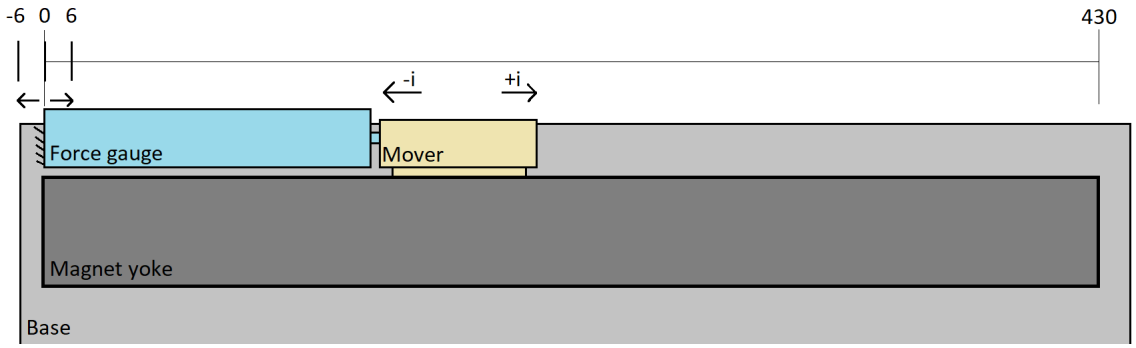

Figure 3.5: Schematic overview of the measurement set-up. Measuring force at a given current

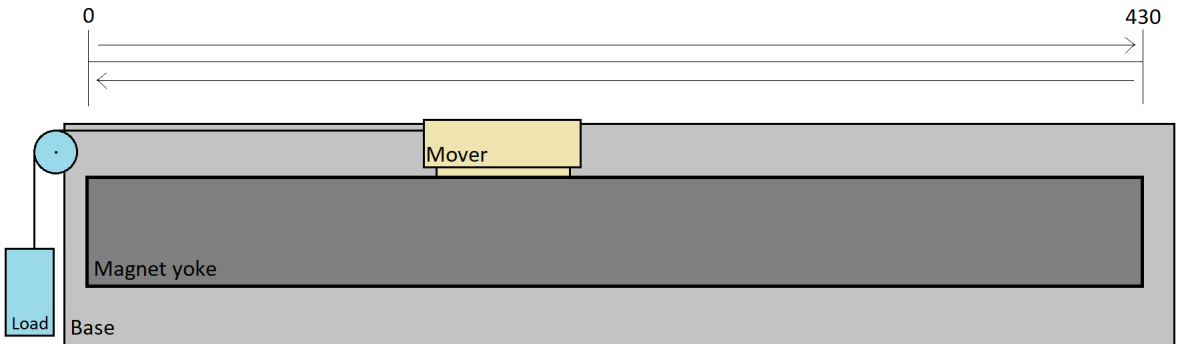

Figure 3.6: Schematic overview of the measurement set-up. Measuring current at a given force

3.4.2. Accuracy and Repeatability

Motivation The user of an Ultimaker 3D printer requires that the printed object resembles the 3D model as close as possible. In order to do so, the motion system of the printer must position the nozzle within a given window from the command position. Accuracy and repeatability characterize the systematic and random errors of the position tracking by the motion system. Ultimaker set this requirement to 10 μm for both the accuracy and the repeatability.

What to measure The accuracy and repeatability can directly be measured using the position setpoint and position data from the reference encoder. A reversal value and mean positional deviation also follows from this measurement, which provides insight in the amount of backlash and the mean deviation of the end effector from the setpoint respectively.

Method ISO 230-2[11] is used to measure accuracy and repeatability of the positioning system. ISO 230-2 specifies test procedures used to determine the accuracy and repeatability of positioning of numerically controlled axes. The tests are designed to measure the relative displacements between the component that holds the tool and the component that holds the workpiece. The machine shall be programmed to move the moving part along the axis under test, and to position it at a series of target positions where it will remain at rest long enough for the actual position to be reached, measured and recorded. The machine shall be programmed to move between the target positions at an agreed feed rate.

The value of each target position shall take the general form:

$$P_i = (i-1)p + r_i \tag{3.2}$$

Where i is the number of the current target position, p is the nominal interval based on a uniform spacing of target points over the measurement travel, r_i is a random number within ± the amplitude of possible periodic errors (such as errors caused by the pitch of linear scales), used to ensure that these periodic errors are adequately sampled. A minimum of five target positions shall be selected. Measurements shall be made at all the target positions according to the standard test cycle. Each target position shall be attained five times in each direction. A schematic overview of this experiment is shown in figure 3.7 and 3.8.

For each target position P_i and for five approaches (n=5) in each direction the target position is registered. The motion is controlled by the to be evaluated encoder and the actual position is measured by the Heidenhain sensor as a reference source. The following parameters are evaluated:

- **Bi-directional repeatability of positioning:** R**.** Maximum value of the repeatability of positioning at any position P_i along or around the axis. $R = max[R_i]$
- **Bi-directional accuracy of positioning:** A**.** Range derived from the combination of the bi-directional systematic deviations and the estimator for axis repeatability of bi-directional positioning using a coverage factor of 2. $A = max[\bar{x}_i \uparrow +2s_i \uparrow; \bar{x}_i \downarrow +2s_i \downarrow] - min[\bar{x}_i \uparrow -2s_i \uparrow; \bar{x}_i \downarrow -2s_i \downarrow]$
- **Reversal value:** B**.** Maximum of the absolute reversal values $|B_i|$ at all target positions along or around the axis. $B = max(|B_i|)$
- **Mean bi-directional positional deviation:** M**.** Difference between the algebraic maximum and minimum of the mean bi-directional positional deviations x_i at any position P_i along or around the axis. $M = max[\bar{x}_i] - min[\bar{x}_i]$

Further details about the parameters used during this measurement can be consulted in ISO 230-2[11].

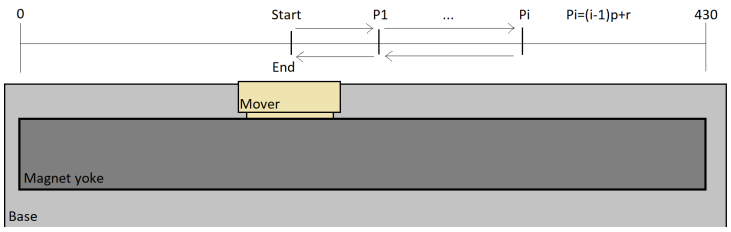

Figure 3.7: Schematic overview of the measurement set-up. Measuring accuracy and repeatability according to ISO230-2

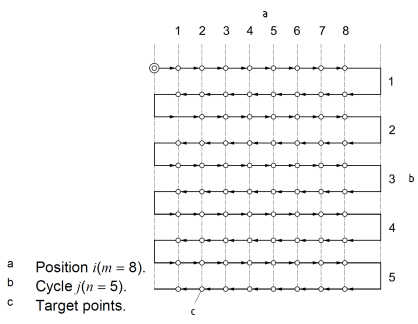

Figure 3.8: Schematic overview of the test procedure according to to ISO230-2[11]

3.4.3. Motor stiffness and bandwidth

Motivation To achieve a certain level of accuracy, the stiffness of a system is a very important property. A system with a high stiffness will deform less in response to an applied force and in most cases that is a benefit for a precision system.[44] When disturbing forces ($F_{disturbance}$) are known, the required stiffness (k_{total}) to achieve a maximum position error x_{max} under these circumstances can be calculated using equation 3.3

$$k_{total} \geq \frac{F_{disturbance}}{x_{max}} \tag{3.3}$$

k_{total} contains both structure stiffness k_s and motor stiffness k_m. When the motor stiffness is known, the position deviation as a result of a disturbance force can be predicted. The higher the motor stiffness, the lower the position deviation at equal disturbance forces.

Bandwidth is an often used term in relation to the complementary sensitivity and the unity-gain cross-over frequency as above this frequency the loop gain becomes smaller than one and consequently the feedback controller becomes no longer effective.[44]

What to measure The motor stiffness follows from the proportional gain of the controller. The control scheme of the ELMO drive is shown in appendix E.1. Since gain of the position controller works trough the velocity control filter, the stiffness of the motor can be calculated by using equation 3.4

$$k_m = KP_p \cdot KP_v \cdot K_e \cdot K_{peak} \tag{3.4}$$

where k_m is motor stiffness $[\frac{\mathrm{N}}{\mathrm{mm}}]$, KP_p is position gain $[\frac{\mathrm{mm}}{\mathrm{s*mm}}]$, KP_v is velocity gain $[\frac{\mathrm{A_{peak}}}{\mathrm{count/s}}]$, K_e is encoder gain $[\frac{\mathrm{counts}}{\mathrm{mm}}]$ and K_{peak} is the motor constant $[\frac{\mathrm{N}}{\mathrm{A_{peak}}}]$.

The bandwidth the is frequency band where the power of the output signal of a system becomes less than -3 dB. This value can be derived from the Elmo application studio.

Method The proportional gain and integral gain of the position and velocity control filter are dependent on the gain margin and phase margin required for the application. To uncouple the achievable motor stiffness and bandwidth from the ability of the user to tune the controller, a fixed gain margin and phase margin is specified. The measurement procedure will be as follows:

- Reset the controller
- Perform a system identification on a fixed position (120 mm)
- Let the software automatically design a PID controller with 50 deg phase margin and 10 dB gain margin
- Manually adjust the acceleration feed forward by a motion move from 100 mm to 300 mm with a 1 g 1 m/s move until the position error is minimized
- Reload the plant from the system identification
- Manually adjust the PID controller until either the 50 deg phase margin or the 10 dB gain margin is exceeded
- Read out the bandwidth and controller gain

3.4.4. Dynamic position error

Motivation Positioning error during the printing process may lead to material deposition at undesirable places. These errors are not covered by the accuracy and repeatability tests, as the definition of these tests is to position and rest long enough for the actual position to be reached. The dynamic performance of a servo control system is therefore evaluated by indicators measuring how closely the objective reference signal is tracked, which is commonly based on the magnitude of the root-mean-square (RMS) tracking error over the profile. For point-to-point tracking (i.e. step change in reference signal), classical performance indicators can be used, including the overshoot, settling time and steady state error.[30] Overshoot is the occurrence of a signal or function exceeding its target. Settling time is the time required for the response curve to reach and stay within a range of certain percentage of the final value.

What to measure The root mean square error and maximum absolute error is measured directly using the current position and position setpoint. The overshoot is measured by taking the current position and observe to what extend it overshoots the setpoint. The settling time is measured by defining an error band, and evaluate the time it takes to enter this window.

Method The error, overshoot and settling time strongly depend on the amount of proportional gain and integral gain of the position and velocity control filter. These are on their own dependent of the gain margin and phase margin required for the application. To uncouple the measurement from the ability of the user to tune the controller, a fixed gain margin and phase margin is specified. The tuning procedure will be the same as stated in the motor stiffness and bandwidth section (see 3.4.3).

During this measurement a series of long and short stroke motions are generated. The measurement is shown in figure 3.9. The following moves will be executed:

- 60 mm to 70 mm @250 mm/s and 1 g
- 60 mm to 70 mm @250 mm/s and 3 g
- 60 mm to 360 mm @250 mm/s and 1 g
- 60 mm to 360 mm @250 mm/s and 3 g
- 60 mm to 360 mm @1000 mm/s and 1 g
- 60 mm to 360 mm @1000 mm/s and 3 g

During these movements the target position (setpoint) and current position (feedback encoder) are recorded. These measurements are repeated for a position setpoint that is shifted 10 mm with respect to the setpoints as stated above to get rid of any periodic effects.

The RMS error and maximum absolute error are measured over the entire range. The overshoot and settling time are measured on the 300 mm, 1 m/s, 1 g step. The position must fall within a ± 10 μm band of the target position.

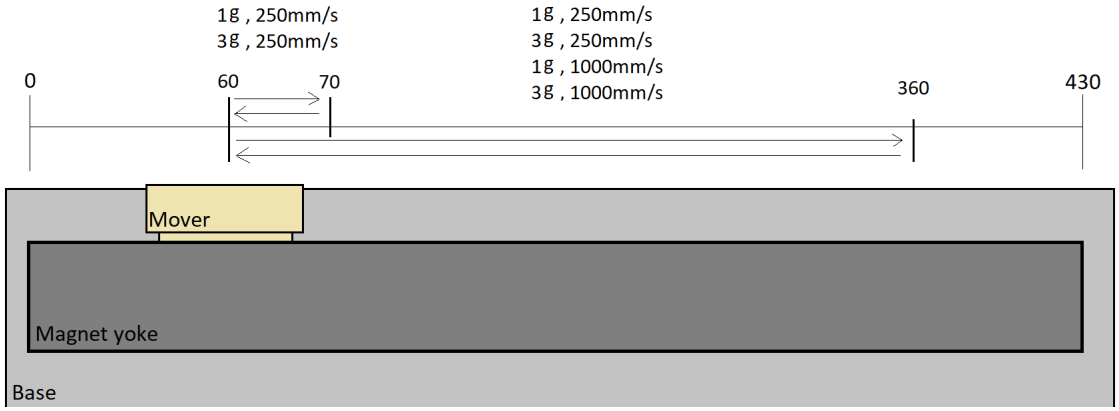

Figure 3.9: Schematic overview of the measurement. The RMS error, maximum absolute error, overshoot and settling time can be determined using this measurement.

3.4.5. Error due to thermal expansion

Motivation Thermal analyses of machine tools and their environment are significant to facilitate their accuracy specifications. Traditional machine tools require a warm up period which has the machine powered and moving in order to reach thermal equilibrium. As the machine warms up, the motors, guideways, bearings, etc. heat up and expand which causes positioning errors.[15] The positioning system in the new Ultimaker 3D printer will be built on top of a heated chamber with varying temperatures. Therefore, it is important to carry out an extensive research regarding thermal behaviour of the motion system.

What to measure The position of the Heidenhain encoder and the position of the evaluated encoder has to be measured. Since the coefficient of thermal expansion of the Heidenhain sensor is known, the expansion of the evaluated encoder at different temperatures can be related to the Heidenhain encoder.

Method During this measurement the mover starts at 0 mm and mover so the end of the encoder track, with low speed (10 mm/s) and low acceleration (0.1 g) to get rid of any stiffness, damping and rotational effects. The position of the evaluated encoder is plotted against the position of the Heidenhain encoder. A position error follows from this measurement. The RMS error is noted along with a maximum absolute error, both at room temperature (20°C) and at 40°C.

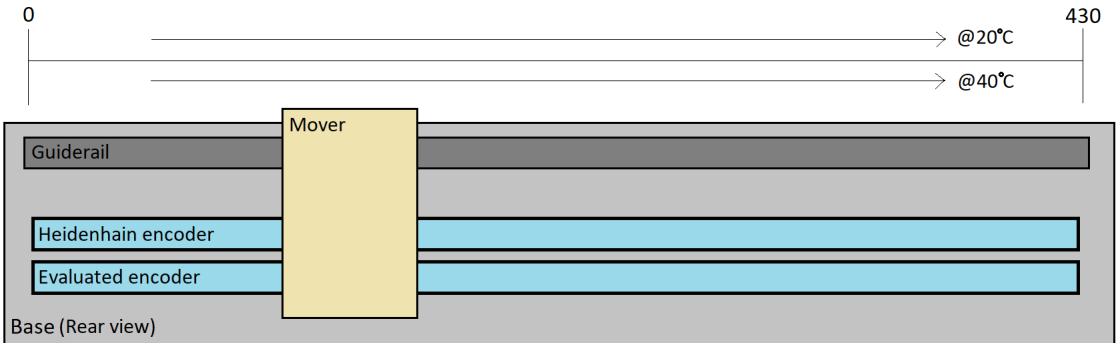

Figure 3.10: Schematic overview of the measurement, determining the thermal error

3.5. Conclusion

A single-axis experimental set-up is created to evaluate the effect of various motor configurations, encoders, guides and controllers on the performance of the positioning system. Also a series of measurements were created, which ensures that the evaluation of the different components can be carried out in a systematic way.

4

Motor configuration

4.1. Introduction

As the linear drive is a costly part of the positioning system, large expenses can be saved by reducing the costs of this subsystem. In this chapter cost optimization of the linear motor is explored. From the literature study it is concluded that a flat, linear, synchronous, ironless motor is most suited for application in an Ultimaker 3D printer. It is however, still the question if a single sided, double sided or semi double sided topology is optimal for this specific application.

In a recent study between different ironless motors Chevailler et al. [43] compare the maximum force per surface unit of four different motor configurations, shown in figure 4.1. These four motor configurations consist of a double sided, a semi-double sided, a singe sided and a Hallbach array single sided magnet configuration. It is predicted that a semi-double sided configuration will generate 69% of the force per surface unit when compared to a double sided magnet configuration. For a singe sided configuration this is 43% and for the Hallbach array single sided configuration this is 79%. This study shows that a reasonable amount of force can be generated with a linear motor, which is built with half of the magnetic material as the normal, double sided, configuration.

The downside of this study is that the generated force by the motor in each motor configuration is analytically determined and there is no proof of the method in practice. Celera Motion [33] applies the concept of a single sided linear ironless motor to their Javelin series, but the difference in dimensions between the single and double sided motors makes it impossible to compare the two.

Apart from the generated force in the motor, the weight of the moving axis also plays a large role in the consideration of the motor configuration. Reducing the amount of yoke material reduces the weight of the axis, lowering the force needed per unit of acceleration. An overview of the weight of a single axis and the force needed for 1 g acceleration is provided in table 4.1. A distinction has been made between the x-axis and y-axis. As shown in figure 4.2, in a typical gantry configuration, the y-axis consists of two motors which are stationary, whereas the x-axis consist of one motor which is mobile.

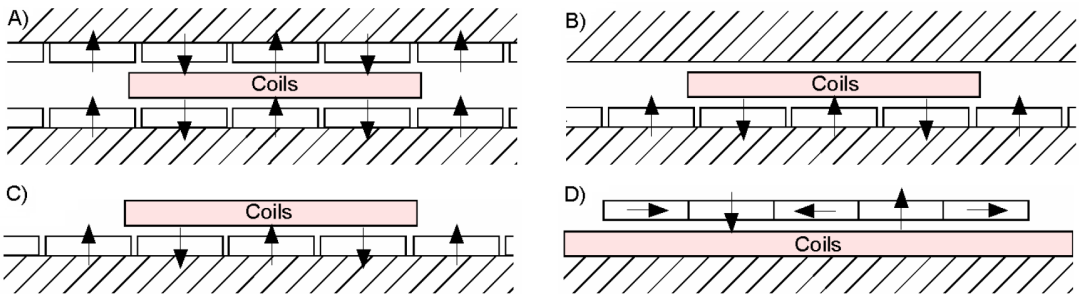

Figure 4.1: Ironless motor variants. A: Double sided, B: Semi-double sided, C: Single sided, D: Hallbach array single sided

Robustness and safety can also be a point of concern in the consideration of motor configuration. In a single sided configuration, the magnet track is exposed and fringe fields may lead to situations where the user can hurt itself or damage the motor. Some encoder types are also sensitive to strong static magnetic fields. In a double sided and semi-double sided configuration the ferromagnetic yoke determines a low reluctance path for the flux and at the same time it puts the exposed magnets out of the user's reach.

Contact has been made with Tecnotion, a Dutch supplier of linear motors. Tecnotion can offer a single sided, double sided and semi-double sided configuration. For a 2DOF, 3 axis system and in ordering quantities of 10K pieces per year, the standard UF double sided configuration will cost €830, the semi-double sided configuration will cost €550 and the single sided configuration will cost €380 (prices are subjected to changes). A cost overview is provided in table 4.2. The UC series of Tecnotion are smaller and 10% cheaper, however, they provide about half the force compared to the UF series. The three motor configurations that are offered by Tecnotion are analysed in this chapter.

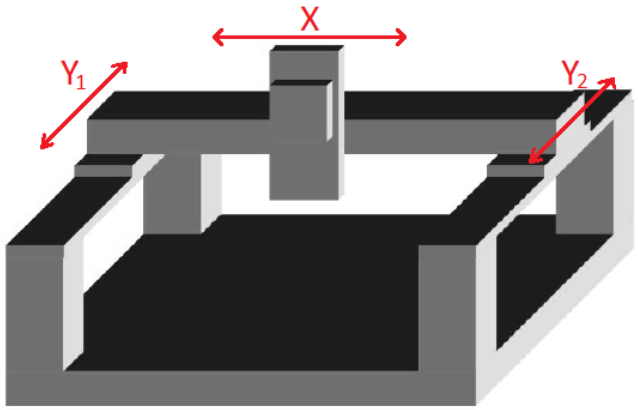

Figure 4.2: Configuration of a gantry positioning system. Freely adopted from [14]

Table 4.1: Weight and force overview motor configurations

		Double sided	Semi-double sided	Single sided
x-axis				
Printhead weight	[kg]	0.5	0.5	0.5
Mover + guide block weight	[kg]	0.2	0.2	0.2
Weight other components	[kg]	0.1	0.1	0.1
Needed force for 1 g in x-axis	[N]	8	8	8
y-axis				
Printhead weight	[kg]	0.5	0.5	0.5
Mover + guide block weight	[kg]	0.6	0.6	0.6
Guide rail weight	[kg]	0.4	0.4	0.4
Magnet section weight	[kg]	1.5	1.5	0.7
Weight other components	[kg]	0.4	0.4	0.4
Needed force for 1 g in y-axis	[N]	17	17	13

Table 4.2: Cost overview motor configurations (Based on a 2DOF, 3 axis system)

		Double sided	Double sided	Semi-double sided	Single sided
Order quantity	[pcs]	1	10000/year	10000/year	10000/year
Magnet section	[€]	12x 205	-	-	-
Coil unit	[€]	3x 332	-	-	-
Total	[€]	3456	830	550	380

4.2. Expectation

It is expected that the change from a double sided to a semi-double sided or single sided configuration affects the magnetic flux density of the magnetic field in the motor, which results in a change in motor force constant. The magnetic force on a wire in a magnetic field is given by equation 4.1

$$F = BIl_w \sin\alpha \tag{4.1}$$

Where B is flux density, I is current, l_w is wire length and α is angle relative to the direction of the magnetic field. In most practical cases the Lorentz force must be maximised, which means that sinα is kept as much as possible equal to one. The magnetomotive force of the permanent magnet creates a flux, proportional to the sum of the internal and external reluctance.[44] When the motor configuration is changed, the internal and external reluctance of the motor change, which directly influences the magnetic flux density B in the air-gap. When the magnetic flux density B decreases, the force F generated by the motor per unit of current I, called the motor constant K, decreases. Because the back EMF is related to the motor constant, the back EMF also decreases. Also expected is that the shape of the magnetic field is changed by removing one half of the magnet track of the motor, which might affect the force ripple.

Because the motor dimensions used in [43] differ from the dimensions of the Tecnotion motor, a COMSOL[7] simulation was made to predict the motor constant of the semi-double sided and single sided configurations. The COMSOL simulation can be found in appendix B. If the force per surface unit generated in the motor is assumed 100% using the double sided magnet configuration, the simulation predicts a motor having a semi-double sided configuration will generate 60% and a singe sided configuration 47% of the force.

4.3. Measurement set-up

The measurement set-up is shown in figure 4.3. Using this measurement set-up, the effect of using a double sided, semi-double sided and single sided motor configuration on the performance of the system is evaluated. None of the components are changed, except the motor configuration. A mass of 0.5 kg was attached to the mover during the tests to represent the weight of the printhead. The following components are used during this test:

- **Linear guideway block:** 2x HIWIN MGN12CZ0HM
- **Linear guideway rail:** HIWIN MGNR12R550HM
- **Reference encoder:** Heidenhain LIC 211
- **Servo drive and motion controller** Elmo G-DCBEL10/100EE

Apart from the standard PID controller, a low-pass filter is added with a cut-off frequency of 500 Hz (about three times the unity gain crossover frequency), limiting the differentiating action at frequencies where resonating mode shapes and sensor noise occur. Also, a notch filter is added at 140 Hz to create an anti-resonance at the eigenfrequency of the first eigenmode of the system.

The maximum acceleration and velocity test (see 3.4.1), motor stiffness and bandwidth test (see 3.4.3) and RMS error, maximum absolute error, overshoot and settling time test (see 3.4.4) are carried out using this measurement set-up.

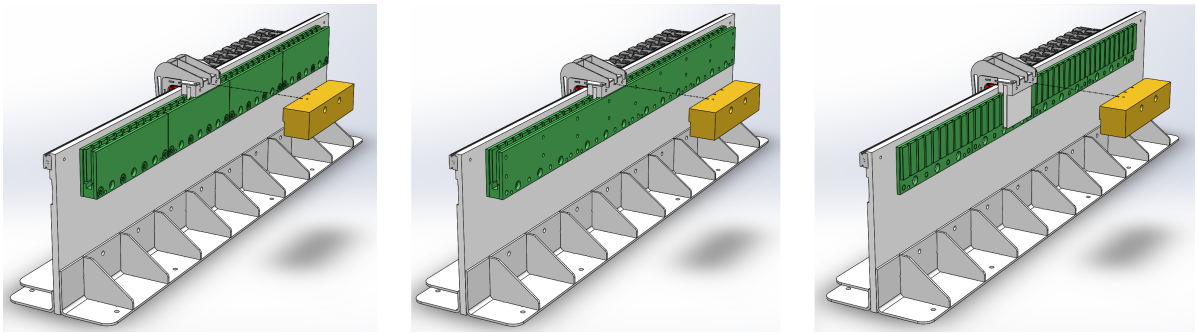

Figure 4.3: Schematic view of the experimental set-up evaluating the motor configuration. The magnet track and yoke are displayed in green. Left: Double sided configuration. Middle: Semi-double sided configuration. Right: Single sided configuration

4.4. Measurement results

The measurement results are shown in table 4.3. During the determination of the RMS error and absolute maximum error when a single sided motor configuration is used, the motor requires 5.8 A to realize a 3 g acceleration. Because this exceeds the peak current of the motor, the motor current starts clipping. This introduces a large position error because the motor cannot keep up with the desired position profile. For this reason, only the 1 g moves are used from the measurement profile to determine the RMS error and absolute maximum error.

Measurements results from the set-up show that the semi-double sided configuration has 54% of the motor force and the single sided configuration has 43% of the motor force with respect to the double sided configuration. This this corresponds to the results of the simulation in COMSOL, but does not correspond to the results from the study of Chevailler et al. This can be explained by the fact that the authors give little insight in the dimensions of their motor used to predict the motor force, but instead the authors give a range of dimensions which are used to model the motor force. In the range of dimensions, a motor exists that has a thinner coil unit than the motor of Tecnotion, which might explain the difference in motor force.
denMeasurements results from the set-up show that the semi-double sided configuration has 54% of the motor force and the single sided configuration has 43% of the motor force with respect to the double sided configuration. This this corresponds to the results of the simulation in COMSOL, but does not correspond to the results from the study of Chevailler et al. This can be explained by the fact that the authors give little insight in the dimensions of their motor used to predict the motor force, but instead the authors give a range of dimensions which are used to model the motor force. In the range of dimensions, a motor exists that has a thinner coil unit than the motor of Tecnotion, which might explain the difference in motor force.

The measurements show that all the motor configurations feature virtually the same stiffness, bandwidth and dynamic position error. Difference can be found in the continuous and maximum force the motor can generate. Both the semi-double sided and single sided configuration cannot reach continuous acceleration of 1 g in the y-axis. All the motor configurations can, however, reach 1 g peak acceleration. Assuming the required printing speed of 250 mm/s, the single sided configuration stays below its continuous acceleration limit of 6.7 m/s^2 when it repeatedly prints line segments larger than 12mm with an acceleration of 1 g (10 m/s^2).

From cost perspective, it would be beneficial to use a single sided configuration for both the x and y axes of the linear motor positioning system.

Table 4.3: Measurement results using different motor configurations

		Double sided	Semi-double sided	Single sided
Motor force constant	[N/A_{rms}]	12.7	6.9	5.5
Continuous(Peak) current	[A_{rms}]	1.58(3.5)	1.58(3.5)	1.58(3.5)
Continuous(Peak) acceleration x-axis	[m/s^2]	25(56)	14(30)	11(24)
Continuous(Peak) acceleration y-axis	[m/s^2]	12(26)	6.4(14)	6.7(15)
Maximum velocity	[m/s]	5.8	11	13
Price per peak force	[€/N_{peak}]	19	23	20
P-gain position	[N/mm]	24	22	21
P-loop Bandwidth	[Hz]	49	48	47
V-loop Bandwidth	[Hz]	91	93	95
RMS error (1 g moves)	[μm]	11	12	13
Maximum absolute error (1 g moves)	[μm]	69	82	80
Overshoot	[μm]	23	35	38
Settling time	[s]	0.08	0.06	0.09

5

Position sensor

5.1. Introduction

A sensor is needed for the commutation of the motor and to read out the position of the mover. Various types of sensors exist, all having their own performance characteristics like accuracy, repeatability and resolution. Various sensor types are mounted on the experimental set-up, in order to evaluate the impact of the different sensor types on the performance of the positioning system. In this way, the ideal sensor is chosen for the application in a linear motor positioning system for an Ultimaker 3D printer.

As concluded in section 2.5, several sensor types are eligible for use in the linear motor positioning system. Despite the fact that all sensors can be used for position determination, there are differences in performance and costs. To be able to compare the different sensor types, a selection of sensors has been made and can be found, along with a cost overview and specifications, in table 5.1. One optical encoder (Heidenhain), one magnetic hall encoder (RLS[40]) and one inductive encoder (POSIC[38]) is selected. The RLS and POSIC encoders are available in SMD versions, which are more economical for larger numbers.

A magnetic scale containing a series of magnetic poles is needed for the hall encoder to work. However, a magnetic scale is already available within the set-up, namely the linear motor itself. In an attempt to cut costs even further, effort has been made to develop a custom position sensor using Honeywell hall effect sensors[22], which can determine the position using the motors magnetic field. A cost overview can be found in table 5.1. Apart from the hall effect sensors, a pair of differential op-amps (LT1994[8]) were needed to correct the offset and gain of the sensors, such that it can be used on the sine/cosine input of the controller. A circuit diagram of this sensor, along with a simulation of the circuit can be found in appendix C.1.3.

Table 5.1: Cost overview and specifications of different sensor types (Based on a 2DOF, 3 axis system)

		Optical Heidenhain LIC211	Hall effect RLS RLC2IC	Inductive POSIC ID1102L	Hall effect RLS RLC2HD	Inductive POSIC ID4501C	Hall effect Honeywell SS496A1
Order quantity	[pcs]	1	1	1	10000	10000	250
Scanning unit	[€]	3x350	3x47	3x68	3x15	3x12	12x2
Scale	[€]	3x117	3x24	3x30	33	~27	-
Op-amps	[€]	-	-	-	-	-	6x3
Total	[€]	1401	213	294	78	~63	42
Resolution	[μm]	0.05	1	0.6	1	0.6	1.5
Maximum speed	[m/s]	10	3.7	2	3.7	2	-
Accuracy	[$\pm\mu$m]	15	10/m	-	10/m	-	-

5.2. Expectation

Based on the specifications of the sensors, it is expected that the Heidenhain optical encoder will yield the highest accuracy, followed by the RLS Hall effect encoder and finally the POSIC inductive encoder. Because of the diversity in calculation time and resolution of the sensors, a difference in position error during movement is also expected.

A downside of Hall effect encoders is that strong static magnetic fields may saturate the sensing elements or damage the magnetic scale. For the RLS encoder, the maximum magnetic flux density for safe operation is 50 mT. In appendix C.3 the 50 mT contour lines are shown for a single sided and semi-double sided configuration. It is important that the sensor and scale stay out of these 50 mT field lines.

It is expected that the performance of the Honeywell hall effect sensors will be less than the other three sensors. The other sensors provide position information by means of a digital output format, making the position read out resistant to small EMI on the wires. PCB level encoders also often contain lookup tables, in which sensor imperfections are corrected for. The Honeywell sensors do not contain these kind of lookup tables, however, they can be added by means of an intermediate data processing step. The Elmo drive features sensor calibration functions for the sin/cos input, in which signal amplitude mismatch, signal phase shifts and signal offsets are corrected for. After these corrections, it is expected that the Honeywell position sensor will also perform reasonably well. Whether the accuracy and repeatability of this sensor meets the requirements of Ultimaker, is to be determined.

5.3. Measurement set-up

The measurement set-up is shown in figure 5.1. Using this set-up, the effect of different types of position sensors on the performance of the system is evaluated. Only the sensors are changed on the set-up during these measurements. The Heidenhain optical encoder is used as a reference during the measurements, which means that the accuracy and repeatability test cannot be executed with the Heidenhain sensor. This also means that the Heidenhain encoder position is assumed ideal during the accuracy and repeatability tests. The following components are used during this test:

- **Linear guideway block:** 2x HIWIN MGN12CZ0HM
- **Linear guideway rail:** HIWIN MGNR12R550HM
- **Reference encoder:** Heidenhain LIC 211
- **Linear motor:** Semi-double sided Tecnotion UF3, with a 0.5 kg mass attached tot the mover
- **Servo drive and motion controller** Elmo G-DCBEL10/100EE

The accuracy and repeatability test (see 3.4.2), motor stiffness and bandwidth test (see 3.4.3), the RMS error, maximum absolute error, overshoot and settling time test (see 3.4.4) and the thermal error test (see 3.4.5) are carried out using this measurement set-up.

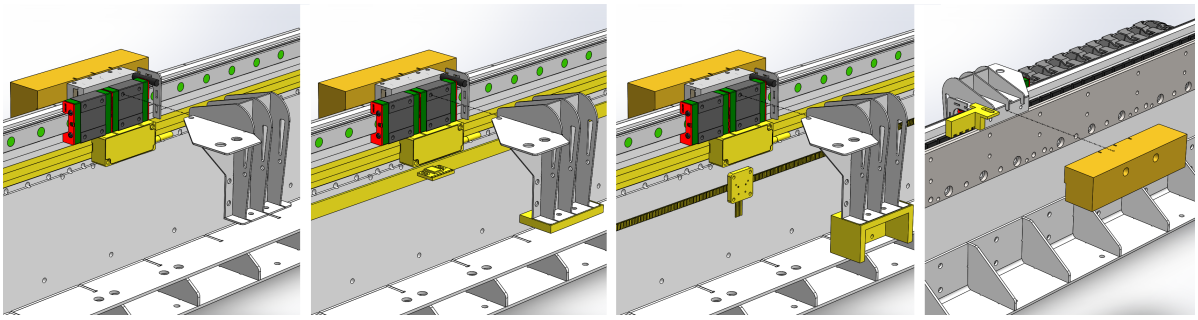

Figure 5.1: Schematic view of the experimental set-up evaluating different sensor types. Sensors and scales are displayed in yellow. From left to right: Heidenhain LIC211, RLS RLC2IC, POSIC ID1102L and Honeywell SS496A1

Apart from these tests, several measures are taken in order to calibrate the sensors. The sensors are corrected for gain errors and errors resulting from time delay. For the POSIC inductive encoder, a lookup table is used to linearise the sensor signal. The Honeywell hall effect sensor is equipped with op-amps that also act as active low-pass filters with a cut-off frequency of 1.8kHz, filtering out the electro magnetic noise from the motor to the sensor signal. More information about the steps taken to calibrate the sensors and the measurements before and after calibration can be found in appendix C.1.

5.4. Measurement results

The measurement results are shown in table 5.2. For comparison, a 550mm scale (MS05) of the RLS sensor has a specified accuracy of ± 6 μm. The results of the thermal error test are shown in appendix C.2. It is shown that the POSIC inductive encoder is sensitive for temperature deviations. The periodic error of this encoder changes at higher temperatures, making it hard to calibrate and compensate for these errors. The RLS Hall effect encoder is less sensitive for temperature deviations.

The performance of the Honeywell position sensor is less than required. Periodic errors of ± 75 μm are visible and are likely to be caused by variations in strength and positioning of the magnets from the linear motor. Appendix C.1.3 shows the periodic errors of the Honeywell encoder and the variation in magnetic field strength of the magnets.

It can be concluded that the choice of sensor type affects the accuracy and repeatability of the system. The accuracy and repeatability of the Heidenhain encoder is not measured because this sensor is used as a reference. The RLS Hall effect encoder can reach an accuracy of 14 μm and a repeatability of 2.8 μm. The POSIC inductive encoder can reach an accuracy of 11 μm and a repeatability of 1.3 μm. The POSIC sensor is very sensitive to temperature changes and deviations in scale distance. The RLS sensor is preferred for this reason, even though the POSIC sensor has better accuracy and repeatability than the RLS sensor. The RLS sensor needs to be mounted in such a way that it is not exposed to magnetic field densities higher than 50 mT. The choice of sensor type only has minor effect on the motor stiffness, bandwidth and dynamic position error.

Using a custom build position sensor has proven to be difficult. Noise on the sensor wires quickly lead to positional deviations of a few micrometers. Even after sensor calibration in the Elmo drive, an accuracy of 110 μm is maximum achievable. Combining the low accuracy with the RMS error of 69 μm at room temperature, this custom built position sensor can be considered unsuitable for position feedback in the Ultimaker 3D printer.

Table 5.2: Measurement results using different sensor types

		Heidenhain LIC211	RLS RLC2IC	POSIC ID1102L	Honeywell SS496A1
Accuracy	[μm]	-	14	11	110
Repeatability	[μm]	-	2.8	1.3	13
Reversal value	[μm]	-	2.1	0.9	4.4
Positional deviation	[μm]	-	12	10	99
P-gain position	[N/mm]	22	25	18	16
P-loop Bandwidth	[Hz]	48	49	45	38
V-loop Bandwidth	[Hz]	93	96	83	57
RMS error	[μm]	18	12	18	-
Maximum absolute error	[mm]	0.14	0.10	0.16	-
Overshoot	[μm]	35	25	35	-
Settling time	[s]	0.06	0.07	0.09	-
RMS error @20°C	[μm]	-	5.0	9.9	69
RMS error @38°C	[μm]	-	5.6	21	-
Coefficient of expansion	[10^{-6}/K]	10	12	13	-

6

Linear guide

6.1. Introduction

A guide constrains the motion to the desired direction. It is the main component that determines the trajectory accuracy, stiffness and load capacity. The trajectory accuracy is characterized by the straightness, flatness, or maximum angular deviations required for the application. To some extent, guide stiffness in directions perpendicular to the motion is also related to trajectory accuracy, but it is also a large contributor to dynamics and thus has some impact on axial accuracy and stability. Of course, these considerations of trajectory and stability are taken into account not only on the guiding mechanism itself but also on the support and structure that holds it.[4] Because of the large contribution of the guiding system to the accuracy and stiffness of the linear motor positioning system, the effect of using different number of guide blocks is investigated in this chapter.

The number of guide blocks on the guide rails used in an application has an influence on the system characteristics of the linear guide. The number of guide blocks installed also makes certain demands on the overall machine design, e.g. the required accuracy of the mounting bases and mating surfaces.[2] For these reasons, this chapter answers the question if a single or double guide block configuration is preferred in the case of a linear motor positioning system. Linear recirculating ball bearings of HIWINs MGN series are used for this evaluation. A cost overview is presented in table 6.1.

6.2. Expectation

First of all, an estimation for the sensor displacement as a result of an applied motor force has to be made. This sensor displacements is dominated by the yaw stiffness of the bearing, which is not given in the data sheet of the manufacturer. The derivation of the yaw stiffness and the displacement of the sensor as a result of a force applied by the motor can be found Appendix D. Assuming that the accelerated mass is placed in the bearings center of rotation, a 1N motor force will lead to a position error of 0.2 μm between the reference and evaluated encoder. Because the yaw stiffness of the bearing is high enough to prevent large sensor errors due to rotational effects (Abbe errors), it is expected that the increase of yaw stiffness by addition of an extra guide block will not be of great influence. Because a single guide block has less contact area with the guide rail, it is also expected that a singe guide block will provide less friction and thus smoother motion. The single guide block is expected to be preferable for the application of an Ultimaker 3D printer.

Table 6.1: Cost overview number of guide blocks (Based on a 2DOF, 3 axis system)

		Single guide block	Double guide block
Order quantity (3 axis system)	[pcs]	1	1
Guide block (HIWIN MGN12CZ0HM)	[€]	3x23	6x23
Rail (HIWIN MGNR12R550HM)	[€]	3x66	3x66
Total	[€]	267	336

6.3. Measurement set-up

The measurement set-up is shown in figure 6.1. This set-up is used to evaluate the effect of using one or two guide blocks on the performance of the system. Only the guide blocks are changed on the set-up during these measurements. Noted should be that the two guide blocks must be perfectly aligned in the direction of motion, to prevent the guide blocks from clamping on the rails. The following components are used during this test:

- **Linear guideway rail:** HIWIN MGNR12R550HM
- **Reference encoder:** Heidenhain LIC 211
- **Evaluated encoder:** RLS RLC2IC
- **Linear motor:** Semi-double sided Tecnotion UF3, with a 0.5 kg mass attached tot the mover
- **Servo drive and motion controller** Elmo G-DCBEL10/100EE

The accuracy and repeatability test (see 3.4.2), motor stiffness and bandwidth test (see 3.4.3) and the RMS error, maximum absolute error, overshoot and settling time test (see 3.4.4) are carried out using this measurement set-up.

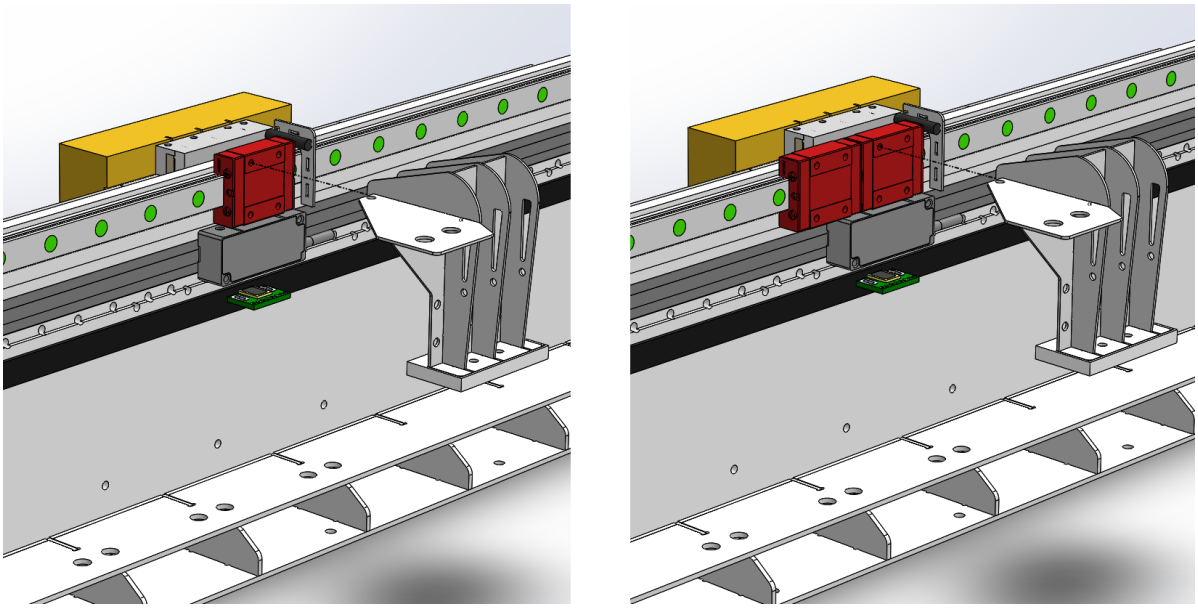

Figure 6.1: Schematic view of the experimental set-up evaluating the number of guide blocks. Guide blocks are displayed in red. Left: one guide block. Right: two guide blocks

6.4. Measurement results

The measurement results are shown in table 6.2. The first eigenmode of the system using two guide blocks is located at 120 Hz. After equipping the mover with accelerometers, it is concluded that this eigenmode is a yaw mode with a node in the centre of the attached mass. When two guide blocks are used, the frequency of the first eigenmodes shifts to 140 Hz. For this reason, the notch filter is placed at 120Hz when a single guide block is used and at 140 Hz when two guide blocks are used.

Measurements show that there is a slight performance gain of the positioning system when two guide blocks are used instead of one. A decrease in dynamic position error is noticeable, the RMS error, maximum absolute error, overshoot and settling time all decrease when two guide blocks are used. The accuracy and repeatability stay virtually the same when two guide blocks are used instead of one. Concluded can be that the gain in stiffness outweighs the extra friction introduced by an extra guide block. Because of the increase in performance, and because the guide blocks are relatively inexpensive compared to the rails, the double guide block is preferable in this specific application.

Table 6.2: Measurement results using different number of guide blocks

		Single guide block	Double guide block
Accuracy	[μm]	14	14
Repeatability	[μm]	2.6	2.8
Reversal value	[μm]	1.9	2.1
Positional deviation	[μm]	12	12
P-gain position	[N/mm]	19	25
P-loop Bandwidth	[Hz]	45	49
V-loop Bandwidth	[Hz]	74	96
Lowest resonance frequency	[Hz]	120	140
RMS error	[μm]	16	12
Maximum absolute error	[mm]	0.15	0.10
Overshoot	[μm]	41	25
Settling time	[s]	0.09	0.07

7 Controller

7.1. Introduction

A control system is used to enable the positioning system to perform according to the prescribed specifications. Many different controllers are available on the market. They are distinguished by communication interfaces, feedback interfaces, user interfaces, control strategies and hardware components. Which of these functions are needed for a controller in an Ultimaker 3D printer and what effect these functions have on the performance of the motion system, is investigated in this chapter.

The Elmo drive that is used in the reference set-up is an industrial grade controller that features an user-friendly GUI and different type of connections for feedback encoders. For a prototype set-up where multiple encoders need to be tested, these functions are very useful. However, for implementation in an end product, these functions are no longer necessary and cause an unwanted increase in the bill of materials. There are industrial grade controllers available that support only one sensor connection, no GUI and have only PID control functions. The downside of these controllers is that the software is closed off and no adjustments can be made to improve the controller. Since Ultimaker has a history in developing motion planners, building their own motion controller might be feasible. The ODrive controller[41] is an open source controller, both in hardware and software, which means that the controller can be adjusted to the needs of Ultimaker. If the control strategies from the ODrive are sufficient to control the motion system without noticing difference in performance, the ODrive will be a more economical solution for the linear motor positioning system. If control strategies are missing, they can be built into the ODrive because of the open-source software. A cost overview along with specifications is provided in table 7.1. Note that the components on the ODrive, when ordered in a quantity of 5000 pieces, will cost around €60 for a 2DOF, 3 axis system.

Table 7.1: Cost overview and specifications of the different controllers (Based on a 2DOF, 3 axis system)

		Elmo Gold DC Bell 10/100EE	ODrive V3.5 48V
Order quantity	[pcs]	1	1
Servo drive	[€]	3x1115	2x130
Total	[€]	3345	~260
Maximum supply voltage	[VDC]	95	48
Continuous current	[A]	10	40
Communication interfaces		USB, Step&Dir, PWM, CAN, RS-232, EtherCAT, TCP/IP	USB, Step&Dir, PWM, CAN, UART
Feedback interfaces		Quadrature, Sine/Cosine, Digital hall Pulse&Dir, Absolute serial	Quadrature, Sine/Cosine
Control functions		PID, Cogging compensation, Advanced filtering, Peak current limit Gains&Filter scheduling vs. position	PID, Cogging compensation

Both the Elmo and the ODrive are single axis controllers. During a 3D print, circular movements are common and the position commands are cut into small line segments. When the build-in trajectory control of the drives are used for control, the print head will stop at each end of a small line segment. Therefore, it is unfavourable to use the build in motion planner of the drives and both the controllers will need a master to synchronize the motions of the x and y-axis when implemented in a 3D printer. Elmo offers a master controller, ODrive robotics does not. Within Ultimaker, a motion planner is in development which eventually will be able to control multiple drives. A pulse and direction or CAN interface is sufficient for communication between a master and the controllers. Both the Elmo as the ODrive feature these communication interfaces.

7.2. Expectation

There are many differences between the two motion controllers. The Elmo drive has several advantages. Where the ODrive uses Python for communication, the Elmo comes with an extensive software package. The configuration time of the ODrive controller during the prototyping phase might take longer because of the lack of a GUI, but the performance will not suffer from this. The Elmo also features advanced filters, such as a notch and a low-pass filter. During the tests from the previous chapters it became clear that eigenmodes of the positioning system are excited and cannot be controlled because they are outside of the bandwidth of the controller. These unwanted vibrations may be excited when using the ODrive, because of the absence of a notch filter. Finally, the Elmo has a build-in option to adjust the sensor signal and control parameters by position, such as error mapping and gain scheduling.

When using a linear motor positioning system, the linearity of the mechanical system makes sure that most of the gain and filter scheduling functions are not needed. Some functions depend on the performance of the feedback encoder and the stiffness of the frame, such as error mapping. Apart from the just mentioned functions, the Elmo drive is just a PID controller, as the ODrive is. The control schemes of the Elmo drive and the ODrive are shown in appendix E. If the feedback sensor can be positioned at the location of the end-effector, the PID controller will ensure that the setpoint is reached by the end-effector, making the accuracy and repeatability of the system only depended on the sensor characteristics. Altogether, it is expected that the use of the ODrive instead of the Elmo controller will not have a noticeable effect on the performance of positioning system.

7.3. Measurement setup

The measurement set-up is shown in figure 7.1. This measurement set-up is used to compare the performance of the positioning system using the two different controllers. Also, the effect of error mapping techniques on the accuracy and repeatability of the system is investigated. Error mapping enables the controller to compensate for encoder errors by creating a lookup table using the reference encoder. The following components are used during this test:

- **Linear guideway block:** 2x HIWIN MGN12CZ0HM
- **Linear guideway rail:** HIWIN MGNR12R550HM
- **Evaluated encoder:** RLS RLC2IC
- **Reference encoder:** Heidenhain LIC 211
- **Linear motor:** Semi-double sided Tecnotion UF3, with a 0.5 kg mass attached tot the mover

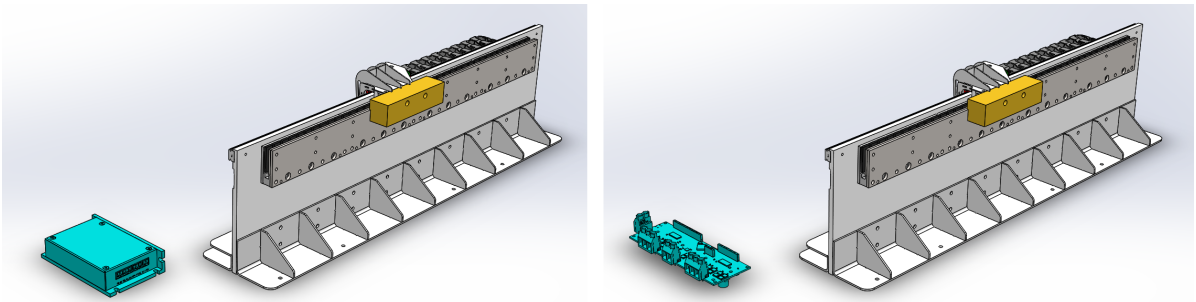

Figure 7.1: Schematic view of the experimental setup evaluating two different controllers. Controllers are displayed in blue. On the left: Elmo Gold DC Bell. On the right: ODrive V3.5 48V.

The accuracy and repeatability test (see 3.4.2) is carried out with the ODrive and the Elmo controller, with and without the error mapping function enabled. The RMS error, maximum absolute error, overshoot and settling time test (see 3.4.4) is carried out for the ODrive and the Elmo with disabled error mapping. The maximum velocity is the theoretical value calculated using the supply voltage of the controller to the motor. The proportional gain is set in the controllers.

7.4. Measurement results

The measurement results are shown in table 7.2. The sensor error of the Elmo controller, before and after error mapping is shown in appendix E. The response of the system to a 300 mm step, for both the Elmo drive as the ODrive, is also shown in appendix E.

From the measurements it can be concluded that the error mapping improves the accuracy of the system significantly, reducing from 15 μm to 7.3 μm. The error mapping from the Elmo drive uses a correction table through which the sensor signal is corrected. It is believed that the same error mapping technique can be implemented in the ODrive.

Also concluded can be that the ODrive is a promising controller for the linear motor positioning system. Before the ODrive is eligible as controller for implementation in a final product, there are few essential functions which are needed to be built in and tested. One of these functions is the acceleration feed-forward, which is essential when the error during motion needs to be minimized. The acceleration feed-forward is available in the trajectory control mode, but lacks when a step and direction input is used. Another very useful function that the ODrive lacks is a peak current limitation. Since a semi-double sided or single sided motor configuration is not capable of producing 1 g accelerations with continuous current, the controller must allow for the violation of the maximum continuous current level of the motor to reach 1 g peak accelerations. Finally, a notch filter has proven to be an important addition to the control loop to reduce eigenfrequencies from the positioning system. During the measurements in the previous chapters the Elmo drive excited the first eigenmode of the system several times, causing positional deviations around the setpoint and undesirable noise from the system. Because the ODrive offers open source software, it is believed that the implementation of these functions can be done relatively quickly, making the reduction in cost of the control system outweigh the effort of adjusting the firmware.

Table 7.2: Measurement results using different controllers

		Elmo (Error mapping enabled)	Elmo (Error mapping disabled)	ODrive
Motor force constant	[N/A_{rms}]	6.9	6.9	6.9
Maximum velocity	[m/s]	11	11	8.5
Accuracy	[μm]	7.3	15	14
Repeatability	[μm]	4.1	3.9	4.1
Reversal value	[μm]	3.6	3.1	3.2
Positional deviation	[μm]	3.3	12	10
P-gain position	[N/mm]	25	25	25
Overshoot	[μm]	-	33	44
Settling time	[s]	-	0.09	0.11

8

Conclusion and Recommendations

8.1. Conclusion

The aim of this project is to demonstrate the feasibility of a low-cost linear motor motion system for use in a 3D printer. A single-axis experimental setup is realized to evaluate the effect of different drives, sensors, guides and controllers on the performance of the system.

Starting off with a literature study, it can be concluded that linear motors are not commonly implemented in commercial 3D printers. Linear motors are common in other type of positioning systems found in both commercial products as in research papers. All of these systems are either too expensive for implementation in an Ultimaker 3D printer or they lack data about the performance of the positioning system. Therefore, this thesis provides a new approach combining the cost optimization for a linear motor positioning system with the proof of performance through measurements.

On the single-axis experimental setup, three different motor configurations were compared. The measurement results show that the semi-double sided configuration produces 54% force and the single sided configuration produces 43% force compared to the double sided configuration. The measurements show that all the motor configurations feature virtually the same stiffness, bandwidth and dynamic position error. An acceleration of 1 g is required for the motion system. Both the semi-double sided and single sided configuration cannot reach continuous acceleration of 1 g in the y-axis. All the motor configurations can, however, reach 1 g peak acceleration. The single sided configuration stays below its continuous acceleration limit of 6.7 m/s^2 when it repeatedly moves 12mm with an acceleration of 1 g. From cost perspective, it would be beneficial to use a single sided configuration for both the x and y axes of the linear motor positioning system.

It can be concluded that the choice of sensor type affects the accuracy and repeatability of the system. The RLS Hall effect encoder can reach an accuracy of 14 μm and a repeatability of 2.8 μm. The POSIC inductive encoder can reach an accuracy of 11 μm and a repeatability of 1.3 μm. Even though the POSIC encoder has better accuracy and repeatability than the RLS encoder, it became clear that this encoder is very sensitive to temperature changes and deviations in scale distance. For this reason, the RLS encoder is preferred, A disadvantage of these Hall effect encoders is that they are sensitive to strong static magnetic fields, so it must be mounted out of range from magnetic field densities higher than 50 mT. The choice of sensor type only has minor effect on the motor stiffness, bandwidth and dynamic position error. Using a custom built position sensor has proven to be difficult. Even after sensor calibration in the Elmo drive, an accuracy of 110 μm is maximum achievable. Combining the low accuracy with the RMS error of 69 μm at room temperature, this custom build position sensor can be considered unsuitable for position feedback in the Ultimaker 3D printer.

Measurements show that there is a slight performance gain of the positioning system when two guide blocks are used instead of one. The frequency of the first eigenmode shifts from 120 Hz to 140 Hz when two guide blocks are used. A small decrease in dynamic position error is also noticeable. The accuracy and repeatability stay virtually the same when two guide blocks are used instead of one. Because of the increase in performance, and because the guide blocks are relatively inexpensive compared to the rails, the double guide block

is preferable in this specific application.

From the measurements it can be concluded that the error mapping improves the accuracy of the system significantly, reducing from 15 μm to 7.3 μm. It is believed that the same error mapping technique from the Elmo drive can be implemented in the ODrive and that therefore the ODrive can also reach an accuracy of 7.3 μm. Also concluded can be that the ODrive is a promising controller for the linear motor positioning system. The ODrive lacks some essential functions, like the acceleration feed-forward during a step and direction input, a peak current limitation and a notch filter. Because the ODrive offers open source software, it is believed that the implementation of these functions can be done relatively quickly, making the reduction in cost of the control system outweigh the effort of adjusting the firmware.

A linear motor positioning system that satisfies the requirements set by Ultimaker is feasible, as far as can be concluded from single axis experiments. In the final concept, a single sided Tecnotion linear motor is used combined with a RLS Hall effect encoder, HIWIN guiderail with two runner blocks and an O-drive controller. To answer the question if this linear motor system still outperforms a belt driven system, a comparison is made between this system and the closed-loop rotary servo 3D printer from the literature study. The rotary servo 3D printer can reach speeds of 280 mm/s and an static accuracy of $\pm$0.1 mm. The linear motor positioning system can reach speeds of 3.7 m/s with an static accuracy of 0.01 mm. It may thus be concluded that this linear motor positioning system still outperforms a conventional belt driven system.

The requirements of the motion system that were set by Ultimaker, along with the results of the final set-up can be found in table 8.1. A cost overview is provided in table 8.2. Even without taking into account the reduction in cost by ordering the guide system in large numbers, it is shown that the final setup can be realized for €854.

Table 8.1: Requirements for the motion system

	Unit	Requirements	Final set-up
Travel speed	m/s	2	3.7
Acceleration	m/s^2	10	15
Motion accuracy	μm	10	14
Motion repeatability	μm	10	4.1
Total cost (BOM)	€	1000	854

Table 8.2: Cost overview of the complete system (Based on a 2DOF, 3 axis system)

		Order quantity (pcs)	Initial setup	Final set-up
Linear motor (Double sided, 10K/y)	[€]	10k	830	-
Linear motor (Single sided, 10K/y)	[€]	10k	-	380
Encoder (Heidenhain)	[€]	1	1401	-
Encoder (RLS)	[€]	10k	-	78
Guide (Double runner block)	[€]	1	336	-
Guide (Single runner block)	[€]	1	-	336
Controller (Elmo)	[€]	1	3345	-
Controller (O-drive)	[€]	10k	-	60
Total	[€]	-	5912	854

8.2. Recommendations

This thesis demonstrates the feasibility of a linear motor motion system for use in a 3D printer in one single axis. The xy motion system for the Ultimaker 3D printer needs two degrees of freedom. Errors that are not visible in the single-axis setup, like the guide stiffness perpendicular to the direction of motion, can become suddenly visible in a 2DOF system. Also, the stiffness of the frame and housing, which are not included in the single-axis setup, become important in the 2DOF motion system. Ultimaker needs to continue this research until a final statement can be made about the feasibility of a 2DOF linear motor motion system in a 3D printer.

Regarding the linear drive, it might be useful to use a semi-double sided configuration for the y axis while keeping the light single sided configuration for the x axis. This adds the benefit of the extra motor force in the y axis and contributes to the safety and robustness of the system. The ferromagnetic yoke puts the exposed magnets out of the users reach. A print head will consist of ferromagnetic material increasing the cogging effects on the motor which are also less when the magnets are covered by a ferromagnetic yoke. It can also be examined if another coil unit might be better suited for this application. A coil unit with thinner an longer copper wires produces more force, but lowers the maximum speed of the motor. Because the maximum speed of the current motor is beyond the required speed, it might be useful to design such a custom coil unit. Tecnotion has indicated that such a motor can be built, which has a force constant of 11 N/A in a single sided magnet track configuration. Compared with the standard double sided UF03 motor having a force constant of 12.3 N/A, this seems a good solution to gain some extra motor force for the system. Expected is that the heat distribution within the coils adds thermal resistance to the system and therefore affects the maximum continuous current allowed in the motor. To what extend this custom motor actually improves the continuous and peak force of the motor, is an interesting topic for further research.

During this research only one type of ball bearing is used from the 'very light preload' class of HIWIN. The measurements showed that the gain in stiffness outweighs the extra friction introduced when two guide blocks are used instead of one. Because it seems that the extra friction does not affect the performance of the system, a ball bearing from the 'light preload' class might increase the performance of the system even further and shift the first (yaw) eigenmode to a higher frequency.

Taking into account all the production tolerances, sensor non-linearities and the fact that the motion system is built on top of a heated chamber, it might be inevitable to implement a calibration step in the production process, to meet the strict requirements of Ultimaker to the motion system. A calibration device, containing multiple reference encoders, can be used to perform a set of test movements. From there a lookup table can be generated to calibrate the position sensors that are mounted in the motion system of the printer. The ODrive does not yet contain an error mapping functionality. When the ODrive is chosen as controller for the motion system in the printer an error mapping function has to be written and tested.

The task for Ultimaker is to finish the stepper and belt drive h-bot motion system, which is planned for use in the new Ultimaker series. This system is cheaper than a linear motor motion system, however, as stated in the introduction, the performance of the h-bot system is expected to be worse than a linear motor system. When this system is finished, it can be checked whether the system is performing according to expectations. If this is not the case, Ultimaker can continue developing the linear motor system, which is proven in this thesis to perform according to the requirements.

A

Conceptual design

A.1. Solidworks simulations of the bracket

The coupling between the end effector and encoder has to be stiff enough to avoid position errors that cannot be measured and controlled. A SOLIDWORKS static deformation analysis is performed on the bracket, which couples the motor to the sensor. Because no end effector is installed on the set-up, the simulation assumes it to be at the bottom of the mover. In figure A.1 a displacement of 1 μm is shown as a result of a driving force of 10 N.

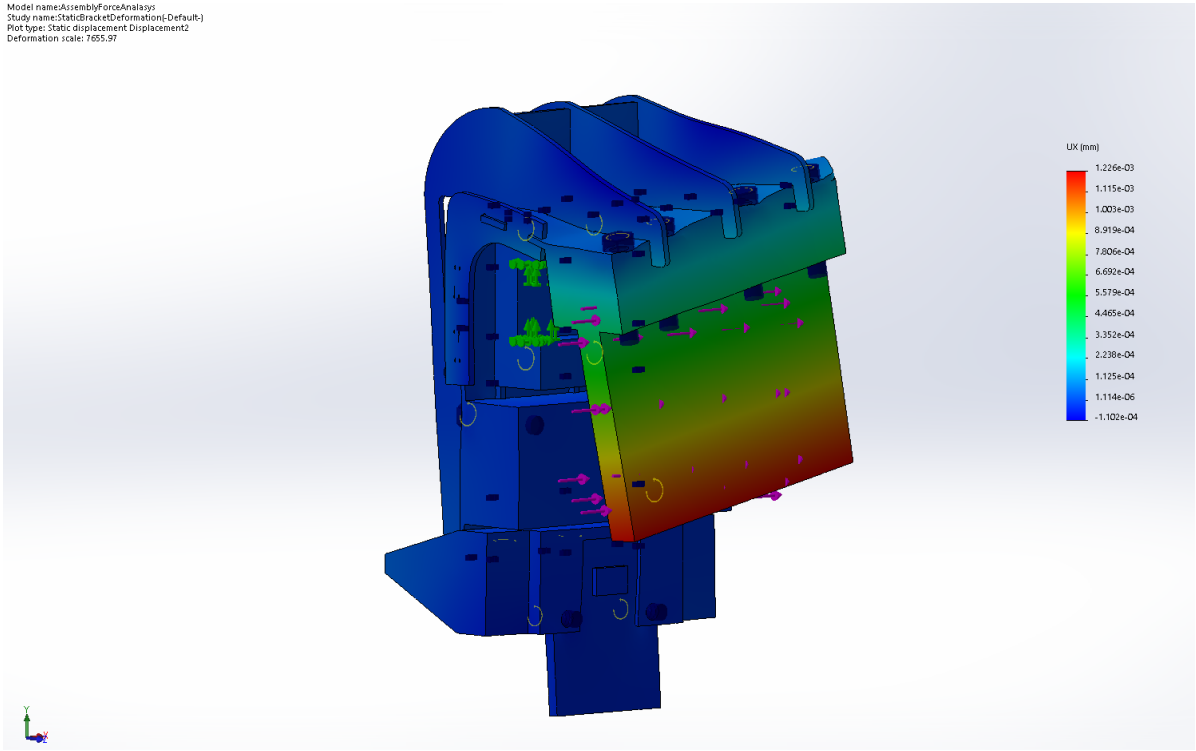

Figure A.1: Deformation of the bracket as a result of a 10 N driving force. Bracket in fixed on the bearing (green arrows), force is applied on the mover (pink arrows).

A.2. Position plant bode plot

A system identification is performed using the Elmo controller and Elmo Application studio. A semi-double sided magnet configuration is used, along with a double guiding block and the Heidenhain optical encoder. Figure A.2 shows the position plant magnitude and phase. A resonance frequency around 140 Hz is visible when two guide blocks are used.

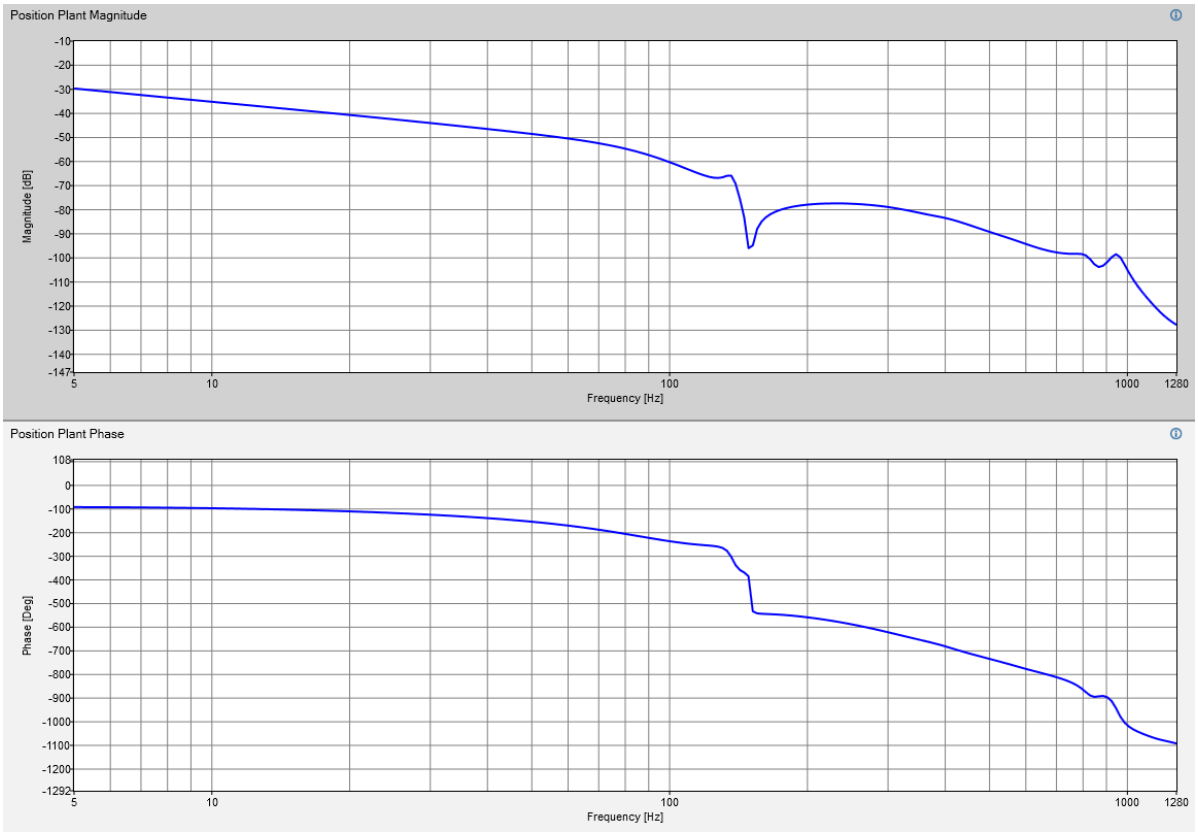

Figure A.2: Position plant bode plot of the linear motor. Obtained using the Elmo Application studio.

B

COMSOL model of motor configurations

This appendix shows the results of three simulations done in COMSOL. Three motor configurations are simulated, the double sided, semi-double sided and single sided magnet configurations. Each magnet is given a remanence of 1 Tesla. Displayed is the z component of magnetic flux density in the air gap at the center of the coils.

Concluded can be that the maximum flux density in the airgap at the hight of the coils is 0.53 for the double sided, 0.32 for the semi-double sided and 0.25 for the single sided magnet configuration.

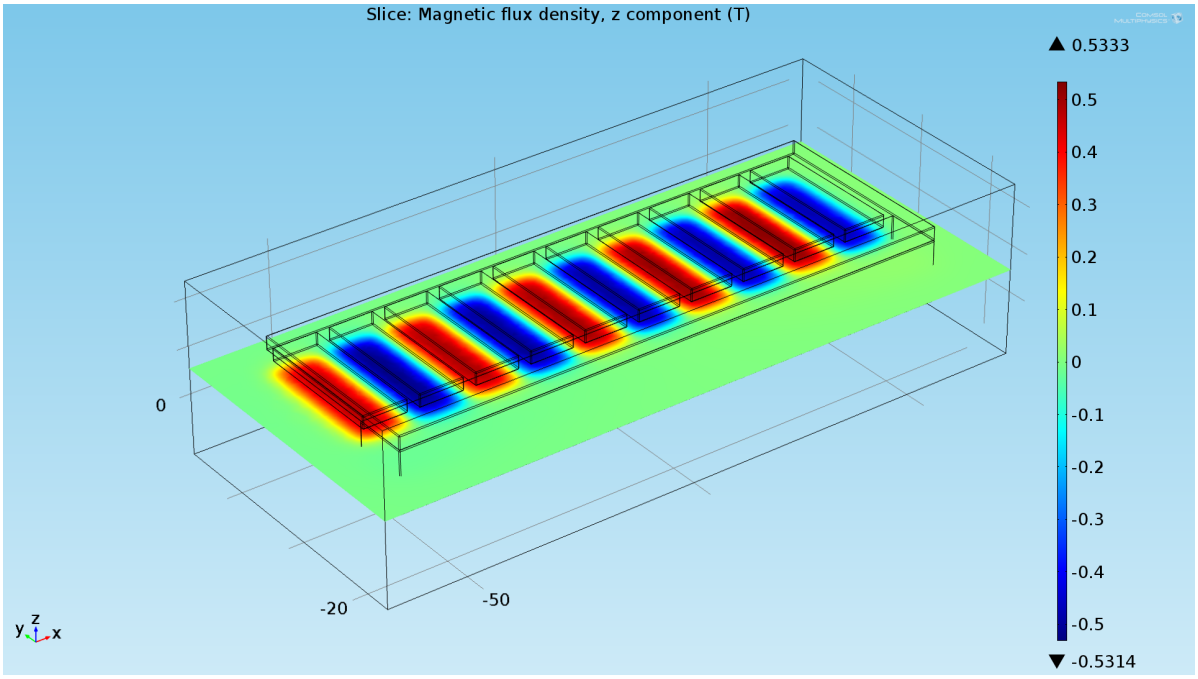

Figure B.1: Z-component of magnetic flux density. Simulated in COMSOL using double sided magnet configuration.

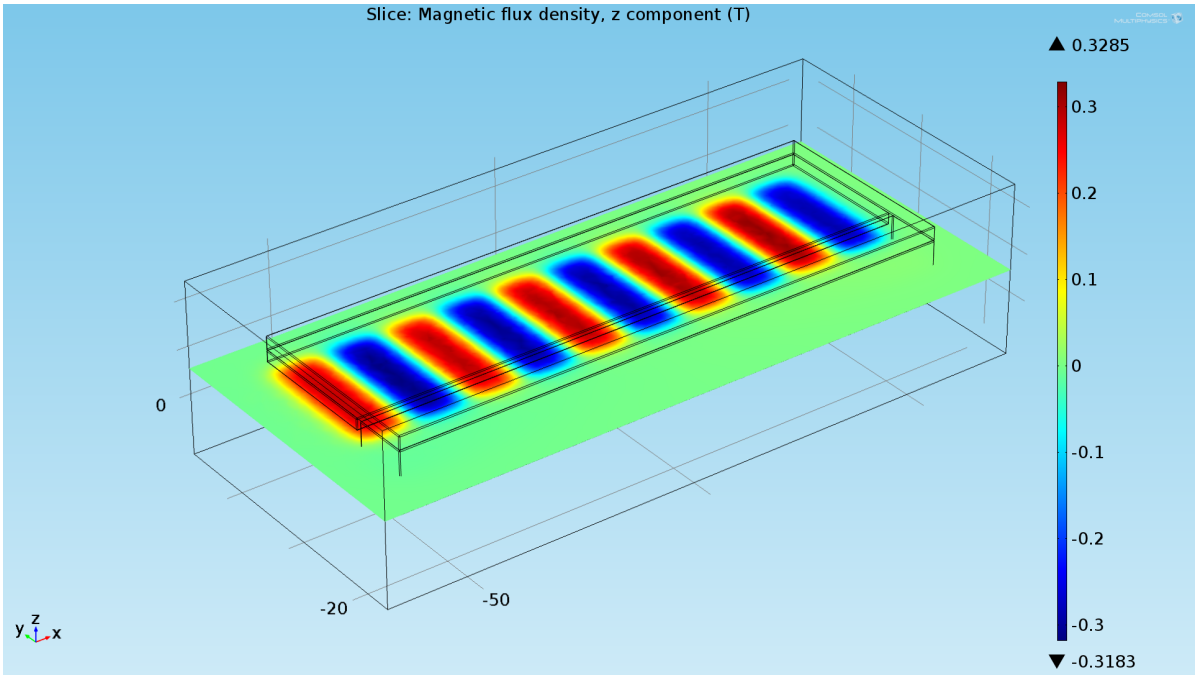

Figure B.2: Z-component of magnetic flux density. Simulated in COMSOL using semi-double sided magnet configuration.

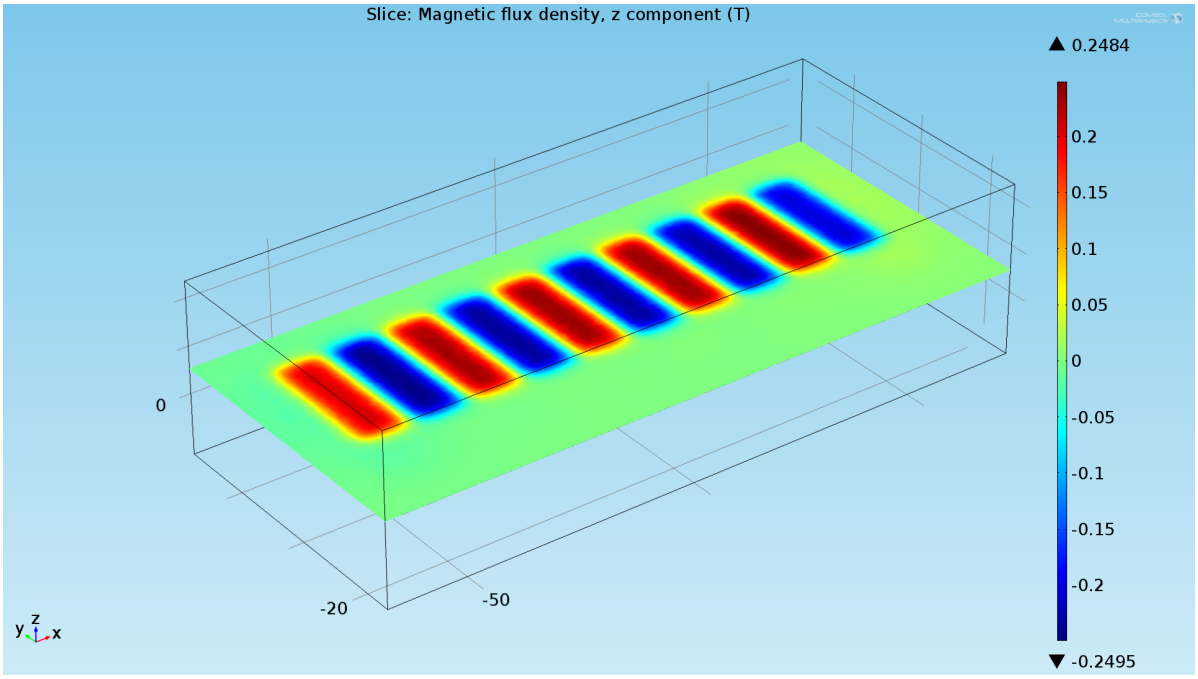

Figure B.3: Z-component of magnetic flux density. Simulated in COMSOL using single sided magnet configuration.

C

Position sensor

C.1. Sensor calibration

This appendix shows several steps that are taken to improve the performance of the sensors. During these measurements, a semi-double sided motor configuration, HIWIN rail with two guide blocks and the Elmo drive are used. The Heidenhain sensor is used as a reference. Every sensor that is used will be discussed in the coming subsections.

C.1.1. RLS

The RLS encoder does not need any calibration. As shown in figure C.1, the RLS encoder falls within a band of ± 10 μm compared to the Heidenhain encoder. The spike that is visible at 5 seconds is caused by the reference mark on the scale. Normally, this reference mark should be placed at the beginning of the scale, but it will still cause a slightly lower accuracy around this mark. A 550mm scale (MS05) of the RLS sensor has a specified accuracy of ± 6 μm. The specified accuracy around reference mark is ± 22 μm for a 550mm scale.

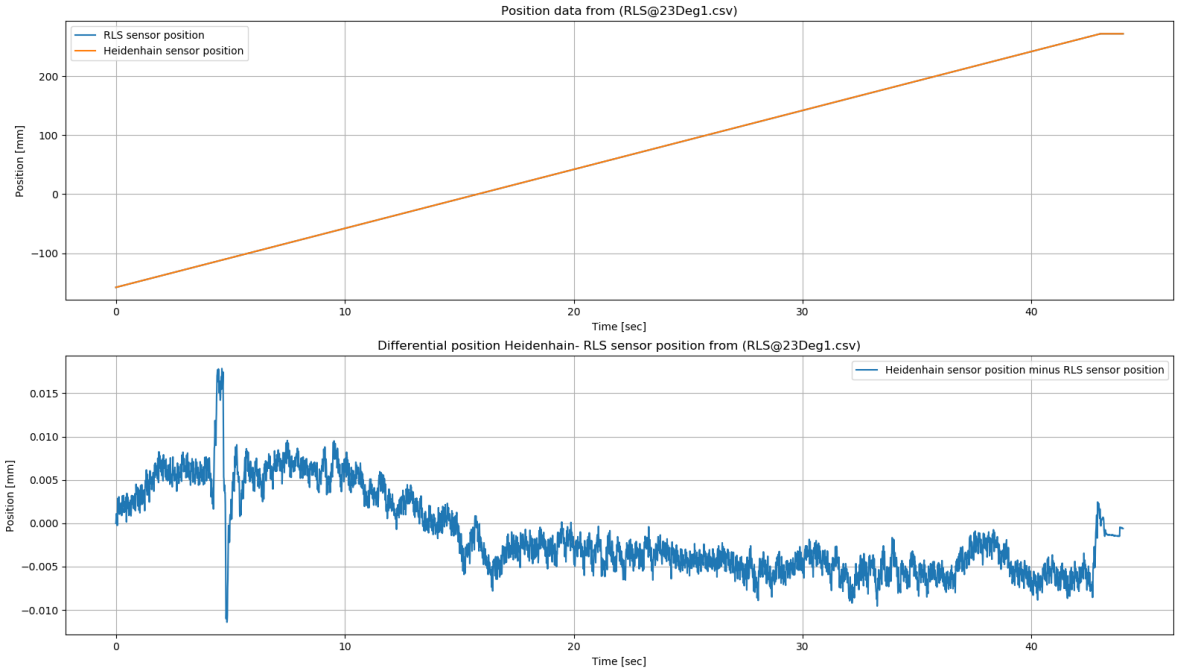

Figure C.1: Position error of the RLS sensor without any calibration. Heidenhain sensor used as reference encoder. The motor moves at 10 mm/s, 1 m/s^2 during this measurement.

C.1.2. POSIC

The POSIC encoder comes with an evaluation & programming tool to program the lookup table of the sensor. The user can input a series of positions setpoints, which are used by the software to calculate the lookup table. Figure C.2 shows the position of the reference encoder minus the position of the POSIC encoder before programming the lookup table, together with the same data after programming the lookup table. Before programming the lookup table the POSIC encoder falls within a band of ± 50 μm compared to the Heidenhain encoder. After programming the lookup table the POSIC encoder falls within a band of ± 30 μm compared to the Heidenhain encoder.

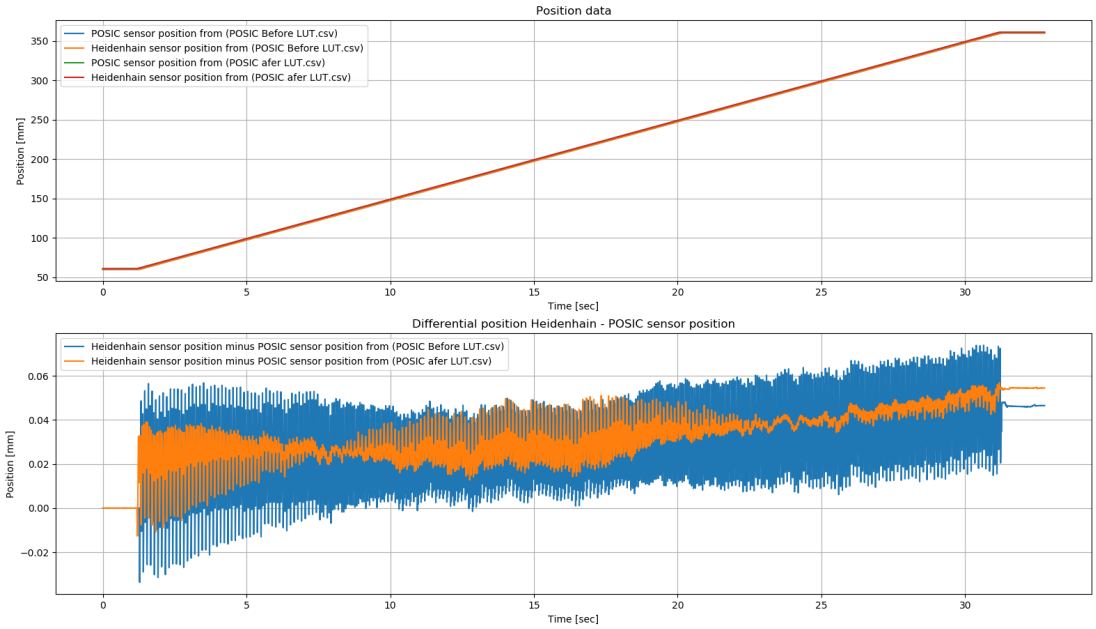

Figure C.2: Position error of the POSIC sensor without any calibration, together with programmed lookup table. Heidenhain sensor used as reference encoder. The motor moves at 10 mm/s, 1 m/s^2 during this measurement.

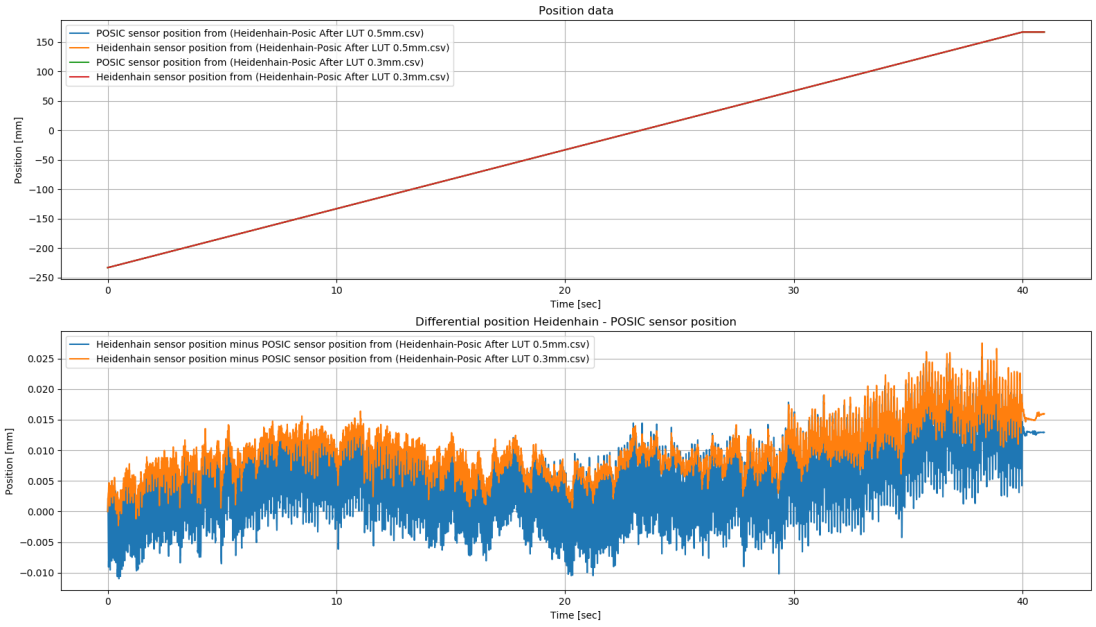

Figure C.3: Position error of the POSIC sensor with programmed lookup table, for a sensor-scale distance of 0.3 and 0.5 mm. Heidenhain sensor used as reference encoder. The motor moves at 10 mm/s, 1 m/s^2 during this measurement.

A FFT on the position error shows that the period of the error signal is 0.64 mm and 1.28 mm. The scale pitch is 1.28mm. It is noted that the distance between the scale and the sensor varies over the length, caused by incorrectly mounted backing tape. After reinstalling the scale without backing tape, the sensor error decreased significantly. Figure C.3 shows the difference in sensor error, for a sensor with a distance of 0.3 and 0.5 millimeters from the scale. It can be concluded that the sensor is very sensitive for variations in sensor to scale distances.

The sensor is mounted on a distance of 0.3 mm from the scale. The sensor error before and after calibration of the lookup table is shown in figure C.4. The repeatability of the sensor is shown in figure C.5.

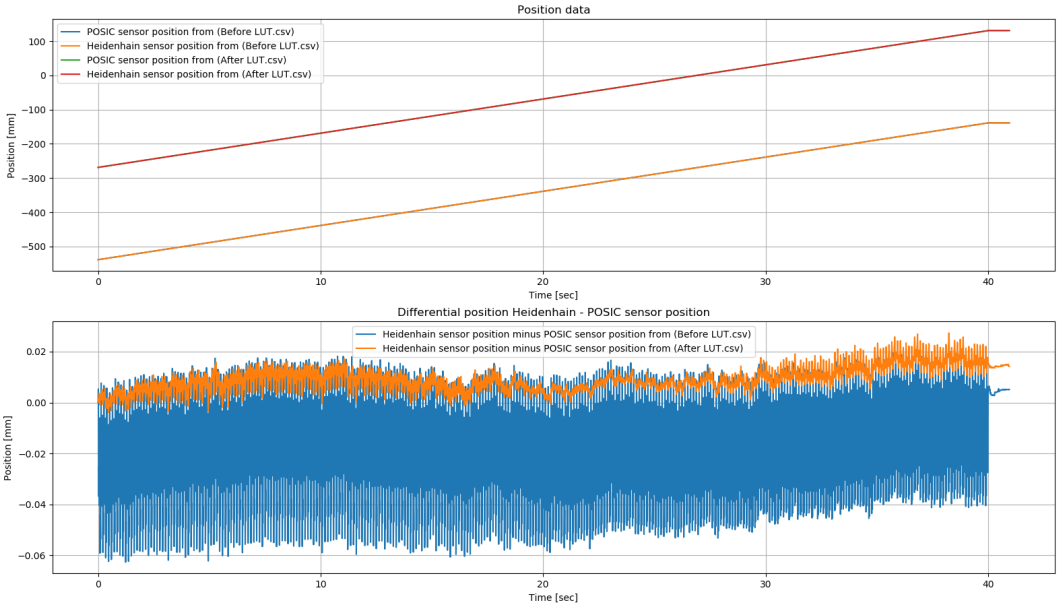

Figure C.4: Position error of the POSIC sensor with and without programmed lookup table, for a sensor-scale distance of 0.3 mm. Heidenhain sensor used as reference encoder. The motor moves at 10 mm/s, 1 m/s^2 during this measurement.

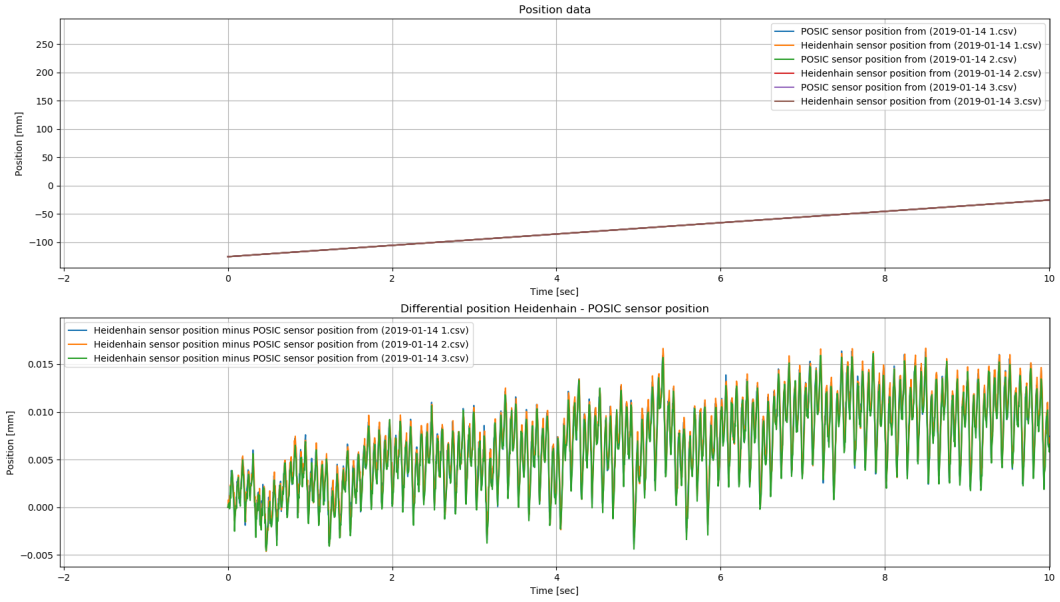

Figure C.5: Position error of the POSIC sensor with programmed lookup table. Measurements are taken at different time instances, showing the repeatability of the sensor. Heidenhain sensor used as reference encoder. The motor moves at 10 mm/s, 1 m/s^2 during this measurement.

C.1.3. Honeywell

Four Honeywell SS496A1 sensors are used to to provide positional feedback to the controller. Two differential op-amps were needed to correct the offset and gain of the sensors, such that they can be used in combination with the Elmo drive. The circuit diagram of this sensor is made using EasyEDA circuit designer[10] and shown in figure C.6. A simulation of the circuit is made in LTspice[9] and shown in figure C.7. It shows that the cut-off frequency of the low pass filter is 1.8 kHz.

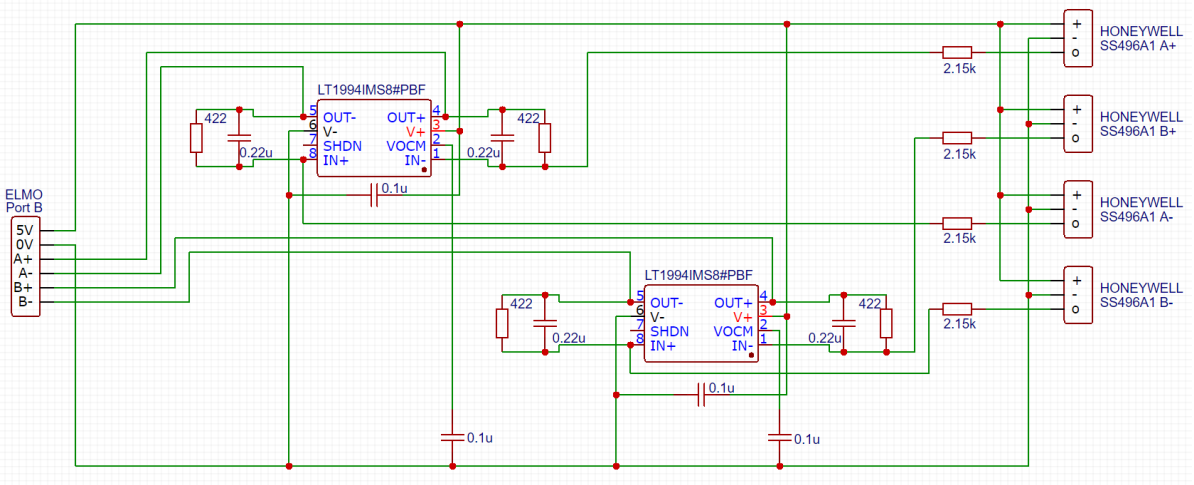

Figure C.6: Circuit diagram of the Honeywell sensors and op-amps. Created using EasyEDA

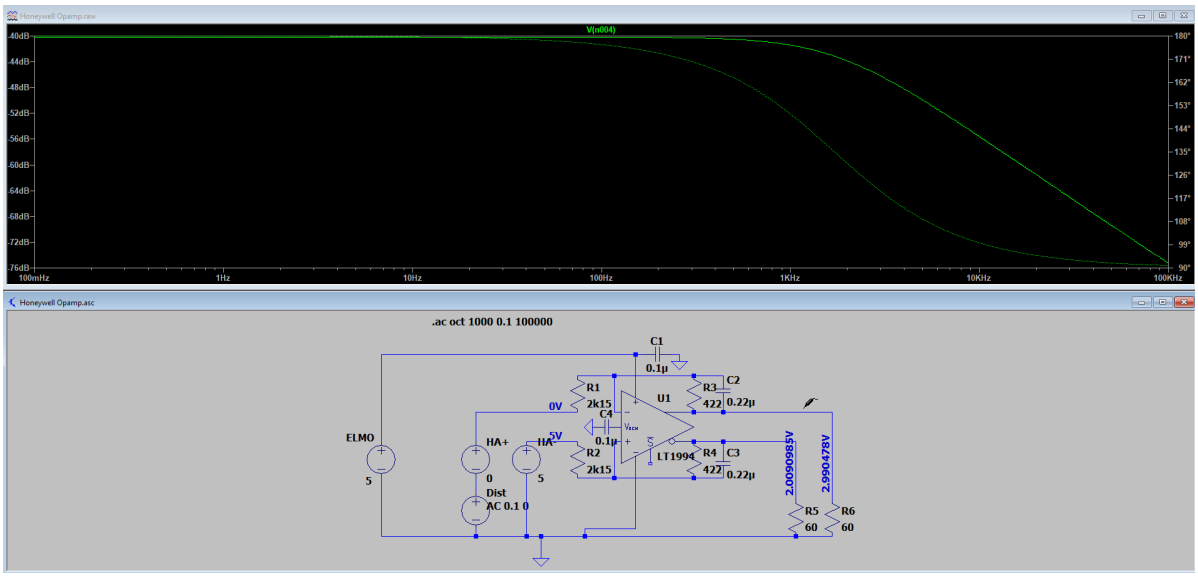

Figure C.7: Simulation of the circuit of the Honeywell sensors and op-amps. Created using LTspice

Figure C.8 shows the position of the reference encoder minus the position of the Honeywell encoder after the sensor calibration using the Elmo drive. The Honeywell encoder falls within a band of ±160 μm compared to the Heidenhain encoder. The period of the error is 6 mm, which is a quarter of the magnet pitch. Although the Honeywell sensor position deviates much from the Heidenhain position, the data is quite repeatable, as shown in figure C.9. The noise on the sensor signal falls within ±4 counts, which corresponds to 6 μm, shown in figure C.10.

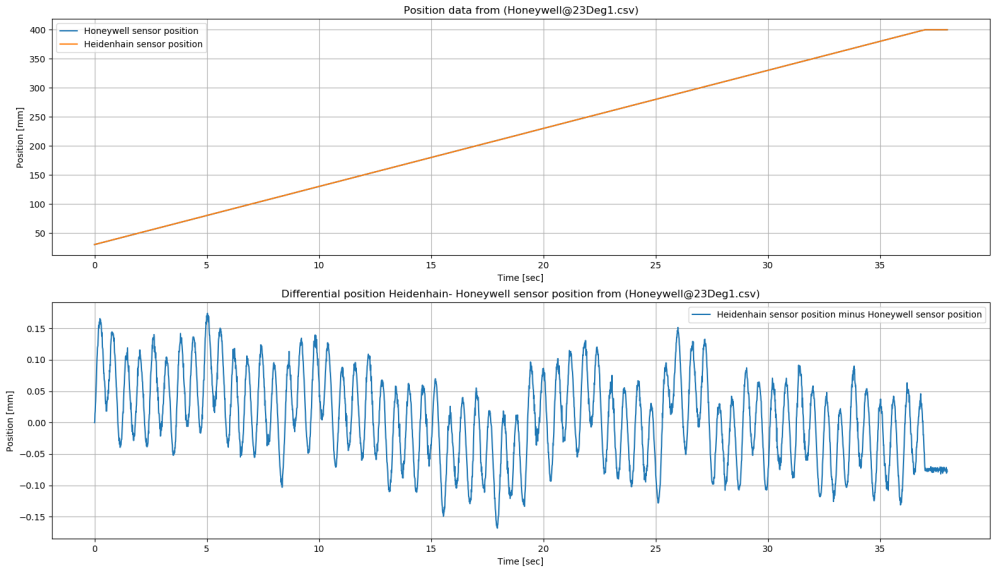

Figure C.8: Position error of the Honeywell sensor, calibrated using the Elmo drive 'sensor. Heidenhain sensor used as reference encoder. The motor moves at 1 0mm/s, 1 m/s^2 during this measurement.

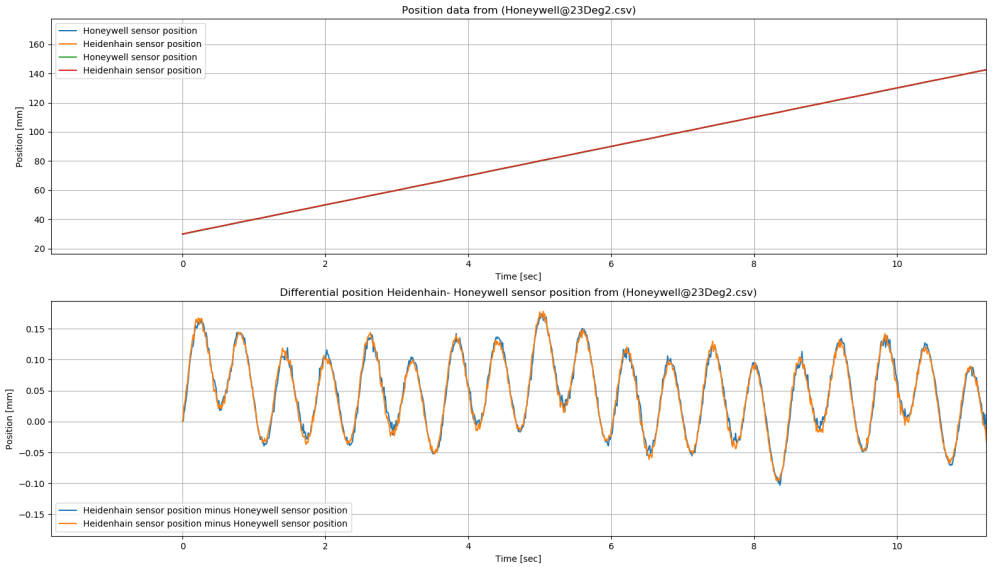

Figure C.9: Two position error measurements of the Honeywell sensor, showing the repeatability of the measurement.

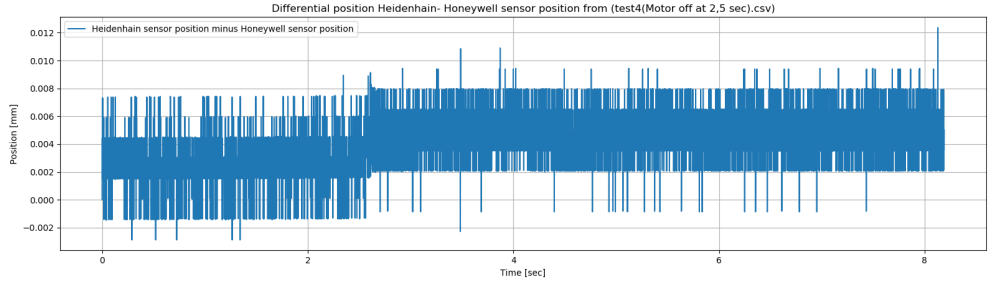

Figure C.10: Position error of the Honeywell sensor during stand still, showing the noise on the position measurement. The motor is turned off at 2.5 seconds.

The periodic error of the sensor suggests that the error is caused by imperfections of the magnetic field. In figure C.11 the magnetic field strength of the magnets is shown as function of the position of the mover. The magnetic field strength is measured by one of the Hall sensors mounted in the Honeywell position sensor. It is shown that maximum amplitude of the magnetic field strength varies from 70mT to 80mT over the entire range of the motor. This may case the sensor errors as shown in figure C.8

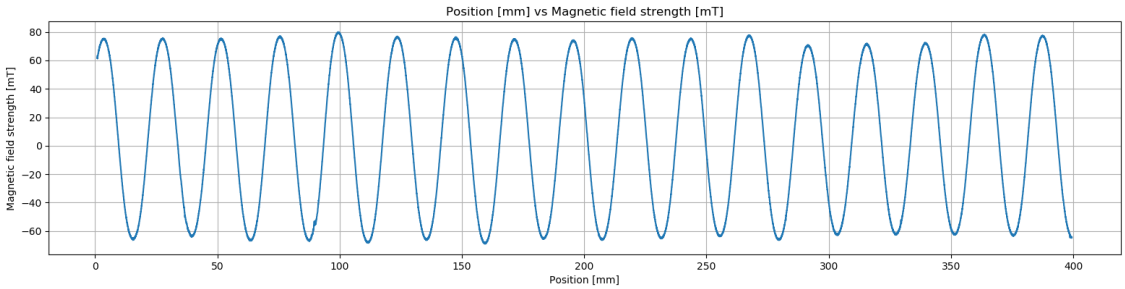

Figure C.11: Magnetic field strength as sensed by the Honeywell Hall sensors as function of position.

C.1.4. AMS

The forth sensor that is used is the AMS AS5311. The sensor was short-circuited during the measurement phase and is therefore not further implemented in the evaluation. Nevertheless the collected data is presented here. Figure C.12 shows the raw sensor data without any correction. A gain error is visible in this graph and is corrected for in figure C.13. In figure C.14 it is shown that the position error of the AMS sensor, compared to the Heidenhain sensor, is closely related to the velocity. This is caused by delay of the AMS output signal compared to the Heidenhain sensor. The time delay between the two outputs is about 0.15 ms. In figure C.15 the same movement is shown, but with corrected time delay. Finally, in figure C.16 the AMS position error compared to the Heidenhain sensor is shown for a variety of movements. The sensor stays within ± 10 μm from the Heidenhain sensor.

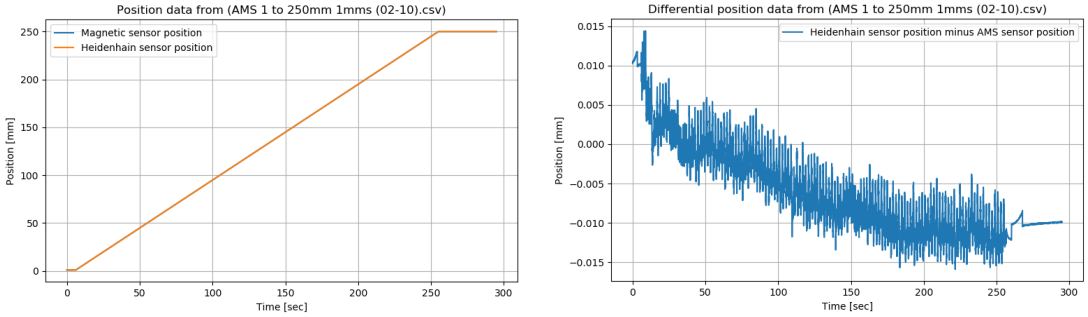

Figure C.12: Position error of the AMS sensor without calibration. Heidenhain sensor used as reference encoder. The motor moves at 1 mm/s, 0.1 m/s^2 during this measurement.

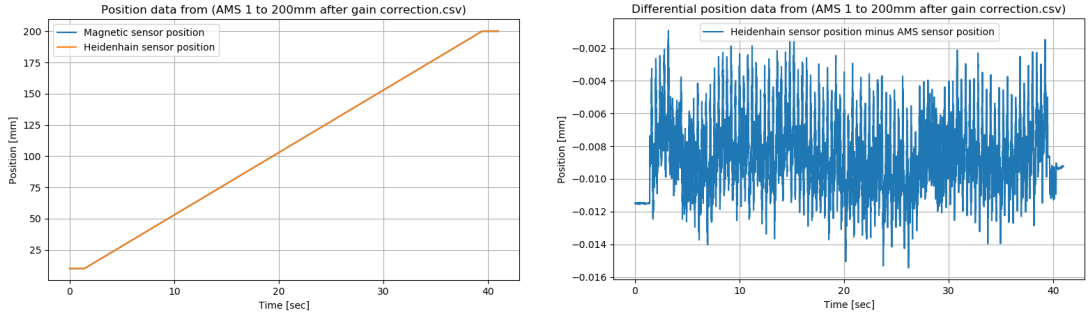

Figure C.13: Position error of the AMS sensor after gain correction. Heidenhain sensor used as reference encoder. The motor moves at 5 mm/s, 0.1 m/s^2 during this measurement.

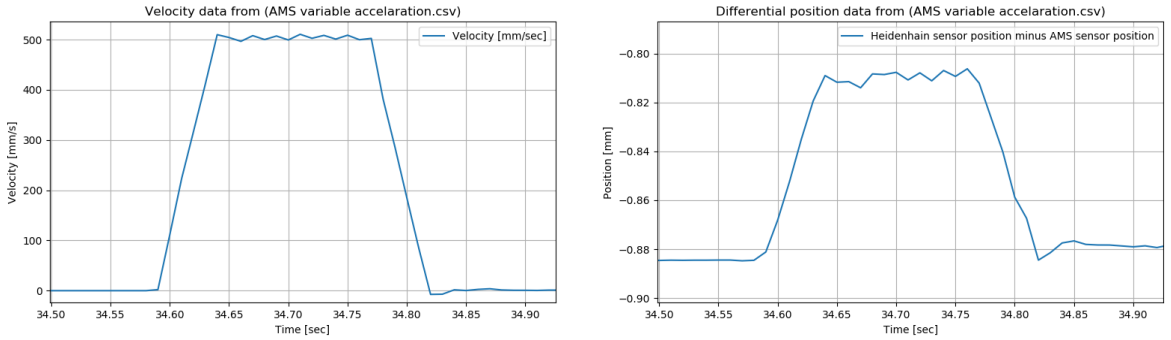

Figure C.14: Position error of the AMS sensor without calibration. Heidenhain sensor used as reference encoder. The motor moves at 500 mm/s, 0.1 m/s^2 during this measurement.

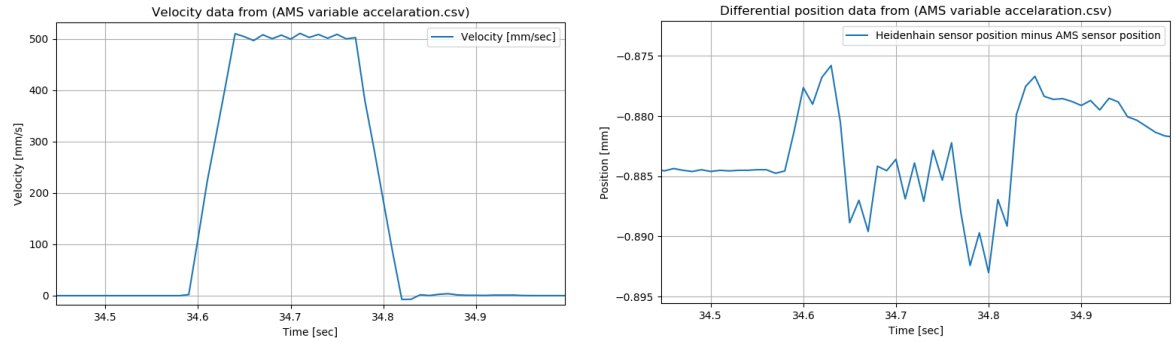

Figure C.15: Position error of the AMS sensor after compensation for time delay. Heidenhain sensor used as reference encoder. The motor moves at 500 mm/s, 0.1 m/s^2 during this measurement.

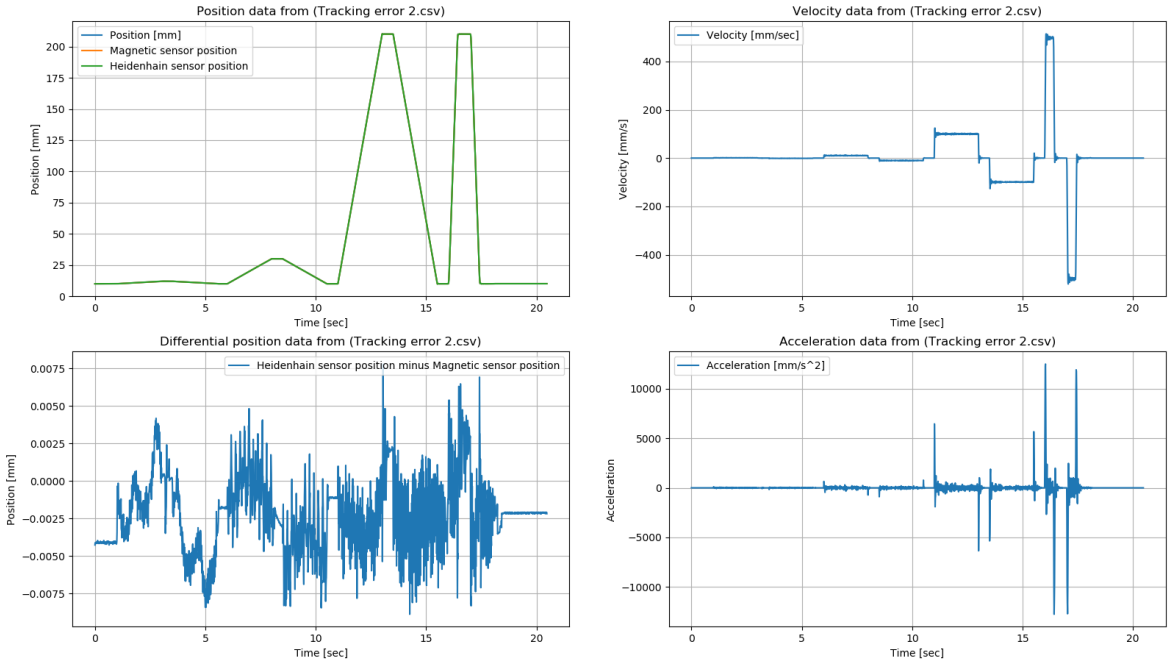

Figure C.16: AMS position error compared to the Heidenhain sensor for a variety of movements.

C.1.5. Comparison of the sensors

Figure C.17 shows a comparison of the three discussed PCB level sensors, after calibration. The Honeywell sensor is not included in this figure, because the position error is an order of magnitude higher.

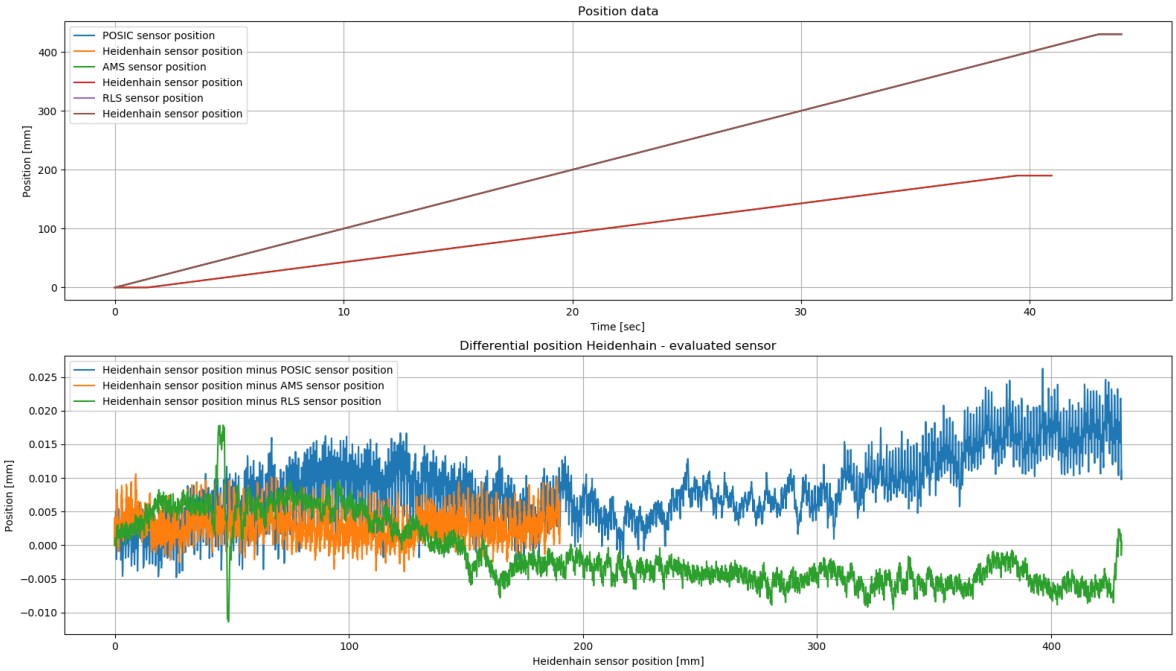

Figure C.17: Comparison of the three discussed PCB level sensors after calibration.

C.2. Measurement results thermal error

This section highlights the thermal measurements from chapter 5. Figure C.18 is included to show the difference between the RLS sensor and the POSIC sensor when heated to 38 degrees Celsius. The figure shows that the POSIC sensor is more sensitive to deviations in temperature.

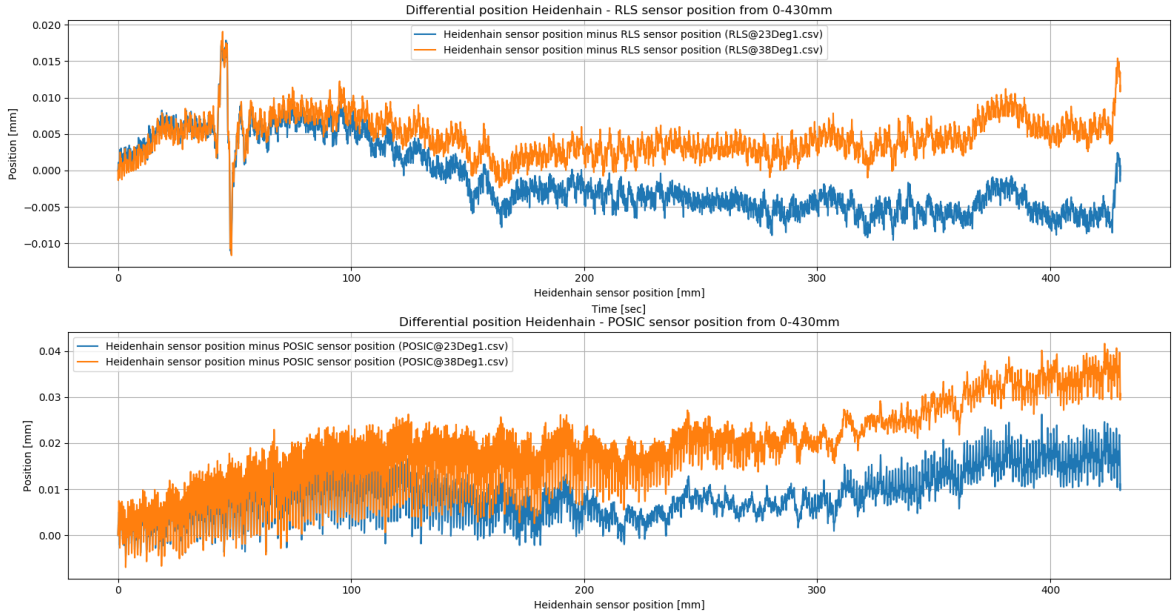

Figure C.18: Comparison of the RLS sensor and POSIC sensor when heated to 38°C.

C.3. Contour lines of 50 mT magnetic field strength

This appendix shows the contour lines where the magnetic field strength exceeds 50 mT. The RLS Hall effect encoder is unable to operate within these contour lines. In figure C.19 the field lines are shown for a single sided and semi-double sided configuration.

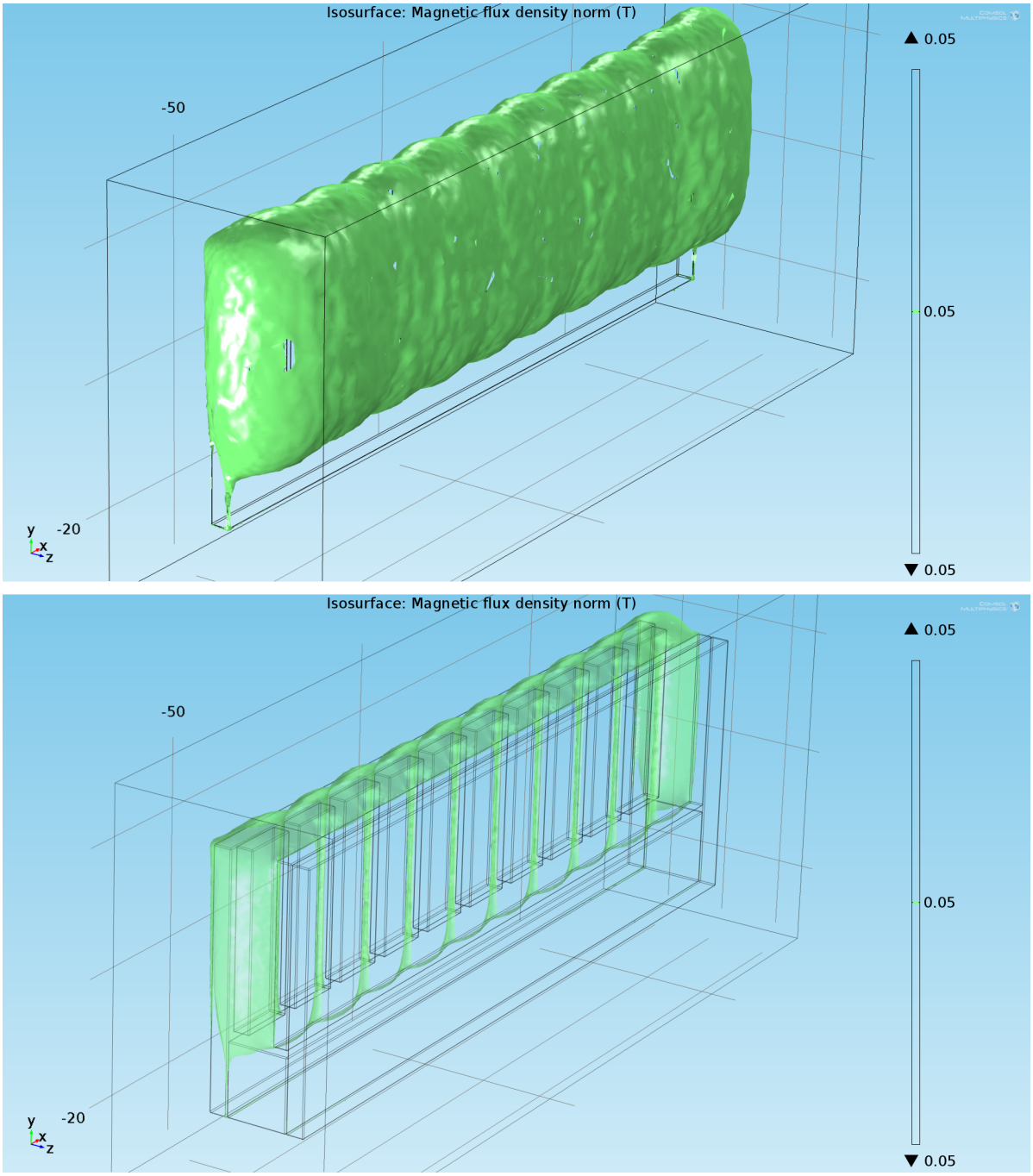

Figure C.19: Comparison of the 50mT contour lines for a single sided configuration (top) and a semi-double sided configuration (bottom).

D

Yaw stiffness guide

This appendix describes an estimation for the sensor displacement as a result of an applied motor force. This estimation has to be made, because this data is not available in the data sheet of the bearing manufacturer. The only stiffness that is given, is the radial stiffness of the bearing k_r = 44e6 $\frac{\text{N}}{\text{m}}$. Taken into account the length of the bearing, this stiffness can be expressed as stiffness per bearing length which equals $k_{r,l}$ =1.0e9 $\frac{\text{N}}{\text{m·m}}$. Assuming small angles, the linear deflection can be related to an angular deflection as $\delta = \theta x$, where x is the distance from the centre of the bearing to the position where the bearing applies the force to the rail. A sketch is shown in figure D.1. The forces applied by the linear springs can be converted to an equivalent torque, given by equation D.1.

$$M = 2\int_0^l (Fx)dx = 2\int_0^l (k_{r,l}\delta x)dx = 2\int_0^l (k_{r,l}\theta x^2)dx = \frac{2}{3}k_{r,l}\theta l^3 [Nm] \tag{D.1}$$

The yaw stiffness k_θ is related to the torque from equation D.1 and given by equation D.2. As length l=11 mm for the HIWIN runner block, the yaw stiffness is given in the equation.

$$k_\theta = \frac{M}{\theta} = \frac{2k_{r,l}\theta l^3}{3\theta} = 0.9e3[\frac{Nm}{rad}] = 16[\frac{Nm}{deg}] \tag{D.2}$$

The angular deflection θ can now be related to a motor force F_m using the distance between the motor and the rotation center of the bearing d_{mb}.

$$\theta = \frac{F * d_{mb}}{k_\theta} \tag{D.3}$$

Finally, the displacement at the position of the sensor δ_s can be expressed as a function of an applied force by the motor F_m, the distance between the sensor and the rotation center of the bearing d_{sb}, the distance between the motor and the rotation center of the bearing d_{mb} and the yaw stiffness k_θ .

$$\delta_s = \theta * d_{sb} = \frac{F_m * d_{mb} * d_{sb}}{k_\theta} [m] \tag{D.4}$$

Given that the Heidenhain sensor has a distance d_{sb}=26 mm from the bearing and the evaluated sensor has a distance d_{sb}=43 mm from the bearing, per Newton of motor force, the Heidenhain sensor will displace 0.35 μm and the evaluated sensor will displace 0.57 μm. The bearing stiffness k_y, as a result of an applied motor force F_m can be expressed as $k_y = \frac{F_m}{\delta_s}$ and thus is equal to $k_{y,H}$=2.9e6 $\frac{\text{N}}{\text{m}}$ and $k_{y,e}$=1.7e6 $\frac{\text{N}}{\text{m}}$.

Apart from the stiffness of the bearing, also the stiffness of the bracket needs to be considered. Solidworks is used to estimate the displacement on the sensor side of the bracket, in relation to a force applied in the motor. The sensor displacement related to bracket deformation is so low that it can be neglected compared to the yaw stiffness of the bearing.

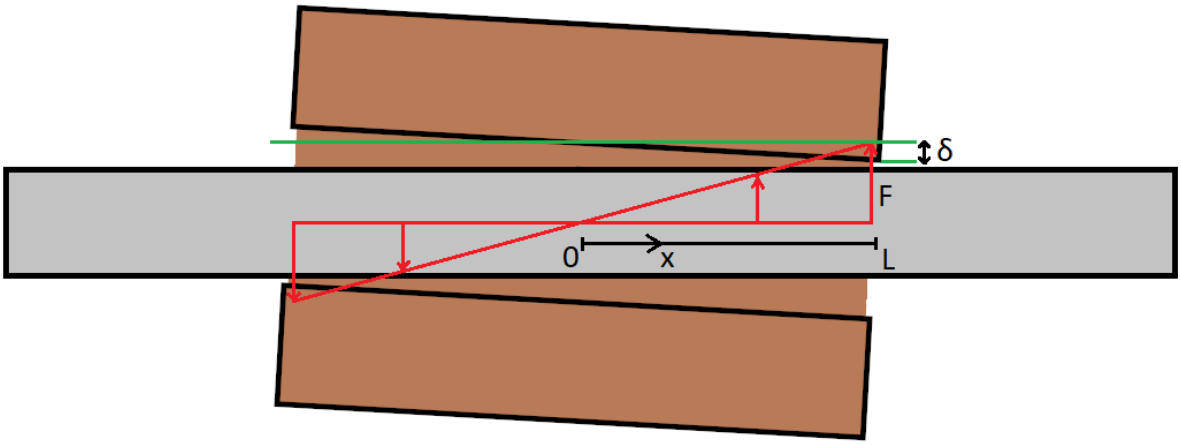

Figure D.1: Sketch and variables used in yaw stiffness calculation

E

Controller

E.1. Elmo control loop

This appendix shows the control scheme of the Elmo controller. The position, velocity and current loop is drawn. Advanced functions like gain and filter scheduling are not implemented in this figure.

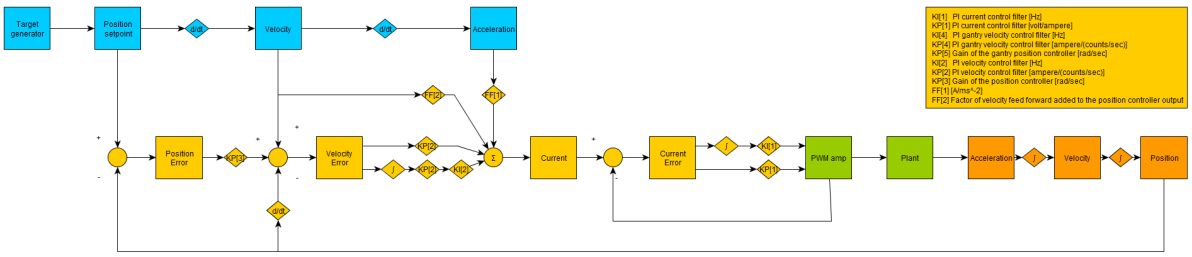

Figure E.1: Sketch of the Elmo control scheme. Freely obtained from the Elmo manual: Command Reference for Gold Line Drives.[35] Gain and filter scheduling is not implemented in this figure.

E.2. ODrive control loop

This appendix shows the control scheme of the Odrive controller.

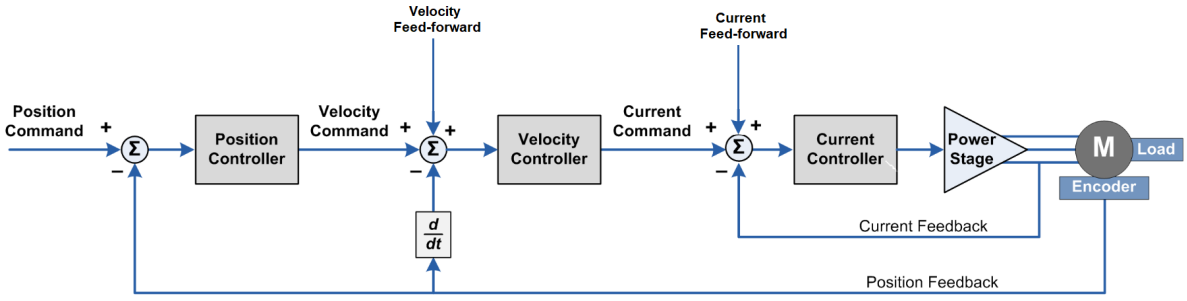

Figure E.2: Sketch of the ODrive control scheme. Obtained from the ODrive documentation, control section.[42]

E.3. Error mapping

Figure E.3 shows the error of the RLS encoder compared to the Heidenhain encoder. The build-in error mapping function of the Elmo controller is used to obtain the error of the encoder for both the error mapping disabled as enabled. It is shown that the error of the RLS sensor becomes significantly less.

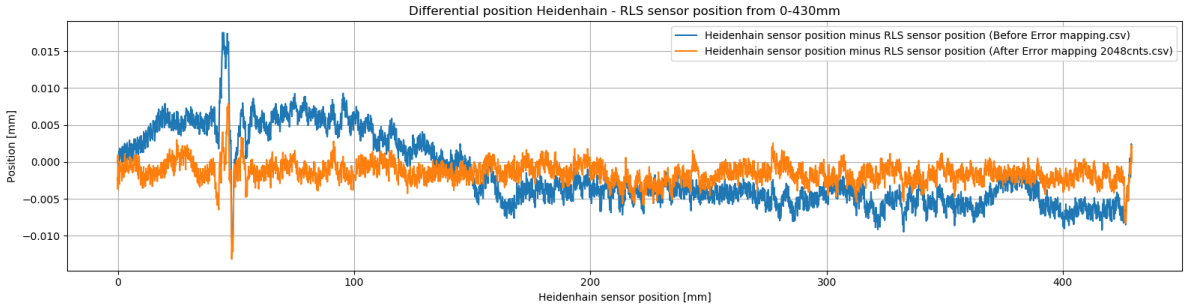

Figure E.3: Error of the RLS encoder before and after error mapping.

E.4. Step responses of Elmo and ODrive

The comparison of the step responses from the Elmo and ODrive are shown in figure E.4 and figure E.5 for two different positions on the axis.

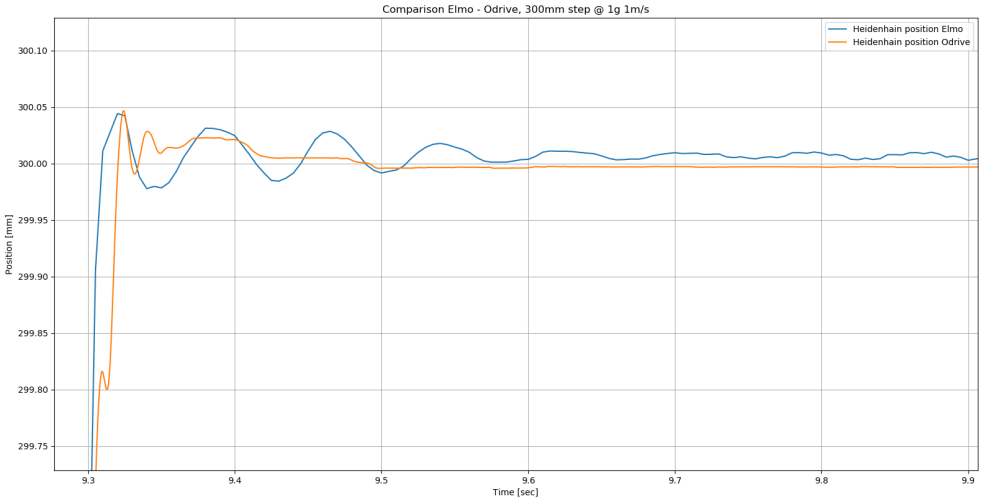

Figure E.4: Response to a 300mm, 1g, 1m/s step for both the Elmo as ODrive controller. Starting at 60mm

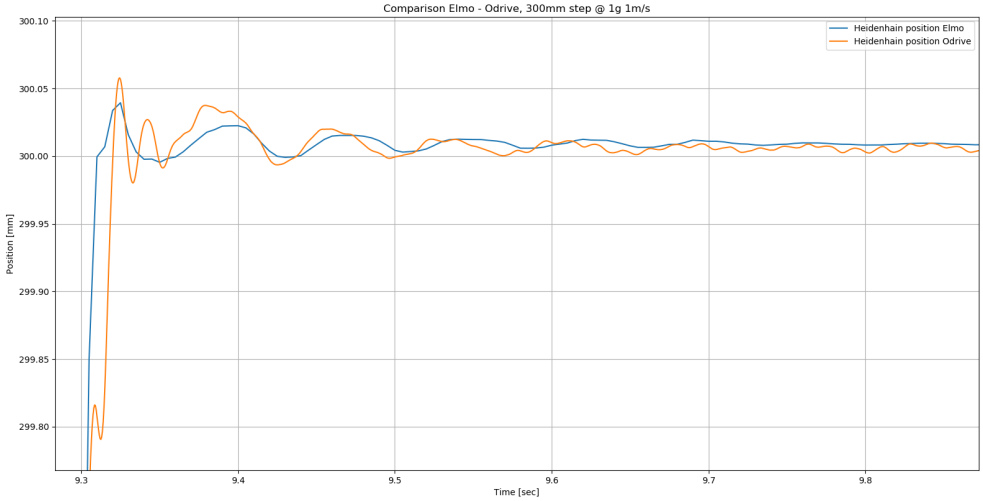

Figure E.5: Response to a 300mm, 1g, 1m/s step for both the Elmo as ODrive controller. Starting at 80mm

F

Supplementary figures

This chapter shows several pictures of the setup, intended as a reference for Ultimaker.

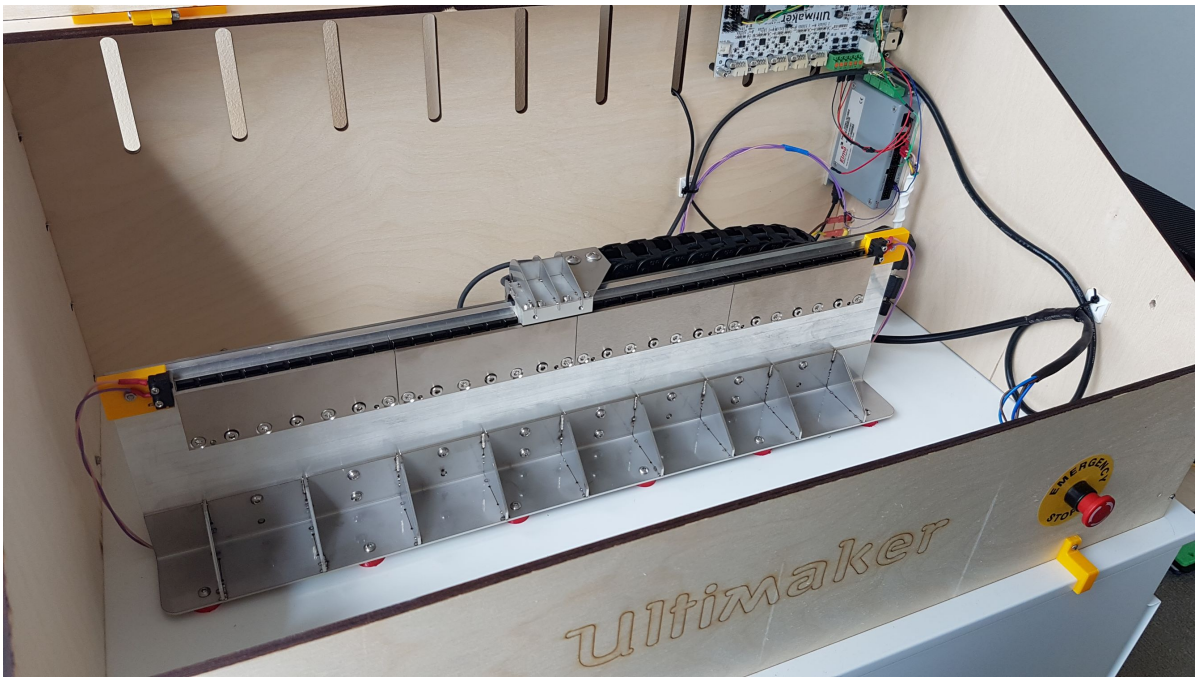

Figure F.1: First impression of the reference measurement setup. At a later stage the home switch was changed for one that features better repeatability.

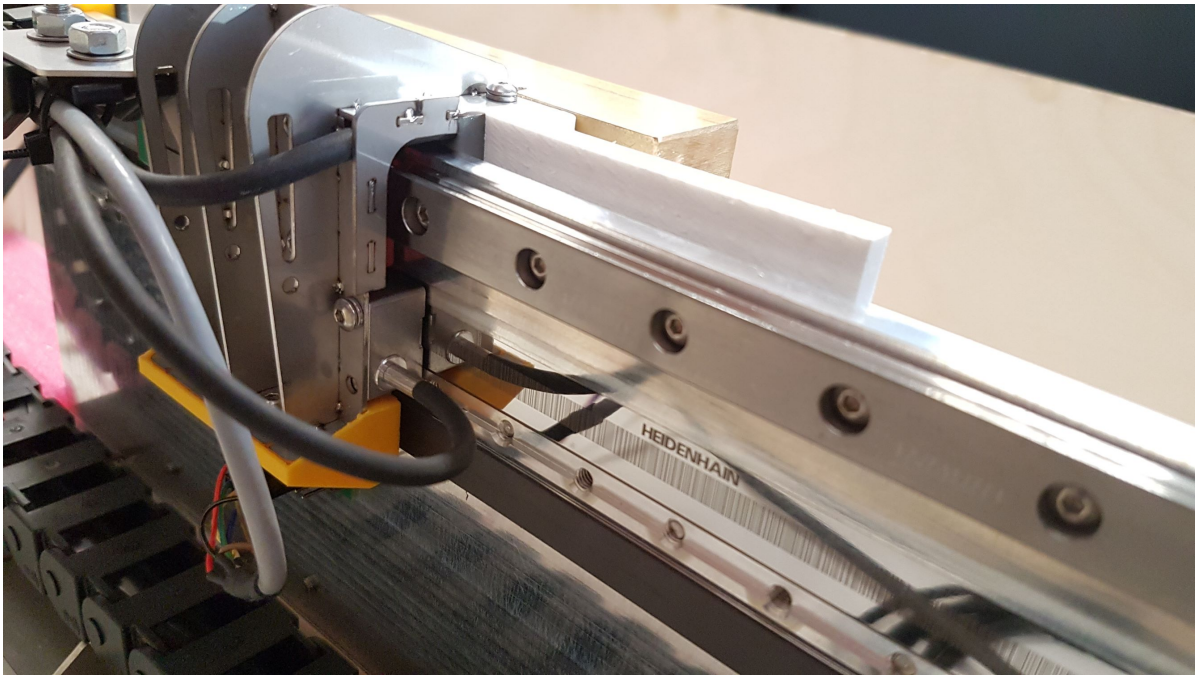

Figure F.2: The back of the reference measurement setup. The AMS sensor is mounted as evaluated sensor.

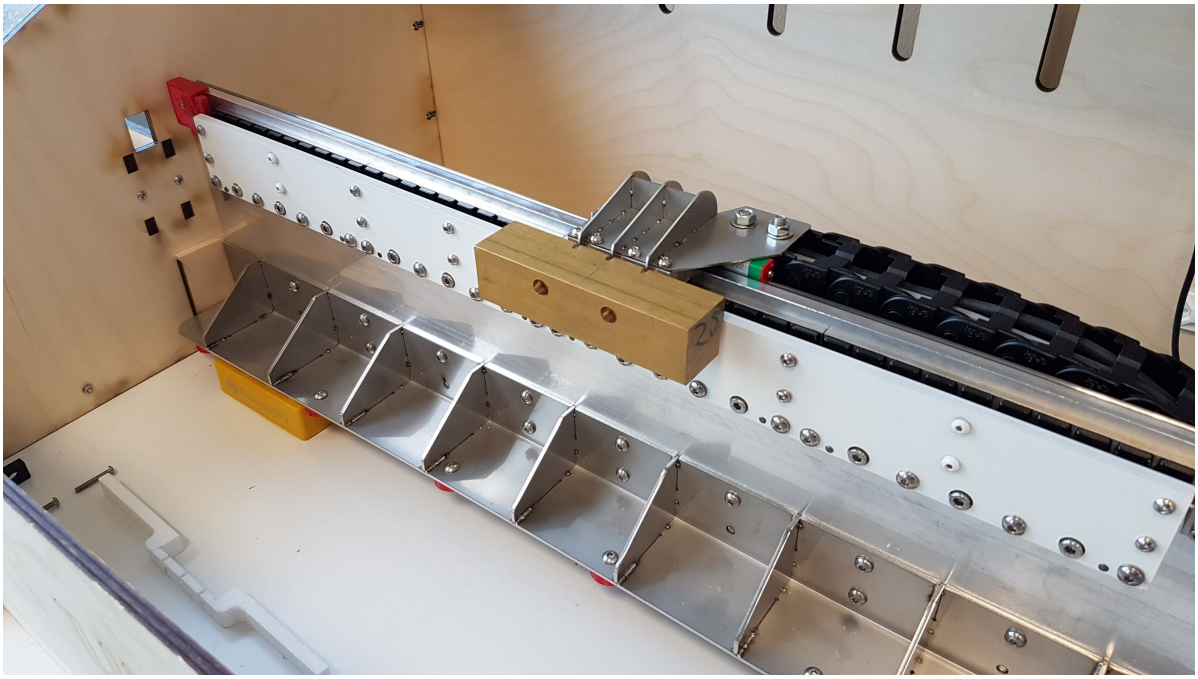

Figure F.3: Semi-double sided motor configuration.

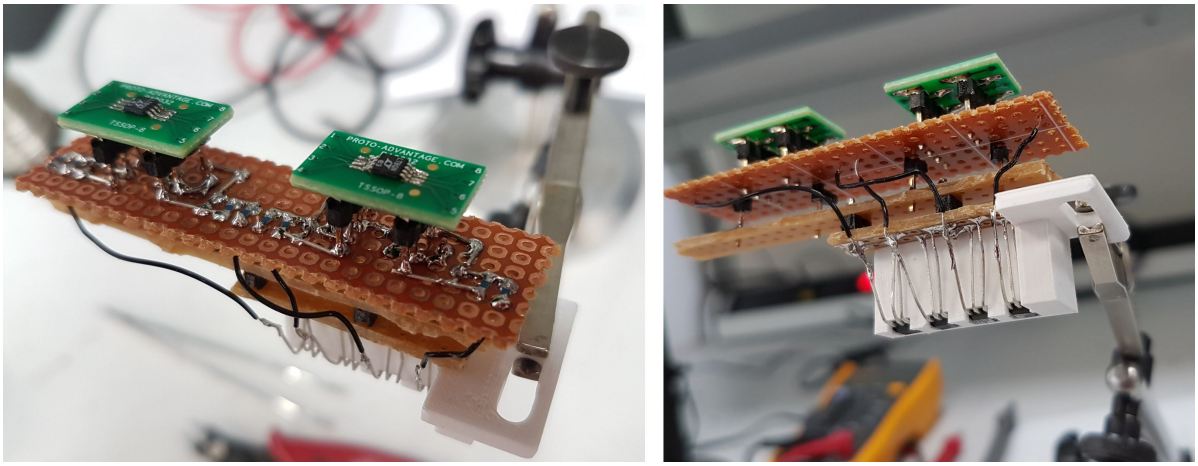

Figure F.4: Position sensor build with Honeywell hall sensors and LT1994 op-amps.

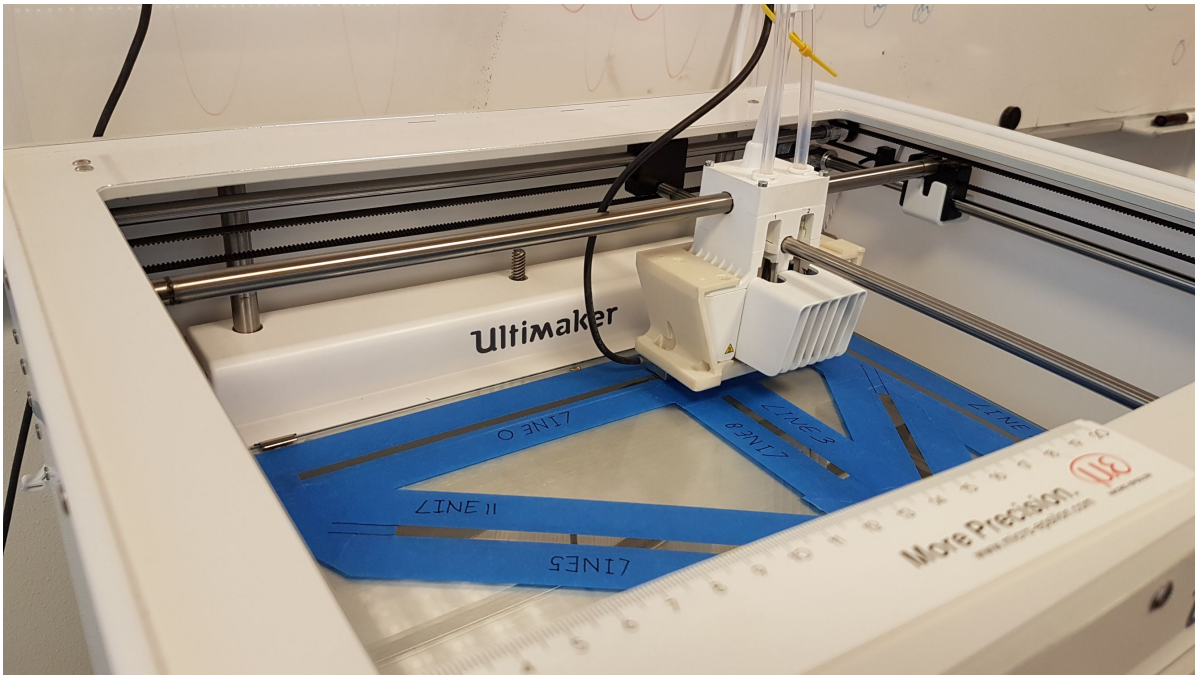

Figure F.5: The measurement setup used to determine the S5's accuracy and repeatability. Stepper motors and the Heidenhain encoder are connected directly to the Elmo drive.

Bibliography

[1] Aerotech. Linear motors application guide. https://www.aerotech.com/media/136335/linear-motors-application-en.pdf. Consulted on 20-06-2018.

[2] Bosch Rexroth AG. Linear motion technology handbook - r310en 2017. http://www13.boschrexroth-us.com/catalogs/LMThandbook/LMT_handbook_07.pdf.

[3] R.J. Cruise-C.F. Landy A.W. van Zyl, C.G. Jeans. Comparison of force to weight ratios between a single-sided linear synchronous motor and a tubular linear synchronous motor. *IEEE International Electric Machines and Drives Conference*, 1999.

[4] T. Baldacchini. *Three-Dimensional Microfabrication Using Two-Photon Polymerization*. Elsevier, 2016. ISBN 978-0-323-35321-2.

[5] WHO Media centre. Electromagnetic fields and public health. https://www.who.int/peh-emf/publications/facts/fs299/en/.

[6] Samuel Chevailler. Comparative study and selection criteria of linear motors. Master's thesis, Ecole polytechnique fédérale de Lausanne, Suisse, 2006.

[7] COMSOL. Comsol multiphysics 5.4. https://www.comsol.com/release/5.4.

[8] Analog Devices. Lt1994 fully differential amplifier. https://www.analog.com/en/products/lt1994.html, .

[9] Analog Devices. Ltspice xvii. https://www.analog.com/en/design-center/design-tools-and-calculators/ltspice-simulator.html, .

[10] EasyEDA. Easyeda circuit designer. https://easyeda.com/.

[11] International Organization for Standardization. Iso 230-2:2006. Test code for machine tools Part 2: Determination of accuracy and repeatability of positioning numerically controlled axes.

[12] Jacek F. Gieras. *Linear Induction Drives*. Oxford University Press, 1 edition, 1994. ISBN 0 19 859381 3.

[13] Jacek F. Gieras. *Linear Synchronous Motors*. CRC Press, 2 edition, 2012. ISBN 978-1-4398-4222-5.

[14] Jacek F. Gieras. Linear electric motors in machining processes. *International Conference on Electrical Machines and Systems*, 2:380–389, 2013. doi: 10.11142/jicems.2013.2.4.380.

[15] Jeffrey Michael Gorniak. Design and metrology of a precision xy planar stage. Master's thesis, University of Waterloo, Waterloo, Ontario, Canada, 2010.

[16] A.S. Gaunekar T.H. Kuah G.P. Widdowson, Liao Youyong and N. Srikanth. Design of a high speed linear motor driven gantry table. *IEEE International Conference on Power Electronic Drives and Energy Systems for Industrial Growth*.

[17] Layton Carter Haled. Principles and techniques for designing precision machines. Master's thesis, University of California, Livermore, California, 1999.

[18] Parker Hannifin. Linear motor engineering reference guide. http://www.motionusa.com.s3-website-us-east-1.amazonaws.com/parkertrilogy/Engineering_Reference_Guide.pdf. Consulted on 12-06-2018.

[19] Heidenhain. Lic 2119 / lic 2199 exposed linear encoders. https://www.heidenhain.com/en_US/products/linear-encoders/exposed-linear-encoders/selection-guide-for-lic/lic-2119-lic-2199/.

[20] HepcoMotion. Gv3 lineair guide system. https://www.hepcomotion.com/nl/product/componenten-lineaire-geleiding/gv3-lineair-geleidingssysteem/. Consulted on 28-12-2018.

[21] HIWIN. Mg series miniature linear guideway. https://motioncontrolsystems.hiwin.com/category/mg-series-miniature-linear-guideway.

[22] Honeywell. Ss490 series linear hall-effect sensor ic. https://sensing.honeywell.com/SS496A-linear-and-angle-sensor-ics.

[23] S.A. Nasar I. Boldea. *Linear Electric Actuators and Generators*. Cambridge University Press, Cambridge, 1997. ISBN 0-521-48017-5.

[24] S.A. Nasar I. Boldea. Linear electric actuators and generators. *IEEE Transaction on Energy Conversion*, 14:712–717, 1999. doi: 10.1109/60.790940.

[25] S.A. Nasar I. Boldea. *Linear Motion Electromagnetic Devices*. Taylor and Francis, 1 edition, 2001. ISBN 90-5699-702-5.

[26] A. John Hart Jamison Go. Fast desktop-scale extrusion additive manufacturing. *Additive Manufacturing Journal*, 18:276–284, 2017. doi: https://doi.org/10.1016/j.addma.2017.10.016.

[27] Jong Young Kim Jin-Hyung Shim, Jung-Seob Lee and Dong-Woo Cho. Bioprinting of a mechanically enhanced three-dimensional dual cell-laden construct for osteochondral tissue engineering using a multi-head tissue/organ building system. *Journal of micromechanics and microengineering*, 22, 2012. doi: 10.1088/0960-1317/22/8/085014.

[28] Dong-Woo Cho Jong Young Kim. The optimization of hybrid scaffold fabrication process in precision deposition system using design of experiments. *Microsyst Technol*, 15:843–851, 2008. doi: 10.1007/s00542-008-0727-8.

[29] Shin-Yoon Kim Jung-Woog Shin Jong Young Kim, Eui Kyun Park and Dong-Woo Cho. Fabrication of a sff-based three-dimensional scaffold using a precision deposition system in tissue engineering. *Journal Of Micromechanics And Microengineering*, 18, 2008. doi: 10.1088/0960-1317/18/5/055027.

[30] Tan Kok Kiong and Andi Sudjana Putra. *Drives and Control for Industrial Automation*. Springer, London, 1 edition, 2010.

[31] Samir Mekid. *Introduction to Precision Machine Design and Error Assessment*. CRC Press, Boca Raton, 2009. ISBN 978-0-8493-7887-4.

[32] MiSUMi. Linear motion products. https://uk.misumi-ec.com/vona2/mech/M0100000000/. Consulted on 28-12-2018.

[33] Celera Motion. Javelin ironless linear motor series. https://www.celeramotion.com/products-solutions/direct-drive-motors/linear-motors/portfolio-page#ironless-javelin-series. Consulted on 05-oct-2018.

[34] Elmo motion control. Gold dc bell servo drive. https://www.elmomc.com/product/gold-dc-bell-for-stepper-motors/.

[35] Elmo motion control Ltd. Command reference for gold line drives. Ver. 1.406, February 2013.

[36] David S. Nyce. *Position Sensors*. John Wiley and Sons, 2016. ISBN 9781119069089.

[37] Michael Petch. New essentium high speed extrusion 3d printer runs at 1 m/s. https://3dprintingindustry.com/news/new-essentium-high-speed-extrusion-3d-printer-runs-1-ms-132606/. Consulted on 14-06-2018.

[38] Posic. Id1102l incremental encoder. https://www.posic.com/EN/linear-encoder-id1102l.html.

[39] Günter Pritschow. A comparison of linear and conventional electromechanical dives. *CIRP Annals*, 47:541–548, 1998. doi: 10.1016/S0007-8506(07)63241-7.

[40] RLS. Rlc2ic pcb level incremental magnetic encoder. https://www.rls.si/en/rlc2ic-miniature-linear-pcb-level-incremental-magnetic-encoder.

[41] Odrive Robotics. Odrive v3.5. https://odriverobotics.com/shop/odrive-v35, .

[42] Odrive Robotics. Orive documentation - control. https://docs.odriverobotics.com/control, .

[43] Alain Cassat Samuel Chevailler and Marcel Jufer. High acceleration applications: Design optimization and comparison between different toothless motors. Master's thesis, Ecole Polytechnique Fédérale de Lausanne, CH-1015 Lausanne, 2005.

[44] Robert Munning Schmidt. *The Design of High Performance Mechatronics*. Delft University Press, 2 edition, 2014.

[45] Herve Stampfli. Linear motor applications: Ironcore versus ironless solutions. HST-Etel Inc., 2003.

[46] Tecnotion. Iron core and ironless linear motor series. https://www.tecnotion.com/downloads/catalogue-iron-core-/-ironless-motors.pdf, . Consulted on 08-aug-2018.

[47] Tecnotion. Uf series linear motors. https://www.tecnotion.com/products/iron-less-linear-motors/uf-series.html, .

[48] Sudin Izman V. C. Venkatesh. *Precision Engineering*. Tata McGraw-Hill Publishing Company Limited, New Delhi, 2007. ISBN 0-07-154828-9.